Temporo-frontal Phase Synchronization Supports Hierarchical Network for Mismatch Negativity

by

Shannon Elizabeth MacLean

Bachelor of Child Study, Mount Saint Vincent University 1991

Bachelor of Science, Dalhousie University, 1994

Master of Science, Dalhousie University, 1998

A THESIS SUBMITTED IN PARTIAL FULFILLMENT OF THE

REQUIREMENTS FOR THE DEGREE OF

DOCTOR OF PHILOSOPHY

in

The Faculty of Graduate Studies

(Neuroscience)

THE UNIVERSITY OF BRITISH COLUMBIA

(Vancouver)

April 2011

ABSTRACT

Several cortical regions appear active when the mismatch negativity (MMN) scalp potential is evoked automatically in response to detectable auditory changes. It remains debatable whether the activation of regions beyond the auditory cortex is coincidental or functionally significant to the MMN response. We used independent component analysis (ICA) to separate high density EEG data (64-channel) prior to dipole fitting for two reasons: 1) to enhance the spatial resolution of EEG and 2) to provide temporal and frequency information about the cortical sources needed to evaluate their functional relationships during the MMN response. For a group of young adults (n = 12) passively listening to infrequent changes in complex tones while watching a silent movie, event-related activity within sources localized to the orbitofrontal cortex (OFC) and the bilateral superior temporal gyrus (STG) regions accounted for most of the scalp response variance implicating these regions as driving forces in the MMN. For a second group (n = 14) performing both passive and active listening across the same paradigm, cross-coherence (phase synchronization) during the MMN response was consistently found between the OFC and the STG bilaterally. During both paradigms the source in the right inferior frontal gryus (R IFG) was also synchronous with the STG-OFC network. When responding to deviant targets in the active paradigm, synchrony was more bilaterally distributed across the network. For a third group (n = 14) passively listening to infrequent changes in speech syllables, synchrony during the MMN response was found between the STG-OFC again as well as with regions in the R IFG and Broca's area. This same subject group later attended to the speech syllables responding to deviants and standards with a different button press. Synchrony between the STG-OFC, and Broca's area was found, as well synchrony with a source in the right anterior cingulate. All paradigms showed synchronous interactions both within and between the temporo-frontal

regions that were modulated differentially by deviant and standard stimulus conditions as well as by task demands providing the first evidence of functional coupling within a hierarchical network coinciding with the MMN response evoked at the scalp.

PREFACE

The experiments described herein were approved by the Behavioural Research Ethics Board of the University of British Columbia, and the Certificate Numbers of the Ethics Certificates obtained are: C00-0505, D00-0505, E00-0505 and F00-80505.

TABLE OF CONTENTS

LIST OF TABLES

LIST OF FIGURES

ACKNOWLEDGEMENTS

This work was generously supported by NSERC: a Discovery Grant awarded to Lawrence Ward and a Post Graduate Scholarship Doctoral awarded to Shannon MacLean.

I remain deeply indebted to Lawrence Ward, my supervisor, for his wisdom, compassion, generosity, and patience. As well, for their guidance and generous donation of their time, I am indebted to my supervisory committee members, Drs. Jeremy Seamans, Peter Reiner, and Valter Ciocca, as well as to former members, Drs. Li Yue-Xian and David Stapells. Also I owe a debt of gratitude to Dr. Julie Onton of the SCCN for help with EEGLAB advanced script writing. I am grateful also to Dr. Janet Werker for the loan of speech stimuli. I also wish to especially thank Dan Black for the calibration and loan of audiometric equipment and Dusko Pijetlovic for setting up my remote access to the laboratory computer.

As well, I owe great thanks to the past lab members who assisted me in my research at its various stages: Lauren Emberson for the introduction to EEGLAB; Dr. Alexa Roggeveen for help with programming in Presentation and Acquire; Drs. Kei Kitajo and Sam Doesburg for help with Matlab programming; and Stephani Thái for help running subjects and formalizing experimental procedures. Also special thanks to current lab members Ania Mizgalewicz for help with running subjects; Aaron Kirschner for help with cross-coherence analysis; and Sam Bayless for help with Presentation programming and with the 64-bit operating system setup.

Above all, I thank Keith Burdon for reasons too numerous to mention here.

DEDICATION

To Marjorie & me.

CHAPTER 1: BACKGROUND OF THE MISMATCH NEGATIVITY

Introduction

Automatic change detection is a fundamental capacity of the auditory nervous system. Without it, the ability to respond to potentially relevant sounds outside the focus of attention would be lost, and chances for survival severely diminished. The human brain's involuntary response to rare and unexpected changes to an ongoing acoustic regularity is a negative going potential recorded on the scalp surface shortly after changes occur, roughly 120 - 250 ms post-stimulus onset. This response, aptly named the Mismatch Negativity (MMN), has been extensively studied using EEG/MEG technologies and appears sensitive to both the physical and abstract contextual changes occurring within a stream of regular acoustic input (Dehaene-Lambertz, 1997; Nääatänen, et al., 1997; Näätänen, Paavilainen, Rinne, & Alho, 2007). The MMN is derived by subtracting the event-related response to the regularly repeating event (known as 'the standard') from the response to the infrequent event (known as "the deviant"). If the deviant has been detected, the resulting difference wave displays a negative potential typically between 2-3μV at the midline frontal sites and inverting polarity at the temporal sites (using mastoid reference sites). This scalp potential is thought to arise from the excitatory responses of apical dendritic currents from cortical pyramidal cells resulting in an accumulation of negative charge in the extracellular fluid making the surface of the cortex more negative than its base. See Figure 1.1 for the distribution of MMN difference waveform among a scalp electrode array.

Deviations from the acoustic regularity need not be to stimuli at all: unpredictable gaps or silences where a sound was expected will elicit a MMN response. However, when a gap is masked by broad-band noise creating an illusion of a continuous tone the amplitude of the MMN has been shown to reflect this perception of continuity (Micheyl, Carlyon, Shtyrov, Hauk,

Dodson, & Pullvermüller, 2003). The MMN corresponds closely to the behavioural discrimination threshold for acoustic contrasts, losing amplitude and prolonging latency as the difference between standards and deviants narrows (Nääatänen, et al., 1997; Dehaene-Lambertz, 1997; for exception see Rivera-Gaxiola, Csibra, Johnson, & Karmiloff-Smith, 2000), finally disappearing when contrasts can no longer be discerned.

Intertwined with the brain's ability to detect changes automatically is its capacity to conceptualize aspects of the auditory environment that occur regularly and with high frequency. Therefore the presence of the MMN response to deviant probes provides a measure of the kinds of patterns or stimulus groupings, both learned and innate (Bregman, 1990), a particular auditory system is capable of forming (Ritter, De Sanctis, Molholm, Javitt, & Foxe, 2006; Garagnani & Pulvermüller, 2010). Hence, the MMN is a widely used neurophysiological tool in research and in clinical settings for investigating human auditory perception, in part because it can be recorded noninvasively from the scalp and also most importantly because it can be evoked independent of task or attention (Sussman, Winkler, & Wang, 2003; Atirnza, Cantero, & Dominguez-Marin, 2002; Daltrozzo, Wioland, Mutschler, & Kotchoubey, 2007) to any discernable change in a series of regularly repeating events with a wide variety of stimuli (Näätänen, Paavilainen, Rinne, & Alho, 2007; Atirnza, Cantero, & Dominguez-Marin, 2002). For this reason it has found application in objectively evaluating hearing functions of difficult to test populations, as well as an objective measure of success following cochlear implantation (Sandmann, et al., 2009; Sandmann, et al., 2010). In addition to assessing auditory abilities the MMN has been used to predict recovery from coma (Daltrozzo, Wioland, Mutschler, & Kotchoubey, 2007), to study cortical processing in schizophrenia (Leitman, Sehatpour, Higgins, Foxe, Silipo, & Javitt, 2010; Javitt, Steinschneider, Schroeder, & Arezzo, 1996), in Alzheimer's

disease (Javitt, Steinschneider, Schroeder, & Arezzo, 1996) and in Parkinson's disease (Brønnick, Nordby, Larsen, & Aarsland, 2010).

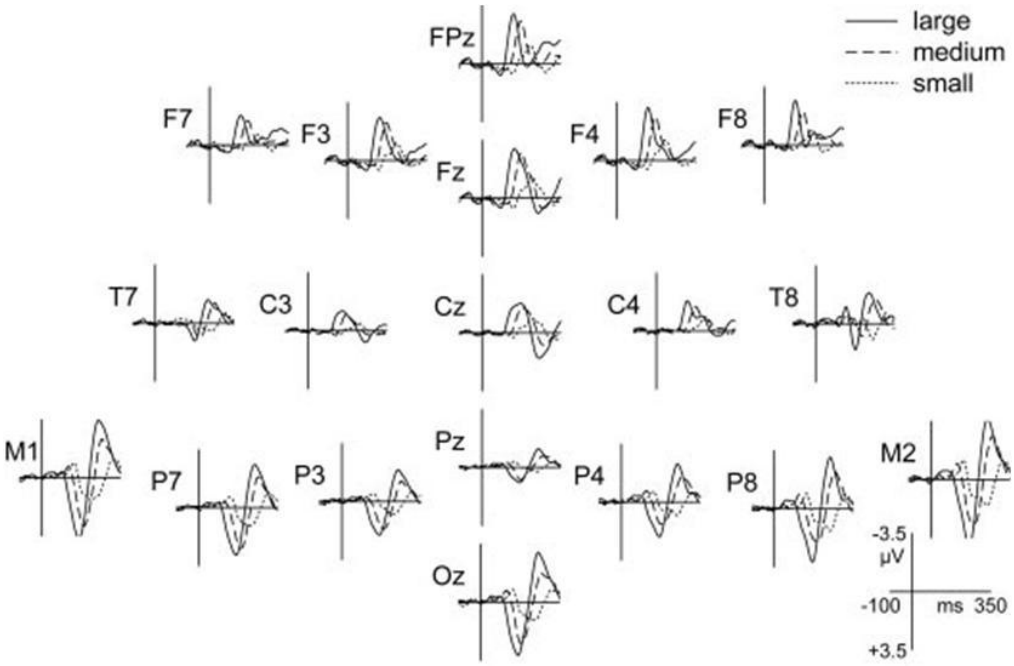

Figure 1. 1. Grand average MMN difference waves (deviant-minus standard) in response to large, medium, and small deviants at different locations across scalp from (Schönwiesner, Novitski, Pakarinen, Carlson, Tervaniemi, & Näätänen, 2007), used with permission.

Models of the MMN

Several models have been proposed to explain aspects of the brain's ability to automatically detect change (Garrido, Kilner, Stephan, & Friston, 2009; May & Tiitinen, 2010). While different models highlight the relevance of different processes, they converge on the importance of short-term mechanisms acting upon, or being driven by, the most recent sensory input. It is debatable whether the MMN response reflects low level mechanisms of sensory adaptation (Butler, 1968; Jääskeläinen, et al., 2004; May & Tiitinen, 2010) or if the response is linked to higher order perceptual processes underlying stimulus discrimination between regular and

deviant sounds (Näätänen, Jacobsen, & Winkler, 2005; Näätänen & Michie, 1979; Näätänen, Paavilainen, Rinne, & Alho, 2007). Initially the enhanced negativity was viewed as the result of fresh neurons coding features in the deviant stimulus that were not present in the standard stimulus (Butler, 1968). The *adaptation model* (Jääskeläinen, et al., 2004) expands this idea further explaining that repetition of the standard eventually engages lateral inhibition and refractory mechanisms in the neural assemblies coding the standard stimulus. Consequently the sensory response (i.e., N1) to the standard is suppressed whereas the sensory response to the deviant activates additional neural assemblies not present in the response to the standard to generate a robust N1. According to this model, the MMN is not considered to be a separate component process but results from subtracting a smaller and perhaps delayed N1 response to standards from the larger N1 response to deviants. The adaptation of neurons generating N1 to standards in conjunction with the fresh afferent N1 response to the deviant serves as a bottom-up mechanism for change detection. This model fails to explain, however, MMN responses in the absence of N1 responses to stimulus omissions (Yabe, Tervaniemi, Reinikainen, & Näätänen, 1997), or the functional separation of these components with NMDA blockers which abolish the MMN but spare the N1 response (Umbricht, Schmid, Koller, Vollenweider, Hell, & Javitt, 2000).

The *model adjustment hypothesis* of the MMN (Winkler, Karmos, & Näätänen, 1996), on the other hand, emphasizes the relationship between the standard and deviant stimuli, rather than the physical attributes of the stimuli. Accordingly, the regular sequence of standard stimuli establishes a pattern or context with which incoming events are compared and therefore involves memory-related processes separate from the afferent process. Evidence for this model comes from the observation that at least 3 to 4 standards must be heard prior to a deviant to evoke the

MMN response suggesting the necessity for a template against which the deviant must be compared (Sams, Alho, & Näätänen, 1993). Also, a pause for 12-15 seconds between stimuli usually results in the loss of this template (Cowan, Winkler, Teder, & Näätänen, 1993). In studies of aging, the MMN response correlates with the duration of auditory sensory-memory traces (Pekkonen, Rinne, Reinikainen, Kujala, Alho, & Näätänen, 1996). As well, the MMN response depends on events stored in long-term memory (Atirnza, Cantero, & Dominguez-Marin, 2002) as demonstrated by paradigms involving violations of complex regularities setup by rhythms (Vuust, et al., 2005), musical sequences (van Zuijen, Simoens, Paavilainen, Näätänen, & Tervaniemi, 2006), or speech segments (Pulvermüller, et al., 2001). Further evidence for the necessity for memory processes for the MMN response comes from studies of humans who have sustained lesions in the memory sensitive regions of the frontal lobe (Alain, Woods, & Knight, 1998; Alho, Woods, Algazi, Knight, & Näätänen, 1998). Such individuals show more disruption to the MMN response than do those with lesions in the medial temporal or parietal regions (Alho, Woods, Algazi, Knight, & Näätänen, 1998). Disruptions of the MMN response also have been associated with Alzheimer's disease (Pekkonen, Jousmaki, Kononen, Reinikainen, & Partanen, 1994).

Unlike the adaptation model, the adjustment model makes no attempt to detail the neurophysiological mechanisms necessary to establish this memory trace or the comparison process, although a temporo-frontal cortical network is implied. Recently the more parsimonious model of *predictive coding* (Garrido, Kilner, Kiebel, Stephan, & Friston, 2007; Garrido, Kilner, Stephan, & Friston, 2009) has been proposed to reconcile the adaptation and adjustment models. Predictive coding is part of a more general theory of perceptual inference that states that our brains are continually drawing inferences from the sensory inputs we receive, taking the neural

signals generated from sensory stimuli (bottom up, data-driven inputs) and fitting them into a repertoire of what we already know (existing top-down models). The mechanism for this process resides in the synaptic connections within the auditory cortex changing in response to the current stimulus (bottom-up) as well as in response to the extrinsic connections linking executive areas in frontal regions to the auditory cortices sources to allow adjustments to the inferences drawn. Specifically, extrinsic connections linking sensory and executive areas reciprocally interact to build and refine interpretations of our experience with forward connections conveying the degree of prediction error resulting from the stimulus experience while backward or feedback connections mediate predictions (Garrido, Kilner, Stephan, & Friston, 2009). The top-down model can be thought of as a matrix of synaptic weights that get enhanced by the matching bottom-up input. In this regard, predictive coding incorporates both adjustments to a top-down model and adaptation due to the increasing precision of predictions. As well it describes more efficient sensory processing accomplished by both feed forward and feedback connections, enabling immediate error correction through dynamic matching of anticipatory intrinsic activity with activity generated by the physical input, in a combined top-down/bottom-up fashion (Engel, Fries, & Singer, 2001). Simulations of the predictive coding model of the MMN in terms of inhibitory and excitatory interactions of dipole sources over time (direct causal modeling) found the best fitting network to be a 3-level hierarchy consisting of both primary auditory cortices, bilateral superior temporal gyri, and the right inferior frontal gyrus (Garrido, Friston, Kiebel, Stephan, Baldeweg, & Kilner, 2008). See Figure 1.2 for a depiction of the MMN network model.

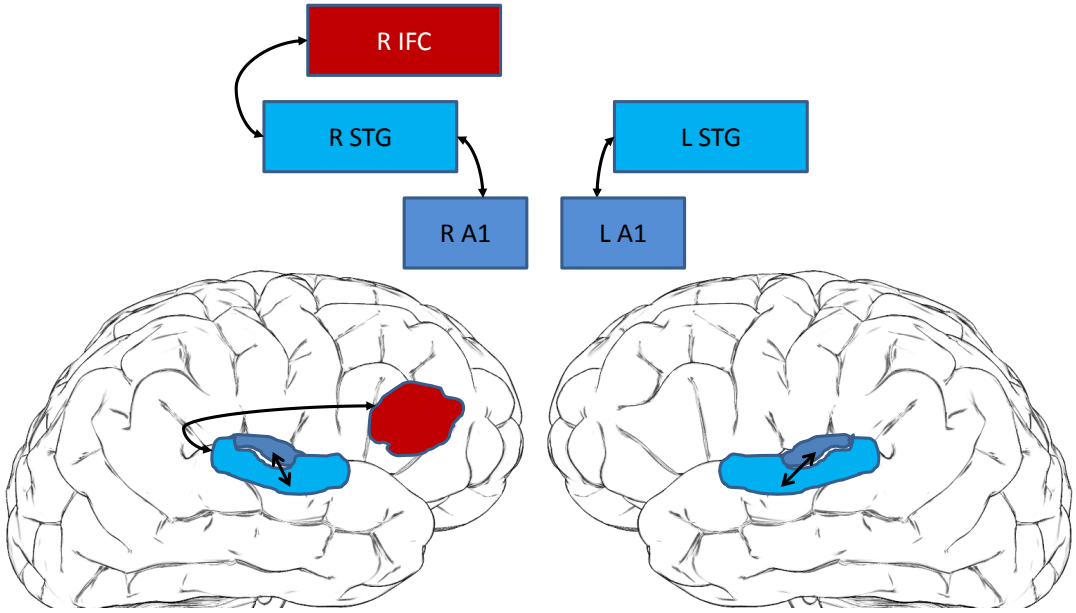

Figure 1. 2. MMN network model as a 3-level hierarchy consisting of both primary auditory (A1) cortices, bilateral superior temporal gyri (STG), and the right inferior frontal cortex (R IFC). Long range (extrinsic) interactions are represented by double ended arrows.

Neural Generators

Shortly after the MMN's discovery, researchers began to suspect that its neural underpinnings involved more than just the auditory cortex (Näätänen & Michie, 1979). Scalp topography and scalp current density studies showed scalp patterns inconsistent with origins solely in sensory cortices, providing tentative evidence for a frontal lobe component (Giard, Perrin, Pernier, & Peronnet, 1990; Alho, 1995; Levänen, Ahonen, Hari, McEvoy, & Sams, 1996; Deouell, Bentin, & Giard, 1998). High density EEG (Jemel, Achenbach, Müller, Röpcke, & Oades, 2002) (Deouell, 2007) and MEG (Kaiser, Lutzenberger, Ackermann, & Birbaumer, 2002) dipole source modeling, fMRI (Molholm, Matinez, Ritter, Javitt, & Foxe, 2005), and combined fMRI/EEG (Opitz, Rinne, Mecklinger, von Cramon, & Schröger, 2002; Schönwiesner, Novitski, Pakarinen, Carlson, Tervaniemi, & Näätänen, 2007) have found activation in the frontal regions in addition

to the auditory portions in the temporal lobes. The localization with fMRI of the frontal generator can include parts of the medial frontal or anterior cingulate cortex (Molholm, Matinez, Ritter, Javitt, & Foxe, 2005), and the caudal or rostral inferior and middle frontal cortex on the right, often accompanied by a strong right superior temporal gyrus (STG) activation (Opitz, Rinne, Mecklinger, von Cramon, & Schröger, 2002; Doeller, Opitz, Mecklinger, Krick, Reith, & Schröger, 2003; Molholm, Matinez, Ritter, Javitt, & Foxe, 2005; Restuccia, Della Marca, Rubino, & Valeriani, 2005; Schönwiesner, Novitski, Pakarinen, Carlson, Tervaniemi, & Näätänen, 2007). The MMN sources can also include the left inferior frontal cortex (Molholm, Matinez, Ritter, Javitt, & Foxe, 2005) with a corresponding left STG activation, or both left and right IFC (Doeller, Opitz, Mecklinger, Krick, Reith, & Schröger, 2003; Rinne, Degerman, & Alho, 2005), and bilateral superior frontal cortex (SFC), (Molholm, Matinez, Ritter, Javitt, & Foxe, 2005). The sources of the MMN may shift depending upon the auditory areas analyzing the deviant acoustic change (Deouell, Bentin, & Giard, 1998). This is not surprising within the sensory cortex where different neuron populations are recruited to respond to the different stimulus features (Giard, et al., 1995). Findings of numerous and variable frontal lobe generators, however, have also been attributed to the varying nature of the stimuli used to elicit the MMN, suggesting feature-specific regions in the frontal cortex (Molholm, Matinez, Ritter, Javitt, & Foxe, 2005). This idea dovetails with previous research that auditory pattern and spatial information are processed in separate ventral and dorsal streams, respectively (Alain, Arnott, Hevenor, Graham, & Grady, 2001; Rauschecker & Tian, 2000)**,** comparable to those in the visual system. In brief, the ventral pathway (also known as the 'what' pathway) originates from the anterior regions of primary auditory areas located in the superior temporal gyrus and projects to the rostral temporal areas, the frontal pole, and the ventral prefrontal region. Auditory

pattern deviants have been shown to activate regions along the ventral pathway (Kaiser, Lutzenberger, Ackermann, & Birbaumer, 2002). The dorsal pathway (also thought of as the 'where' or 'how' or 'action' pathway) originates from the more caudal part of the STG and projects to the dorsal superior temporal sulcus, posterior parietal areas, and dorsal prefrontal regions (Rauschecker & Tian, 2000). Spatial deviants have been shown to activate regions along the dorsal pathway (Tata & Ward, 2005; Levänen, Ahonen, Hari, McEvoy, & Sams, 1996; Kasai, et al., 1999). An alternate explanation for generator variability is that different frontal areas become activated depending on the acoustic stimulus relationship to a specific action program (e.g., speech sounds link to production). The frontal generator's role in distributed neuronal network may be to bind perceptual and action-related information. This notion is consistent with the predictive coding model that sensory processing is accomplished by an interaction of top-down predictive activity with bottom-up stimulus-driven activity. Such interactions could be the means of accomplishing rapid recognition and formulating immediate responses. By evoking predictions for motor output one is able to plan or execute actions and to recognize the actions of others even if they are only heard (Kohler, Keysers, Umilta, Fogassi, Gallese, & Rizzolatti, 2002).

Although there is considerable variability in the number and origin of MMN cortical generators postulated, nevertheless, there is converging evidence for a core set of generators located in the auditory regions of superior temporal gyri and within regions of the prefrontal lobe, and particularly in the right inferior frontal gyrus. Most of the MMN literature has focused on the functional roles of the temporo-frontal network because cortico-cortical connections existing between these areas (Bignall & Imbert, 1969) form a biological basis for maintaining auditory processing for the short term (Romanski & Goldman-Rakic, 2002). Some evidence for

a functional coupling of sensory and executive regions comes from the brain's physical infrastructure. The temporal lobes have long range connections via the superior longitudinal fascicle to the parietal and ultimately the frontal lobes. The uncinate fascicle offers an alternate route although mediated by more limbic regions. See Figure 1.3 for a depiction of these long range fiber tracts using diffusion tensor magnetic resonance imaging (DT-MRI, Makris & Pandya, 2009). Ultimately, there exist auditory sensitive regions in the prefrontal cortex which implies some handling of auditory information received either by way of the auditory cortex, the thalamus, or the parts of the limbic system.

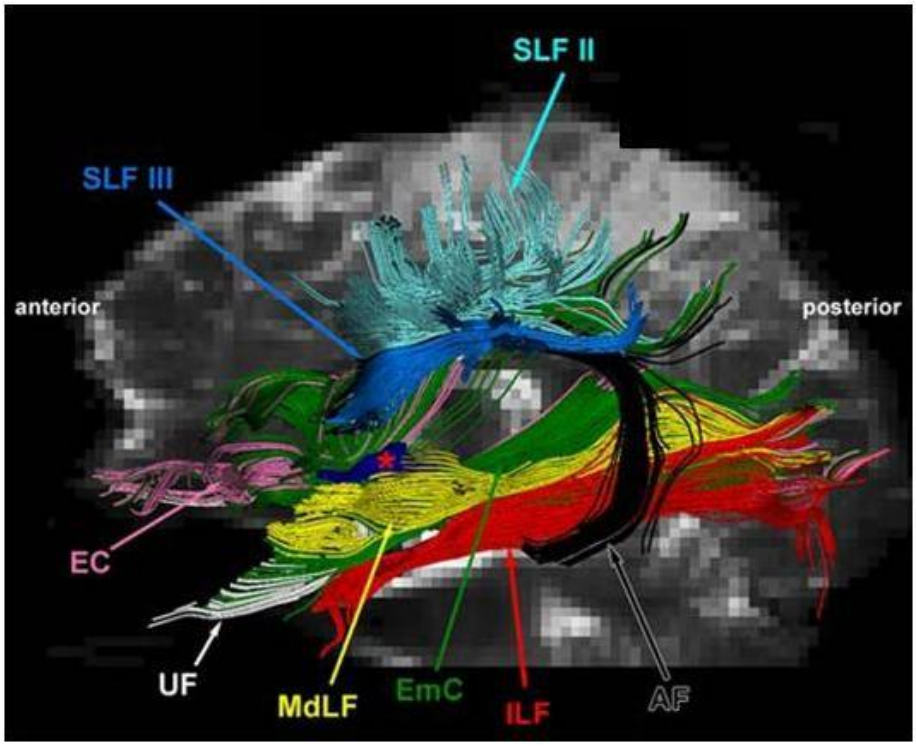

Figure 1. 3. Diffusion tensor based image of fiber tracts connecting cortical areas from (Makris & Pandya, 2009). **AF** arcuate fascicle; **EC** external capsule; **EmC** extreme capsule; **ILF** inferior longitudinal fascicle; **MdLF** middle longitudinal fascicle; **SLF** superior longitudinal fascicles; **UF** uncinate fascicle.

Functional Roles within Temporo-Frontal Network

The frontal and temporal cortical regions are thought to each make distinctive contributions to the change detection process (Näätänen & Michie, 1979; Giard, Perrin, Pernier, & Peronnet, 1990; Garrido, Kilner, Stephan, & Friston, 2009). The temporal generators are believed to perform the initial sensory analysis and transient storage of sensory information, although the asymmetry of bilateral STG activations in many studies suggests that substantial differences exist between generators in the left and right auditory cortices (Pulvermüller & Shtyrov, 2006; Deouell, Bentin, & Giard, 1998; Alho, Woods, Algazi, Knight, & Näätänen, 1998; Giard, et al., 1995; Nääatänen, et al., 1997; Levänen, Ahonen, Hari, McEvoy, & Sams, 1996). The temporal region's sensory analysis role is supported by results of scalp current density analysis of EEG showing that the temporal component is enhanced by stimulation of the contralateral ear (Deouell, Bentin, & Giard, 1998), and attenuated by feature-specific competition where attended and unattended stimuli share the deviant attributes (Shalgi & Deouell, 2007). The generators in the frontal regions are speculated to modulate processing in the temporal regions (Giard, Perrin, Pernier, & Peronnet, 1990; Curtis & D'Esposito, 2003) by exerting top-down control to enhance contrast (Opitz, Rinne, Mecklinger, von Cramon, & Schröger, 2002), switch attention (Giard, Perrin, Pernier, & Peronnet, 1990; Schönwiesner, Novitski, Pakarinen, Carlson, Tervaniemi, & Näätänen, 2007; Shalgi & Deouell, 2007), suppress motor response (Rinne, Degerman, & Alho, 2005), manage attention load (Restuccia, Della Marca, Rubino, & Valeriani, 2005) or to formulate predictions (Garrido, Friston, Kiebel, Stephan, Baldeweg, & Kilner, 2008).

Activation in inferior frontal gyrus (IFG) regions usually occurs after activation in the STG (Rinne, Alho, Ilmoniemi, Virtanen, & Näätänen, 2000; Schönwiesner, Novitski, Pakarinen,

Carlson, Tervaniemi, & Näätänen, 2007; Opitz, Rinne, Mecklinger, von Cramon, & Schröger, 2002; Wolff & Schröger, 2001; for exceptions see Yago, Escera, Alho, & Giard, 2001; Tse & Penney, 2008), but precedes activity in motor preparation areas (Schönwiesner, Novitski, Pakarinen, Carlson, Tervaniemi, & Näätänen, 2007). This pattern is consistent with a recent MEG study (Herdman, Pang, Ressel, Gaetz, & Cheyne, 2007) that found a fast sequence of cortical activations during a word association/word repetition task among these areas. Activity peaked within primary sensory (auditory or visual) cortices between 75 and 130 ms after stimulus onset, within association cortices (inferior temporal gyrus and STG) between 130 and 170 ms, and within inferior frontal and premotor areas between 150 and 240 ms. This fast transition of activity from sensory to association to frontal systems suggests that a rapid feed-forward route exists between sensory and frontal networks. This is consistent with previous findings in the auditory system for a MMN language perception task (Pulvermüller, Shtyrov, & Ilmoniemi, 2005) that have shown that the timing of early evoked activity from sensory-to-frontal systems during verb generation and repeat-aloud tasks occurs within 250 ms. These early EEG component differences in frontal regions might reflect the allocation of top-down resources to processing of low-level perceptions, which are projected to the premotor areas early in preparation for language production. These findings suggest that a feed-forward, modality unspecific, sensory-to-motor processing stream exists within the MMN neural network, at least for expressive language tasks. In contrast, others examining the timing of the MMN generators have reported a frontal component that preceded the temporal cortex component, suggesting that top-down mechanisms could act to modulate the processing of bottom-up information in different ways in order to maximize performance on the task at hand (Yago, Escera, Alho, &

Giard, 2001). In Friston's predictive coding model, prediction errors are resolved through top-down and bottom-up interactions suggesting that feedback and feed forward are concurrent.

Although communication between specialized processing centres is anatomically supported, the exact mechanisms of how neural assemblies within and between regional processing centres interact remains poorly understood. Little is known about the coordinated effort of various cortical regions in the perceptual process or about the mechanism through which information is exchanged between these near and/or distant areas to ultimately achieve perception, action, and cognition. In the following section I discuss neural synchronization as one promising mechanism (Varela, Lachaux, Rodriguez, & Martinerie, 2001) to achieve this end.

Neural Synchronization

Studies employing both near field and far field recordings in animals and humans have shown that oscillatory neural activity along narrow frequency bands is often maintained in a fixed phase relationship (synchrony) between task relevant brain regions (Sirota, Montgomery, Fujisawa, Isomura, Zugaro, & Buzsáki, 2008; Gray & Singer, 1989; Womelsdorf, et al., 2007; Fries, Womeldorf, Oostenveld, & Desimone, 2008; Sederberg, et al., 2007). It appears from these studies that synchronous neural activity is not mere chance coincidence or epiphenomenon but itself serves to modulate the effectiveness of synaptic transmission. The synchronous arrival of excitatory neural inputs imparts a more depolarizing effect on the post synaptic cells than do inputs arriving asynchronously (Fries, 2005). For example, a pyramidal neuron on the brink of firing an action potential will reach threshold more quickly if the excitatory post-synaptic potentials (EPSPs) arrive within a short time period to summate, typically within a time window of 10-30 ms (Buszaki, 2006). Similarly, the timing of inhibitory inputs can regulate when an action potential is fired; a synchronous group of inhibitory post-synaptic potentials (IPSPs) can

delay an action potential whereas asynchronous IPSPs are less likely to do so. The coordination of excitatory and inhibitory inputs by pyramidal neurons and interneuron serves to bring about and maintain synchronous oscillations (Buszaki, 2006). In brief, the interneurons are driven by excitatory input they receive from nearby pyramidal cells. The interneurons in turn provide inhibitory inputs back to these very pyramidal cells, constraining the time interval for subsequent firing. Ultimately, neurons oscillating within narrow frequency ranges can therefore receive and send signals within a critical window for a higher probability of affecting output on downstream target neurons (Salinas & Sejnowski, 2001). In addition, synchronous activity along different frequency bandwidths could be a means to transiently include or remove their participation within particular cell assemblies, therefore changing the nature of neural computations carried out from moment to moment. These rapidly changing network interactions may be a means to encode and retrieve relevant information for immediate use (Engel A. K., Fries, Koenig, Brecht, & Singer, 1999).

Within the auditory modality synchronous oscillations have been associated with a number of integrative functions such as the binding of pitch, timbre, and harmony features (Bhattacharya, Petsche, & Pereda, 2001), representing objects (Kaiser, Lutzenberger, Ackermann, & Birbaumer, 2002) and matching of acoustic cues to representations in long term memory (Lenz, Schadow, Thaerig, Busch, & Herrmann, 2007) and also with the operation of selective attention in the auditory cortex (Debener, Hermann, Kranczioch, Gembris, & Engel, 2003; Tiitinen, Sinkkonen, Reinikainen, Alho, Lavikainen, & Näätänen, 1993).

Early work in audition found local synchrony in the form of increased gamma-band power to be correlated with selective attention but not with changes in stimulus features (Tiitinen, May, & Näätänen, 1997). While important advances have been made with regard to

the functional significance of neural synchronization in the auditory system, very little attention has been given to investigating the role of neural synchrony in the MMN temporo-frontal network. What little evidence there is, however, indicates that such studies could be very informative about the mechanisms through which the MMN is generated in the brain, particularly concerning the roles of the various cortical regions in the process, and the nature and function of communication between these functionally specific brain regions.

Passive auditory change detection and auditory working memory have consistently yielded gamma-band spectral power (>30 Hz) increases at MEG sensors over anterior temporal/inferior frontal areas during auditory pattern processing (Kaiser, Lutzenberger, Ackermann, & Birbaumer, 2002) and over posterior temporo-parietal cortex during auditory spatial processing (Leiberg, Lutzenberger, & Kaiser, 2006). The interpretation of these results was that gamma-band activity (GBA) reflected post-change-detection processing of changed stimulus features in regions related to pattern or spatial processing but was not related to the change detection process itself. In a novelty-oddball task where subjects were instructed to respond to some changes (particular targets) but not others (novelty sounds), GBA was enhanced relative to standards only for targets, implicating a role for attention but not change detection (Debener, Hermann, Kranczioch, Gembris, & Engel, 2003). Similarly, GBA has been associated with top-down processing in a more recent study where increased gamma-band power was found post-omission during a count task of silences occurring randomly in a rhythmic auditory sequence (Gurtubay, Alegre, Valencia, & Artieda, 2006).

The various proposed functions for GBA can be unified under the match-and-utilization model (MUM, Hermann, Munk, & Engel, 2004). Early stimulus-locked GBA (i.e., evoked gamma) in active oddball paradigms is believed to reflect the comparison of memory contents

with stimulus-related information whereas later non-stimulus-locked GBA (i.e., induced gamma) is thought to reflect the utilization of signals derived from this comparison (Debener, Hermann, Kranczioch, Gembris, & Engel, 2003). However, later revisions of this model have eased these latency distinctions to accommodate the occurrence of sensory-motor interactions, allowing that evoked GBA may also reflect aspects of utilization and induced GBA may also reflect memory matches (Herrmann, Fründ, & Lenz, 2010). In keeping with this model, increased GBA was associated with successful sound matching to representations in long-term memory in a task where subjects classified environmental sounds as 'recognized' or 'unrecognized', with significantly stronger GBA occurring about 300 to 500 ms after familiar stimuli (Lenz, Schadow, Thaerig, Busch, & Herrmann, 2007). Compared to novel sounds, familiar sounds produced enhanced GBA, thus reflecting successful sound matching to representations in long-term memory.

A few recent auditory studies examining the oscillatory character of human brain network interactions have moved beyond measures of spectral power to measure the predictive value of spectral activity in one region for activity in other regions using a spectral cross correlation statistic known as coherence. In one study, subjects uttered a sound as they heard it played back with or without a pitch shift. Increased gamma-band coherence was found between EEG sensors over the frontal and temporal regions when what was spoken coincided with what was expected to be heard (no pitch shift), whereas decreased coherence occurred for pitch shifted voices (Ford, Gray, Faustman, Heinks, & Mathalon, 2005). These results suggest that interactions, as indexed by gamma-band coherence, between the frontal and temporal regions are involved in binding expectation with experience very similarly to what is predicted for GBA by the MUM matching memory contents with sensory input. These findings provide preliminary evidence for how GBA

might function within the temporo-frontal network of the MMN. Because oscillatory coherence between scalp sensors is in part the result of volume conduction mixing proximal and distal EEG source signals, there is considerable ambiguity regarding the neural origins of synchronization measured between electrodes. Further studies are therefore required to examine the oscillatory interactions taking place at the level of the neural sources of the MMN. Thus, the main reason for conducting the current series of studies is to provide a demonstration of neural synchronization between temporal and frontal brain sources (not sensors) and thereby provide stronger evidence of a functional network underlying the MMN.

Research Question

If the MMN is generated by temporo-frontal network interactions that match predictions about present auditory experience with sensory activity generated by the current physical input, and if increased GBA is a measure of a sensory input match to existing memory representations (match-utilization model, MUM), GBA in one region of the temporo-frontal network should predict activity in another depending on whether the current stimulus is a standard or a deviant. The research program presented here has two overarching aims:

1) To establish, for the first time, a functional relationship between temporal and frontal brain sources active during the generation of MMN by demonstrating synchronous phase activity of the respective time series between dipole sources (as opposed to between sensors).

2) To explore the effect of other top-down processes known to enhance GBA such as selective attention (Fries, Reynolds, Rorie, & Desimone, 2001), and long term memory (Lenz, Schadow, Thaerig, Busch, & Herrmann, 2007) on the generators of the MMN and their network interactions.

Hypothesis I

(a) If increased GBA reflects the successful match of predictions with auditory experience, then we expect the frequently occurring and hence more predictable standard stimulus to generate increased GBA within the MMN generators than will the infrequent deviant stimulus during passive listening (i.e., when no task is associated with change detection).

(b) If the matching process requires the interaction of the temporal and frontal generators, then we expect GBA to be accompanied by long-range synchronization between these generators.

Hypothesis II

(a) If long term memory and attention enhance the match-to-memory gamma activity, then in target detection tasks where the deviant is the target we expect the deviant stimulus to generate more GBA in the MMN generators than will the standard stimulus.

(b) If the matching process requires the interaction of the temporal and frontal generators, then we expect GBA to be accompanied by long range synchronization between these generators and possibly others related to selective attention.

Significance

Real biological data that demonstrate the functional relationships between active brain sources in the temporal and frontal cortices are necessary for a network model of the MMN to be accepted as a viable explanation for how the human brain operates during auditory change detection. Such a demonstration lays the ground work for objectively assessing auditory processing necessary for both simple and complex auditory discrimination.

CHAPTER 2: ICA REVEALS DRIVING NEURAL SOURCES OF MMN

Introduction

To formulate a brain model of the MMN response it is necessary to determine both the spatial and temporal character of its neural activity. Currently there is no single noninvasive approach that provides this information simultaneously. Combining EEG/MEG and fMRI to reveal the spatiotemporal character of neural sources is one approach that has been untaken to address the limitations inherent in each technique alone; however, the assumption that these measures track similar neural events has been questioned (Ritter & Villringer, 2006). It is worthwhile then to explore ways to improve the spatial resolution of the EEG data alone, and one promising technique is to decompose the EEG data into independent components (ICs) using independent component analysis (ICA, a blind source separation method) prior to any dipole fitting procedure (Makeig, et al., 1999). ICA is a strictly mathematical approach to data analysis, used in a variety of disciplines to separate signal mixtures into a set of statistically independent signals (Stone, 2004). Since the data collected from surface electrodes are recognized as a linear mixture of electrical activity, from both neural and non-neural sources, ICA is an appropriate application for EEG analysis (Onton, Westerfield, Townsend, & Makeig, 2006). Indeed, ICA decompositions have been employed as a method of artifact rejection where irrelevant physiological activities originating from ocular, muscular, and cardiac activity, as well as electrical interference (line noise), are separated into ICs, based on the characteristics of their activity time courses, scalp maps, power spectra, and dipole locations (Viola, Thorne, Edmonds, Schneider, Eichele, & Debener, 2009). Separating these artifactual ICs from the ICs related to brain activity increases the signal-to-noise ratio of the experimental data. Recently, this analysis approach has been

applied to MMN data and was found to better identify the MMN response at the scalp than the classic difference wave procedure (Kalyakinai, Gonzálezb, & Kärkkäi, 2008).

Because ICA renders the scalp data into a format where separate electrical activities can be identified and evaluated based on their time locked activity (event-related potentials, ERPs), spectra, scalp maps, and dipole locations, we reasoned that ICA could be used to identify the unique contributions of the temporal and frontal regions to the MMN. The advantage of the ICA approach is that it does not limit the neural source analysis to just these specific parts of the brain (as no prior assumptions are needed regarding the number of active neural sources) so that other anatomically and physiologically distinct regions can also be evaluated. To determine which ICs are task relevant, plots can be generated showing IC contributions projected back to the scalp average ERP at specified latencies. Recently, EEG data from an oddball task were decomposed into six independent components that accounted for more than 67% of signal variance in the MMN time window of 100 - 300 ms. The corresponding sources associated with these ICs using low-resolution tomography (LORETA) included bilateral STG and right IFG but also the anterior and central medial frontal regions, and the right inferior parietal lobule (IPL)(Marco-Pallares, Grau, & Ruffini, 2005). Unfortunately in this latter study the unique contributions of the temporal and frontal MMN generators could not be evaluated separately as these three were not decomposed as separate ICs but folded into a single IC with three dipoles. This seems inconsistent with one of the principles of ICA, which is to identify ICs that arise from single neural source. The three-dipole IC likely resulted at least partially from the limited number of electrodes employed (i.e., 30 channels yield a maximum of 30 ICs, of which a substantial subset will be related to non-cephalic or artifactual sources) and from applying ICA to a limited dataset

of averaged data, specifically 1800 concatenated difference waves derived by subtracting ERPs to deviants from the grand mean ERP to the standards.

In the present study we employed a 64-channel recording and used a temporal algorithm to decompose the continuous EEG records (approximately one hour of continuous data for each of 10 subjects), including all standards and deviants, into ICs with single dipole sources. We then analyzed IC activity based on approximately 22,000 epochs, 11,000 each for standards and deviants. As the responses to repeated stimuli have a regular time structure, it is a reasonable approach to apply an ICA algorithm that uses the temporal structure of the data (e.g., extended infomax). We predicted that several distinct relevant brain regions would emerge after applying cluster analysis (to group similar ICs from separate subjects). As a fronto-temporal network is thought to contribute to the scalp MMN, the clusters in the right PFC and the bilateral STG were predicted to display significantly different ERPs for the standard and deviant conditions within the latency of the MMN, 120-250 ms. Moreover, these three regions were predicted to be the major contributors to the scalp grand mean ERP, together accounting for the majority of the variance in that ERP when compared to ICs in other brain regions. On the basis of previous studies mentioned above we thought it likely that the temporal sources would account for most variance in the scalp MMN. As this comparison had not been undertaken before, however, it was difficult to predict the relative contribution of the frontal source.

Materials and Methods

Participants

Twelve right-handed volunteers (5 men) attending UBC, aged 18-33 years (mean age 24, SD 4.5 years), were paid to participate. All provided written consent. The experiment was approved by the Behavioural Research Ethics Board of the University of British Columbia. All participants

were assessed by clinical audiometry and found to have hearing within normal range at the time of the EEG acquisition. No history of neurological disorders was reported during a prescreening interview. Data from two men were excluded from the analysis, one for possible history of seizure (reported casually during EEG acquisition) and the other for excessive artifact. All participants had strong right-hand preferences as measured with the Edinburgh Handedness Inventory (Oldfield, 1971).

Stimuli and Procedure

The oddball paradigm was adapted from a previous study (Deouell, Bentin, & Giard, 1998) in which bilateral STG sources and IFG sinks were inferred from scalp current density analysis. Volunteers were instructed to watch a silent video with closed captioning and to ignore the sounds heard through insert earphones. The paradigm consisted of three 20-minute blocks with short breaks (self paced, ~1-5 minutes) between blocks. Each trial (n = 2,400 per block) consisted of two pure tones differing in frequency presented to each ear separately but simultaneously (dichotic presentation). A standard tone pair and two deviant tone pairs characterized the stimuli presented in each block. See Table 2.1 for the types and probabilities of stimuli in each block.

Table 2.1. Types and probability of dichotic stimuli with each block.

	Frequencies (Hz)		
p	Block 1	Block 2	Block 3
.86	660, 932	932, 660	740, 932
.07	740, 932	932, 740	660, 932
.07	660, 830	830, 740	932, 740

Note: tone pairs within each block represent the left and right ear stimuli respectively

Standard dichotic trials occurred most frequently (86% of the time) while deviant trials, of which there were two types (7% each) made up the remaining trials. Standards and deviants occurred in a pseudo-random order, different for each block and subject, according to the listed proportions. Deviant tone pairs were created by changing the tones in the standard dichotic pair, either in the left or right ear alone or in both ears simultaneously. All stimuli were 100 ms in duration and delivered through insert earphones (E.A.R. 3A) at an intensity of 65 dB SPL. ISI was fixed at 500 ms. Block presentation was counter-balanced in this experiment to control for order effects.

EEG Recording

All EEG recordings were acquired in a sound attenuated chamber. Data were collected from 60 scalp electrodes mounted in a standard electrode cap (Electrocap, Inc.) at locations based on an International 10-10 System, and from four periocular electrodes placed above and below the right eye and at the right and left outer canthi. During recording all scalp channels were referenced to the right mastoid with ground at AFz. Data were sampled at 500 Hz through an analog pass band of 0.01-100 Hz (SA Instrumentation, San Diego, CA). Electrode impedance was kept below 20kΩ for all scalp electrodes (sufficient because SA amplifier input impedance was greater than 2 gΩ). Prior to analysis, all signals were re-referenced to an average reference to give equal weight to each electrode, then resampled to 250 Hz, and digitally high-pass filtered at 1 Hz. The continuous EEG data were analyzed with EEGLAB software (Delorme & Makeig, 2004), an open source MATLAB (Mathworks, Natick, USA) toolbox available at http://sccn.ucsd.edu/eeglab. EEG data contaminated by sources of artifacts (blinks, eye movements, muscle tension artifacts, and infrequent single-channel noise) were not rejected prior

to analysis as these spatially stationary artifacts could be separated from other EEG processes using ICA as described below.

ICA Decomposition

The ICA decomposition procedure consisted of the following consecutive steps which are described in more detail below: (1) decomposition of the continuous 64-channel EEG (64 channels reduces to 63 channel with averaged reference) into 63 ICs for each participant, (2) selection and localization in brain space of the valid ICs, (3) dividing the continuous record of each IC into epochs based on whether the stimulus was a standard or a deviant, (4) cluster analysis of valid ICs, (5) evaluation of cluster ERPs for MMN-like characteristics, and (6) projection of selected ICs back to the scalp ERPs to determine their contributions (as indexed by the percentage of variance accounted for, PVAF) to the MMN response at the scalp.

1) Decomposition of the continuous EEG into ICs was done separately for each participant. A problem often faced when using averaged EEG data is that there are not enough conditions in the training set to obtain stable ICs. Another problem with using averaged EEG data is that the averaging process may cancel out the activity of many brain sources. To address these problems we decomposed the single trial continuous data with extended infomax ICA directly – not the concatenated data epochs nor their averages. Continuous data provide ample observations, required by ICA, to separate two or more independent neural processes. We used the EEGLAB *runica* algorithm, which is based on the infomax neural network algorithm (Bell & Sejnowski, 1995), an algorithm that exploits temporal independence to perform blind separation. The 63-channel EEG data were transformed into 63 independent components by multiplying the matrix array of channel data (**X**, 63 channels by time points), by a square scalar matrix of unmixing coefficients, called the weight matrix, **W**. These unmixing coefficients were derived by

obtaining the inner product that yielded 63 non-Gaussian activity sources that were as nearly perpendicular to one another as possible when plotted relative to one another (so to create a maximally independent relationship) (Delorme & Makeig, 2004). Multiplying **X** by **W** gives the matrix **U**, or 63 ICs decomposed from the raw data matrix. See below for an example using just 2 channels decomposed into just two ICs.

$$\begin{pmatrix} u^1_1, u^2_1, \ldots, u^N_1 \\ u^1_2, u^2_2, \ldots, u^N_2 \end{pmatrix} = \begin{pmatrix} \alpha,\beta \\ \gamma,\delta \end{pmatrix} \begin{pmatrix} x^1_1, x^2_1, \ldots, x^N_1 \\ x^1_2, x^2_2, \ldots, x^N_2 \end{pmatrix}$$ where α, β, γ, δ are the unmixing coefficients

$$= (\mathbf{w}_1, \mathbf{w}_2)^T (\mathbf{X_1}, \mathbf{X_2})^T$$

$$\mathbf{U} = \mathbf{WX}$$

2) Selection and localization of valid ICs. Once the ICs were calculated, a scalp map for each IC was computed from the inverse weight matrix, W^{-1} (see Fig 2.1.), giving the relative magnitude and polarity of the IC contribution at each electrode. This scalp map was then compared with the forward solutions for various single equivalent dipoles. The digitized 3-D locations of the electrodes on the scalp were first co-registered with the Montreal Neurological Institute (MNI) average brain. IC sources were then localized with the Dipfit2 algorithm in EEGLAB using a standard boundary element model. Dipfit2 is a BESA derivative in which the location and orientation of an equivalent dipolar source for a given scalp potential distribution is estimated by a gradient descent method. Only ICs with scalp maps having an inverse solution for a single dipole source within Talairach (MRI) space (within the brain) of less than 15% residual variance (RV) were included in the subsequent analyses. Those sourced outside the head were rejected as artifactual. Figure 2.1 demonstrates how each independent component is made up of the time course of its activity during the continuous EEG recording and a scalp map giving the relative weight of the component at each electrode. The IC activations (U), can be regarded as the EEG waveforms of single sources however actual amplitudes at the scalp channels requires

multiplication by the inverse of the unmixing matrix because the original activity units (μV) and polarities (+/-) are distributed between the two IC factors—the IC scalp map and activation time series. For this reason scalp maps do not have absolute amplitudes so the scale in Figure 2.1 has no units.

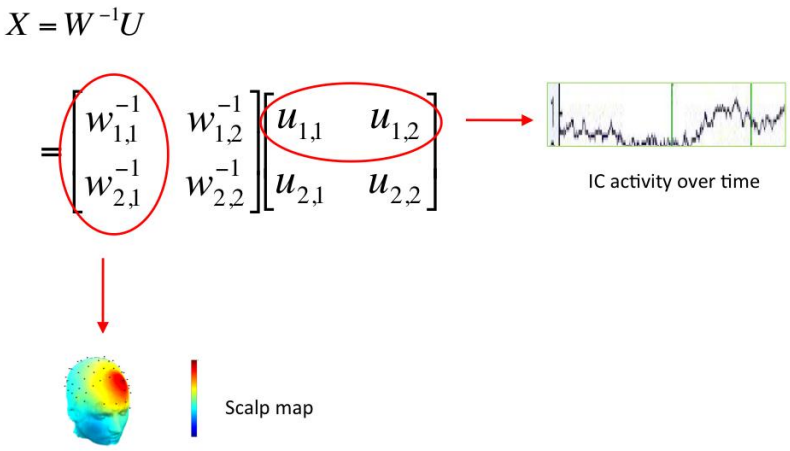

Figure 2. 1. IC scalp map and activations for 2-channel system

3) The continuous record composed of the summed valid ICs was then divided into two groups of epochs, one for standard trials and one for deviant trials. An epoch from -100 ms to +450 ms stimulus onset was considered to be the epoch of interest for the present experiment.

4) To determine which neural sources were common for all subjects, a broad cluster analysis of all valid ICs (dipole fit within the head of RV < 15%) was performed based on the IC scalp maps, dipole locations, and IC event-related activity (ERPs). Because the physiological characteristics of the neural sources are thought to be related to their functions, the occurrence of discrete clusters would indicate the existence of distinct generators. A total of 208 ICs for the 10 subjects were separated into 11 clusters by applying the *k*-means algorithm of EEGLAB. This algorithm attempts to find the centers of natural clusters in the data by minimizing the total intra-cluster variance, or the squared error function. A drawback of the algorithm is that it has to be

told the number of clusters (i.e. *k*) to find. As discussed earlier, the MMN is thought to have multiple generators, including those in the auditory cortex (bilaterally or unilaterally), the inferior prefrontal cortex (bilaterally or unilaterally), and possibly in the anterior cingulate and inferior parietal cortex. Additionally, the visual and motor cortices also should be active during the task as volunteers watched a video. We therefore felt that at least 10-12 significant neural generators might be found. Following the cluster analysis all ICs contained in the clusters will be back-projected to the scalp and compared to the original grand average scalp waveforms. The purpose is to show the validity of the ICs we retained do reflect the actual scalp response. Back-projections are computed by multiplying the components by the inverse of the unmixing matrix.

5) Cluster ERPs will be deemed to have MMN-like characteristics if a significant difference lasting several milliseconds between standard and deviant conditions appears within the time range of 120-250 ms post stimulus onset.

6) The percentage of variance accounted for (PVAF) compares the variance of the channel data minus the back-projected component to the variance of the channel data alone. For an extreme example, if the variance of one component accounted for all the variance in the channel data, the channel data variance minus the component back-projection variance would be zero, and PVAF would be 100%; or alternatively if the component has zero variance, it accounts for none of the data variance and the PVAF would equal 0%.

Results

Scalp ERP Analysis

The amplitudes of the scalp ERPs over 0-250 ms showed no differences among various deviant conditions, i.e. the waveforms obtained for Deviant 1 and Deviant 2 in each block were not significantly different from each other within a block or between blocks. Our findings replicate

previous finding with this same paradigm (Deouell, Bentin, & Giard, 1998) that no difference between the deviant conditions were found when hearing with the left, right or both ears. All deviant trials were thus combined into a single deviant condition (totaling ~1000 trials) for each subject. Similarly, no significant differences in ERP amplitudes were found for the various standard conditions between blocks 1, 2 and 3, so these blocks were combined. To reduce the number of trials in the standard condition so as to make for comparable signal to noise ratios with the deviant condition, only the last standard to precede each deviant was selected.

Selected electrode sites where chosen to the display the grand ERP (see Figures 2.2 A) showing prominent frontal negativity that attenuates and inverts at temporal and posterior sites. The Deviant and Standard conditions did not significantly differ to the early sensory response P1. The grand mean ERPs showed a significant negativity to the deviant tone relative to the standard tone between 100 and 200 ms at Fz and Cz electrode sites (paired *t*-test, $t(9)= 3.25$, $p < 0.01$). Subtracting the ERP for standard tones from that for deviant tones gives a difference wave that shows a clear MMN response that is maximal at frontal midline electrodes (prominent at Fz and Cz). The peak amplitude of the MMN at Fz is -0.8 μV at 172ms. The Deviant condition shows a significant positivity relative to the Standard condition at Fz and Cz between 200 ms and 400 ms (at Fz), peaking at 250 ms. This positive difference represents a P300-type response to the deviant (oddball) that is absent to the standard. The time course implies that this is a P3f component and this conclusion is supported by its localization in the orbital frontal cortex (Delorme, Westerfield, & Makeig, 2007).

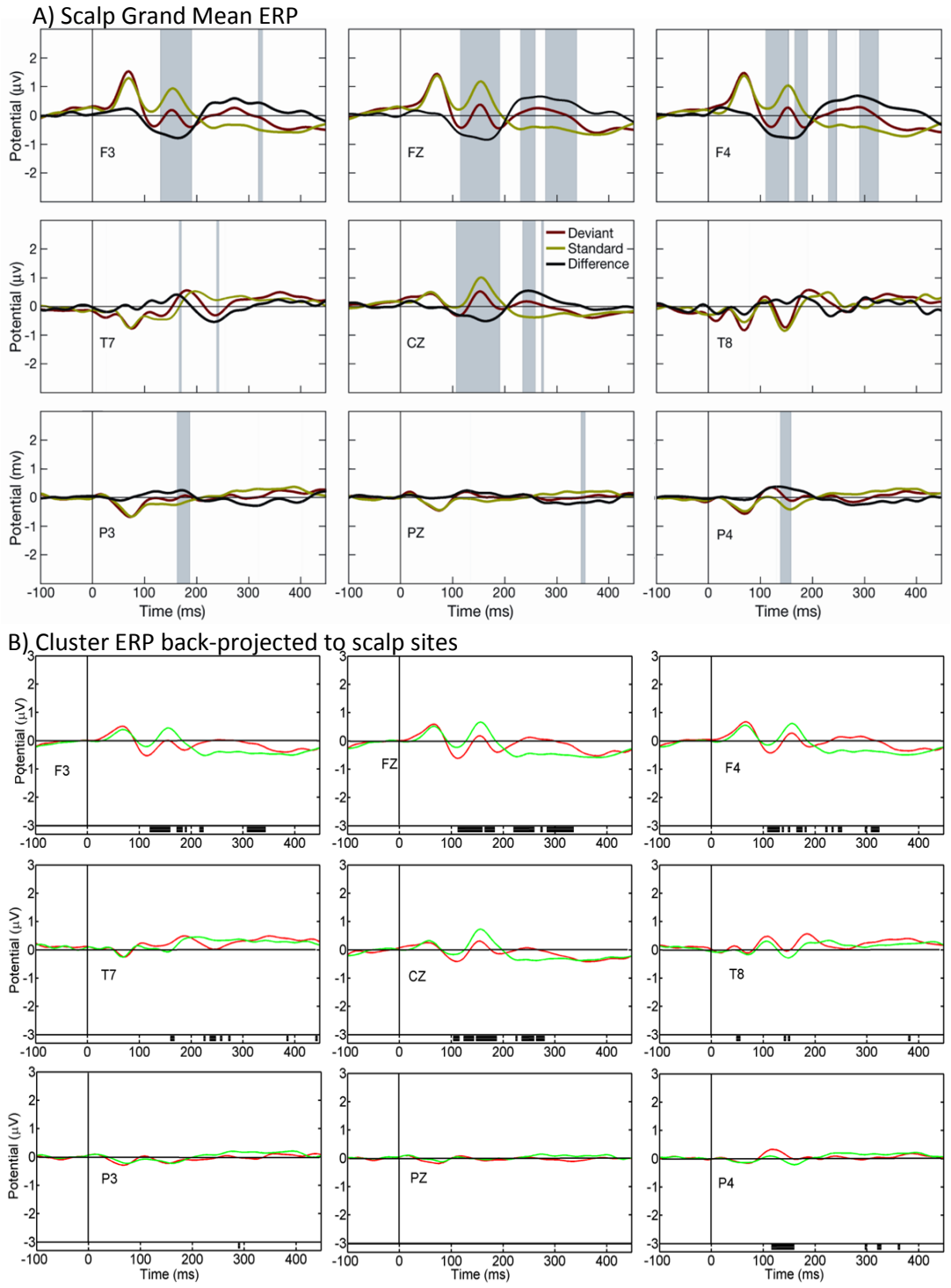

Figure 2. 2. Comparison of grand mean ERP for scalp data (A) and clustered ICs back-projected to the scalp (B) at selected electrodes from -100 to 450 ms. Stimulus onset is at 0 ms. Difference wave with negativity prominent from 120 to 200 ms is MMN response. In (A) shaded regions are significantly different (paired *t*-test, t(9) = 3.25, $p < 0.01$) which are comparable with significantly different regions in (B) represented as dark bars along time line ($p < 0.01$ by permutations). Back-projected waveforms resemble grand mean albeit with reduced amplitude.

Analysis of Independent Component Clusters

Of the 63 ICs decomposed from the 63 channel data for each subject only about a third met our criteria for inclusion in the cluster analysis. Despite this, the back-projected data from all the clustered ICs (n=208) produced comparable waveforms to the grand average scalp data for the deviant and standard conditions, albeit with slightly reduced amplitudes (see Figure 2.2A and B for the comparison). Significant differences between the back-projected ERP (by permutations, $p < .01$) mapped onto similar latency regions that were significantly different between conditions for grand average ERP regions (paired *t*-test, $t(9) = 3.25$, $p < 0.01$). These results validate to a large extent our selection criteria for valid IC.

As expected there was individual variation in the localization of the dipoles from the individual ICs. To group similar ICs across subjects, we performed a cluster analysis based on similarities in the IC event-related activity (0 – 250 ms), scalp map, and dipole location. Setting $k = 11$ clusters yielded clusters with a 3-D spread of less than 2 cm in MRI space to which most subjects contributed. Smaller numbers of clusters (e.g., ≤10 clusters) yielded a larger spread of dipoles with nearly all subjects contributing whereas a larger number of clusters (e.g., ≥12 clusters) yielded a smaller spread of dipoles but with only a small subset of subjects contributing. Eleven clusters struck a balance between the two extremes, so that we were able to characterize the regional sources within which most subjects had a localized IC. Table 2.2 shows a summary of cluster properties. The cluster brain region was determined from the cluster scalp map (see Figure 2.3 A) as the best fit for a single dipole forward model. Each scalp map reflects the mean of all inverse IC weights associated with each cluster. Regional localization represents the nearest grey matter to the Talairach coordinates of the cluster centroid and not necessarily the location of each IC dipole contributing to the cluster.

Regions of Interest (ROI) for the MMN

Clusters in the temporal regions as well as clusters with event related activity significantly different between the Deviant and Standard conditions from 120 -200 ms (see Figure 2.3 B for ERP of each cluster, and Table 2.2. for significance differences falling in MMN period as determined by the scalp grand ERPs) were examined in detail.

Table 2.2. Cluster properties. ROI for the MMN in bold.

Cluster Brain Region*	% of Subjects Contributing	BA	Talairach x, y, z	RV % dipole fit	MMN 120-200 ms $p < .05$
R STG	**70**	**42**	**67, -25, 7**	**10.33**	**-**
L MFG	90	9	-50, 14, 26	11.07	-
L STG	**60**	**42**	**-71, -24, 5**	**10.35**	**190-230**
L SPL	80	5	-16, -40, 47	6.71	-
L MOG	100	19	-36, -72 ,8	9.15	-
FOG	**100**	**11**	**0, 33, -24**	**10.14**	**120-185**
L CT	60	NA	-20, -48, -41	11.35	-
R IFG	70	46	52, 42, 8	11.53	-
R TPJ	**90**	**WM**	**27, -59, 23**	**7.96**	**120-150**
R LG	70	18	9, -91, -14	6.92	-
R MFG	100	6	23, 2, 40	8.05	-

BA Brodmann Area; **CT** cerebellar tonsil, **FOG** frontal orbital gyrus; **IFG** inferior frontal gyrus; **IC** independent component; **L** left; **LG** lingual gyrus; **MFG** middle frontal gyrus; **MMN** mismatch negativity; **MOG** middle occipital gyrus, **NA** not applicable, **R** right; **RV** residual variance; **SD** standard deviation, **SPL** superior parietal lobule; **STG** superior temporal gyrus, **TPJ** temporo parietal junction, **WM** white matter; $p < 0.05$ by permutations. * Regional locations based on centroid mean, not all ICs within a cluster fall within a region.

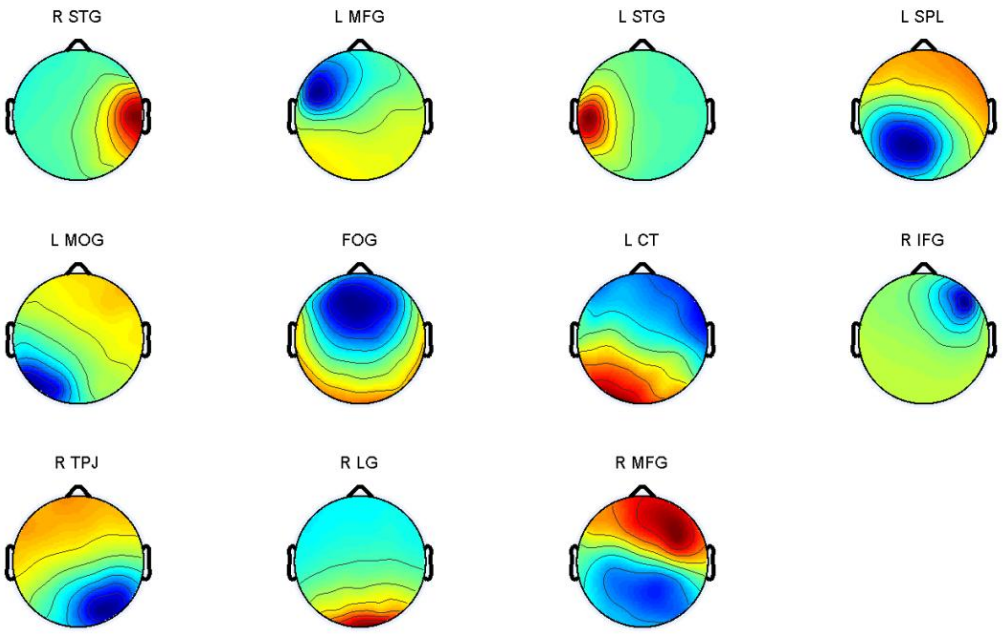

Figure 2. 3. Average scalp maps for clustered ICs with best single dipole fit region indicated above each map.

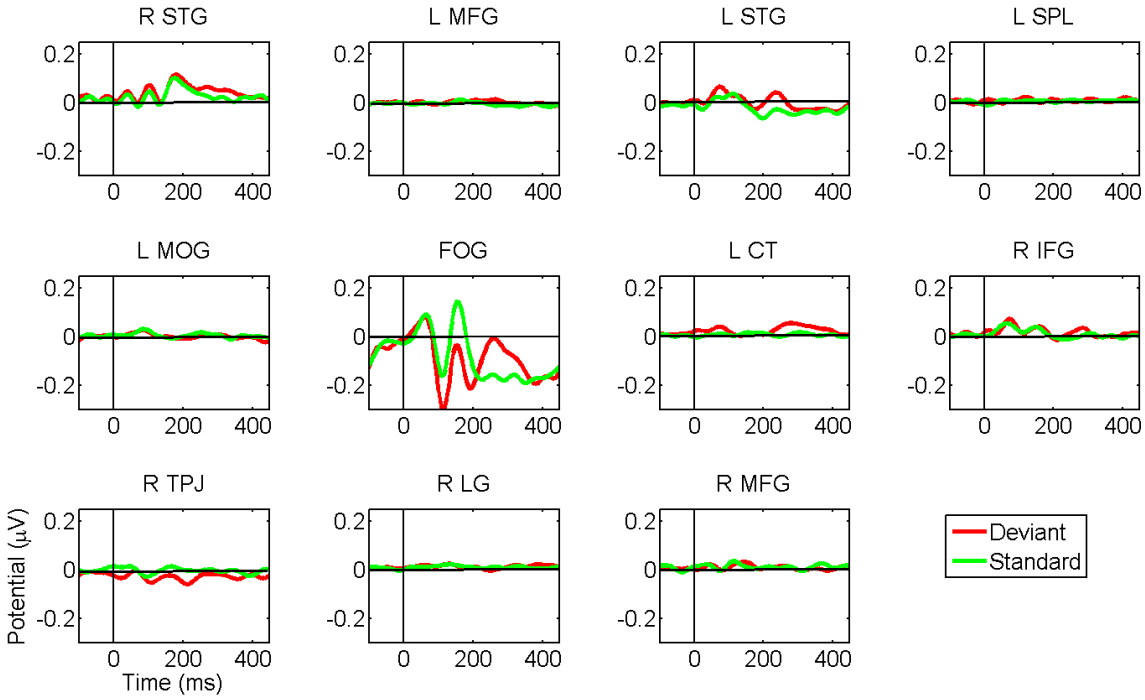

Figure 2. 4. Grand mean component cluster ERP. Only L STG, FOG, and R TPJ are significant differences (by permutation, p <.05) falling within the MMN period (120-200 ms) at the scalp.

Frontal Orbital Gyrus Cluster

Ten subjects contributed a total of 23 ICs with an equivalent dipole fit in or near the frontal orbital gyrus (FOG) with the cluster centroid (i.e., the dipole mean RV = 10.14%, SD = 2.92%) localized at midline in BA 11 (Talairach coordinates 0, 33, -24, *Note:* Attempts to fit this IC with a symmetrical two-dipole model were unsatisfactory, yielding dipoles localized outside the head or with RV exceeding 25% in all cases). We inspected the frequency spectrum of each IC and rejected those with spectral components that would imply that they might have any contribution from an artifactual source (http://sccn.ucsd.edu/eeglab/eeglabdocs). We further pruned the remaining ICs so that each subject contributed only one IC, to minimize any bias from individual subjects contributing multiple ICs. Multiple ICs were present for all subjects (except subjects 5 and 7) and the IC with the largest MMN-related response and/or the best looking frequency spectrum was selected in these cases. After this pruning the mean RV = 9.21%, SD = 2.53% and the centroid remained in BA 11 (Talairach coordinates 3, 27, -25), just inside the right hemisphere along the midline. The dipoles were dispersed about the midline with a slight right hemisphere weighting, although given the close relationship between medial structures and the relatively poor spatial resolution of EEG, a strictly unilateral or bilateral activation cannot be determined.

The cluster mean event related activity shows a prominent waveform with a peak to peak amplitude of 0.2 μV for 2 cycles of alpha-like oscillation beginning about 60 ms post stimulus onset (Figure 2.4, middle row, second column). The waveform morphologies of the deviant and standard conditions closely resemble one another, reminiscent of the P1-N1-P2 complex of late cortical sensory responses. A significant difference between standard and deviant conditions appears at 120 ms post stimulus and lasts until 185ms, with the deviant condition more negative relative to the standard condition, a classic MMN effect. At 200 ms the deviant response shows

a positive deflection compared to the standard response, becoming significantly different ($p < 0.05$) beginning at 225 ms and lasting until 250 ms. The cluster ERP shows a clear resemblance to the scalp grand mean in morphology, and regions of significant difference between conditions. When back projected to the scalp, each individual subject IC accounts for between 21% and 59% of the variance (PVAF) for their respective subject scalp ERP, (see Table 2.3). The mean of these individual values gives the PVAF for the cluster of > 40% . The PFC cluster therefore contributes about 40% of the variance to the grand mean scalp ERP in the time interval of the MMN, by far the most of any cluster.

Table 2.3. Pruned clusters showing contributing ICs and respective PVAF to scalp MMN.

FOG Cluster		R STG Cluster	L STG Cluster
9 Subjects, 9 ICs (PVAF)		5 Subjects, 5 ICs (PVAF)	5 Subjects, 5 ICs (PVAF)
S01 IC1 (34.18)	S07 IC1 (30.29)	S02 IC21 (0.20)	S02 IC22 (0.15)
S02 IC1 (58.66)	S08 IC11 (16.97)	S05 IC7 (12.07)	S04 IC15 (3.12)
S03 IC1 (59.09)	S09 IC1 (48.38)	S07 IC8 (2.05)	S08 IC6 (6.35)
S04 IC2 (35.39)	S11 IC12 (57.38)	S08 IC15 (0.60)	S09 IC17 (-0.90)
S05 IC6 (21.18)		S11 IC24 (0.84)	S11 IC17 (0.62)
Mean (40.16)		**Mean (3.15)**	**Mean (1.86)**

Right Superior Temporal Gyrus Cluster

Seven subjects contributed a total of 19 ICs with an equivalent dipole fit within or near the right STG with the cluster centroid (mean RV = 10.69%, SD = 3.0%) in the right BA 42, Talairach 71, -15, 8. After again rejecting possibly artifactual ICs based on their frequency spectra, we then pruned the ICs down to one per subject. The pruned cluster had just five subjects contributing an

IC meeting our inclusion criteria, with the mean RV = 9.25%, SD = 3.64% and with the centroid remaining in the right STG (BA 42, Talairach 63, -38, 5). Because of the close relationship between temporal lobe structures and the relatively poor spatial resolution of EEG, however, participation of secondary auditory areas (e.g., BA 22) and or medial temporal structures cannot be excluded.

The cluster ERP (Figure 2.4, first row, first column) shows an activation pattern resembling a sensory-like response (i.e., P1-N1-P2 complex) with peak to peak deflection for 2 cycles of beta-like oscillation beginning about 40 ms post stimulus onset. The overall amplitude of the cluster ERP is small however, < 0.5 microvolt. The pruned cluster ERPs show no significant difference in ERP between the standard and the deviant condition.

Left Superior Temporal Gyrus Cluster

Seven subjects contributed a total of 20 ICs within or near the left STG, with the centroid (mean RV=10.26%, SD=3.5%) localized in left BA 42, (Talairach -68, -24, 8. From this we pruned the ICs to one per subject using the same criteria as described earlier. The pruned cluster had only five subjects contributing dipoles with the centroid (mean RV=11.29%, SD=2.1%) in the left STG (BA 42, Talairach -70, -28, 6). Because of the close relationship between temporal lobe structures and the relatively poor spatial resolution of EEG, however, participation of secondary auditory areas (e.g., BA 22) cannot be excluded.

The ERP for this cluster (Figure 2.4, first row, third column) has low amplitude overall with no pronounced peaks. The responses for standards and deviants, however, significantly differ from one another beginning around 190 ms until 230 ms post stimulus onset, during the latency window for the MMN.

Remaining Clusters

Table 2.2 also summarizes the characteristics of 8 additional IC clusters. We did not analyze these clusters in detail. Only one of them shows significant modulation during the MMN period by the auditory stimulus types: the cluster localized to the right temporo-parietal junction (TPJ). Nonetheless, their relationship to the temporal and orbital clusters that we did analyze is of some interest and will be addressed in the Discussion.

Discussion

Frontal Orbital Gyrus Area Exceed Superior Temporal Areas for Contribution to MMN

The FOG cluster displayed a grand mean ERP for deviant and standard conditions that clearly reflected a significant MMN effect. Interestingly, this cluster ERP when back projected to the scalp channels closely resembled the morphology of the scalp recorded grand average waveforms for the deviant and standard conditions at the Fz electrode site. The ICs in FOG cluster accounted for on average > 40% of the variance in the back-projected ERP of all of the valid ICs during the time range of the mismatch negativity (120-200 ms), meaning that this particular cluster is a driving force behind the back-projected ERP, and by extension behind the MMN recorded at the surface of the scalp for this particular paradigm. The relatively large influence of the orbital region in the MMN response is revealed we believe, by the use of our particular approach to EEG analysis. ICA performed on large continuous datasets of significant duration (60 minutes) is especially sensitive to those physiological processes that are sustained throughout the recording period. During the repetitive stimulation from the oddball paradigm habituation of neural responses will occur, although there will be regional differences as to the extent of this affect. Recent findings with fMRI using repeated stimulation with melodies demonstrated that long term (43 min) habituation of brain responses occurred in the right and left

superior temporal gyri extending to the primary auditory cortex, in the right inferior frontal cortex, and in the left hippocampal region (Mutschler, et al., 2010). Sustained responses throughout the same period, however, continued in the left ventrolateral prefrontal cortex. As well, intracranial electrophysiological recordings from macaque monkeys showed differences in the way individual brain regions react to stimulus repetition. In comparison to neurons in the inferior temporal cortex, neurons in the prefrontal cortex demonstrated only weak size-contingent repetition effects (Verhoef, Kayaert, Franko, Vaneneugden, & Vogels, 2008). These findings provide a neurophysiological reason for why the FOG cluster would emerge as a driving force within our paradigm. When ICA is performed over a continuous dataset consisting of 60 minutes of data, large amplitude brain responses in the prefrontal region that are sustained throughout the task will emerge as larger components than those brain responses in the temporal regions that, although large initially, more quickly habituate to the repetitive nature of the odd-ball paradigm.

Sustained responses in the FOG not only help explain our findings with ICA but also shed light on the role the prefrontal region has in the MMN response. Sustained responses are a means for maintaining information. With this capability the FOG could extract the statistical regularities occurring among transient acoustic events and compute predictions about the sensory data. Such a mechanism is a viable explanation for the MMN's sensitivity to abstract contextual changes. Recent findings indicate that the orbital prefrontal cortex is a region capable of integrating high-level information, maintaining information for significant durations, and generating predictions (Barbas, 2000). Predictions can be used to modulate the processing occurring within sensory regions through a process of inhibition (Barbas, Medalla, Alade, Suski, Zikopoulos, & Lera, 2005). Our findings are in keeping with the predictive coding model of the

MMN that asserts that the processes that give rise to the MMN necessarily involve more than just adaptive processes in the auditory cortex.

The amplitude of the ERPs displayed by temporal clusters is only about half that of the ERP in the frontal orbital gyrus cluster and the temporal clusters together account for only about 5% of the variance in the scalp ERP. This result should be interpreted with caution. First, only five subjects had ICs meeting the criteria for inclusion in the analysis. Temporal regions are susceptible to artifact from muscle tension from the jaw (e.g., temporalis muscle), so the ICs in the STG area that had a power spectrum resembling muscle artifact were removed from the cluster, despite having dipoles in MRI brain space and an ERP modulated by stimulus condition. A smaller number of ICs will account for smaller percent of variance for that simple reason. Second, the low amplitude and poor morphology of the cluster ERP is likely largely related to our analysis approach. Because sensory areas activated by the same features of the auditory stimulus likely will be temporally correlated (Gray & Singer, 1989; Pantev, Makeig, Hoke, Galambos, Hampson, & Gallen, 1991), we expect ICA algorithms operating over the entire continuous dataset to assign these activities to a single source signal across the various blocks, that is, a single source that has similar physiological response to the stimuli across the entire paradigm. The oddball effect (larger responses to infrequent deviants) might be attenuated because the physical features of a stimulus to which temporal sources are sensitive serve as both deviants and standards overall (see Table 2.1). Future experiments with these stimuli should concatenate blocks only if the stimulus probabilities are maintained.

Distinction Between Various PFC Clusters

Our analysis found independent frontal sources in the FOG, right IFG and bilateral MFG during the passive oddball paradigm, but among these only the FOG displayed a significant condition

effect during the MMN latency period. These findings are consistent with recent fMRI results examining the roles of the PFC in bottom-up and top-down processing of auditory stimuli which also found the VMPFC to be involved with bottom-up processing of infrequent deviants (Salmi, Rinne, Koistinen, Salonen, & Alho, 2009). In contrast to previous studies, we did not find the right IFG to be modulated by the MMN. Evidence from a previous imaging study of the MMN using fMRI (Molholm, Matinez, Ritter, Javitt, & Foxe, 2005) shows activations in the right IFG and left superior frontal gyrus (SFG) for frequency deviants. We show similar clusters of activations in left superior frontal cortex and right IFG, however we cannot ascribe the same roles to those generators as do the previous studies. By our account just the orbital frontal region participates in the MMN whereas the right IFG exerts little influence on the MMN, at least as measured by its ERP and PVAF. There are MMN paradigms, as Opitz (Opitz, Rinne, Mecklinger, von Cramon, & Schröger, 2002) suggested, where the IFC is not engaged at all, for instance when the deviant is easily detected, which may be the case in our paradigm. Overall, we demonstrate what many studies have previously: there is much variability in the neural sources for frequency deviants. The discrepancy between our data and those of Molholm et al. (Molholm, Matinez, Ritter, Javitt, & Foxe, 2005) may be explained, however, by differences between our block design and analysis and those required for fMRI. The sequencing of their block design aimed to control for overall sensory stimulation by comparing a predictable pattern of two alternating tones (the control block) with an oddball sequence of the same two tones (the MMN block). While this approach makes sense for equating activation in sensory regions arising from different neural assemblies coding for frequency, activation in some frontal regions may be compromised if the region detected in our analysis is synchronizing or desynchronizing already active neural assemblies rather than recruiting or suppressing additional assemblies.

The assumption by Molholm et al. (and other fMRI researchers) is that the MMN is indexed by an increase in regional activation, likely related to the recruitment of additional neural assemblies responsible for switching attention (Molholm, Matinez, Ritter, Javitt, & Foxe, 2005; Giard, Perrin, Pernier, & Peronnet, 1990), reorienting, and preparing motor responses if necessary. Although such recruitment may indeed occur, we would argue that likely prior to any attention switching, neural assemblies in the orbital frontal cortex (OFC) region are continuing to refine predictions about incoming auditory stimuli through interactions with the STG. This OFC region would therefore be active in both the control and deviant conditions of the fMRI study. We would argue that the deviant causes changes in synchronization in these assemblies compared to that prevalent for standard stimuli, and that these changes in synchronization in turn entail changes in the EEG signal recorded at the scalp. Our future studies with this paradigm will examine the regional synchronization occurring in different frequency bands (gamma-, beta-, alpha- and theta-bands) that may be contributing to the scalp MMN.

Attention Networks

Consistent with other studies, the elicitation of the MMN attracts attention to the deviant (Escera, Alho, Winkler, & Näätänen, 1998) as indexed by our finding of the P3f that followed the MMN response and has neural sources in the frontal and parietal regions. Additional resources may be recruited to shift attention to relevant changes. Two independent but related attention networks likely operated in our experiment, and several of these network loci are among our clusters (see Table 2.2). Voluntary attention to sensory stimuli based on goals and expectations is mediated by the dorsal fronto-parietal network (bilateral intraparietal sulcus, IPS; bilateral superior parietal lobule, SPL, and R MFG) (Corbetta, Patel, & Shulman, 2008). In our context, the dorsal network is engaged primarily in directing visual attention to the movie video; thus we observed

activations of neural sources in middle occipital gyrus, left SPL, and in right MFG in the absence of significant modulations by stimulus type. Unexpected stimuli activate the ventral fronto-parietal network (bilateral TPJ, R MFG, and R IFG), which serves to interrupt the ongoing focus of attention (in our case, the movie video) to transiently orient attention to the infrequent changes in the acoustic regularity. In some cases these unexpected events may require the dorsal network to be reconfigured, but in our experiment the occurrence of the deviant was to be ignored. The poor response of the ventral network, indexed by a condition effect in the right TPJ cluster but in neither the right IFG nor right MFG, prevents shifts of attention, allowing subjects to maintain focus on their task of watching the movie video.

The subcortical source in the vicinity of the left cerebellar tonsil is speculated to be related to the sensory subcortical processing within the various auditory brainstem nuclei or possibly within the locus coeruleus (LC) in the dorsal pons area. Certainly both are reasonable. Recent work with invasive recordings in animals have shown stimulus-specific adaptation, i.e., a reduced neural response to a commonly occurring "standard" tone than to the same tone when it is rare or "deviant", in subcortical neurons in the inferior colliculus (Malmierca, Cristaudo, & Covey, 2009) and the medial geniculate body (Anderson, Christianson, & Linden, 2009). A rationale for the involvement of the LC in the MMN is related to its proposed involvement in the ventral attention network and in the generation of the P3f scalp response (Corbetta, Patel, & Shulman, 2008). With regard to active oddball paradigms, the LC phasic response is thought to be triggered by prefrontal inputs after the sensory evidence meets criteria for target identity.

In summary, the MMN may recruit or subsume smaller neural assemblies (Giard et al., 1995) or itself may be a subset neural process involved in a more complex neural network evaluating auditory stimuli (Salmi, Rinne, Koistinen, Salonen, & Alho, 2009). Our findings may

help explain the reduced MMN after prefrontal cortical damage (Alho, Woods, Algazi, Knight, & Näätänen, 1998; Alain, Woods, & Knight, 1998). Similar behavioural and neurophysiological correlates have been reported for aged humans, suggesting that neural changes in prefrontal cortices reduce inhibitory influences in auditory areas, and impair the ability to ignore irrelevant sounds (Chao & Knight, 1998).

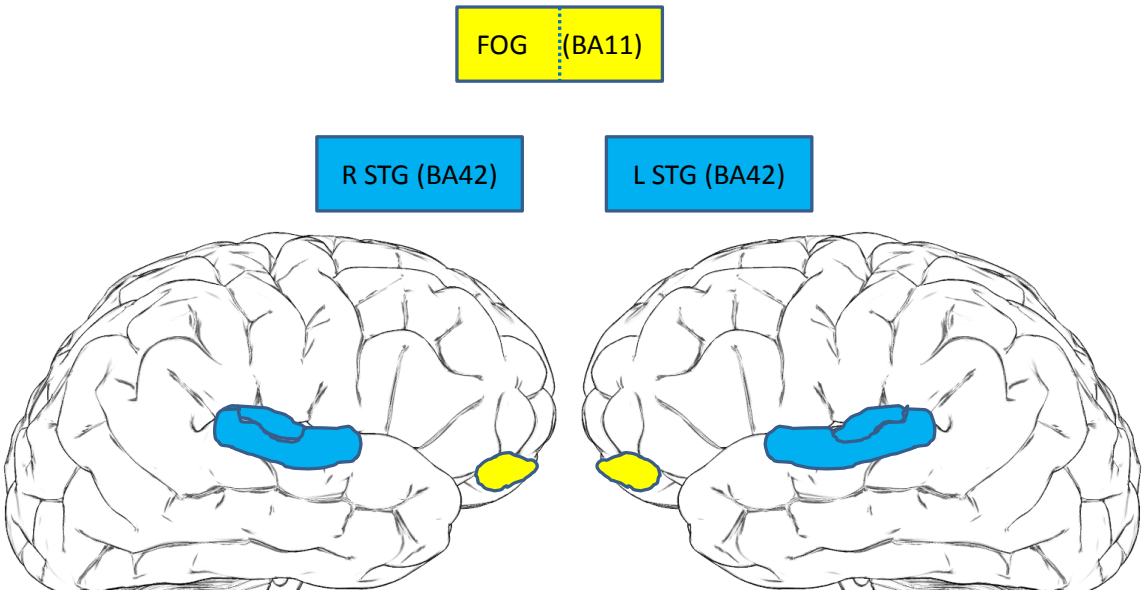

Figure 2. 5. ICA sources related to MMN scalp activity in the paradigm of Experiment 1.

Note: Dotted line through the FOG source represents possible bilateral sources.

Future Directions

Applying ICA to EEG data allows the activity from certain brain sources to be better quantified. In our dichotic listening study using complex tones we show that sources localized to regions in the left superior temporal gyrus, the orbital frontal cortex and the right temporal parietal junction have event related activity that is significantly different for deviant and standard conditions during the MMN response at the scalp. As well, we see the source in the orbital frontal cortex is

the largest contributing factor (and the source in the R STG, a distance second) to the brain response recorded at the surface of the scalp during this dichotic MMN paradigm. This evidence echoes previous findings that regions beyond the auditory cortex are involved in the generation of the MMN. What we have found is how these regions relate to the scalp response or to the stimulus conditions but not how these brain regions relate to one another. The next question to be address is when and how these brain regions interact during the process of change detection. This is fundamental to understanding the roles these key regions play in the neural mechanism of change detection. To claim that interactions between these areas are needed for change detection requires evidence from some measure of temporal dynamics. Future studies in this series are directed toward analysis of the synchronous interactions within and between these three brain regions and others that may play subsidiary roles.

CHAPTER 3: SYNCHRONIZATION SUPPORTS HIERARCHICAL MMN NETWORK

Introduction

In recent years, EEG has gained renewed interest in the field of neuroscience for the temporal information it provides about how the intact human cortex works as a network of specialized processing centres. Synchronous neural oscillations between disparate brain regions are thought to be the means for globally integrating the results of local computations from specialized processing centres to achieve meaningful perceptions, awareness, cognition and consciousness. The neural interactions between functionally distinct processing regions in the temporal and frontal cortices during the perceptual event of change detection are thought to culminate in the MMN scalp response. The evidence for this temporo-frontal network, however, is somewhat circumstantial, being based on topographic maps of EEG data, equivalent dipole modeling of both EEG and MEG, co-activating brain regions from BOLD response of fMRI data, simulations with computational modeling, and from neuropsychological performance of brain damaged individuals.

Previous studies with non-human primates have examined the relationship of prefrontal connections to local inhibitory neurons in the STG and have shown that feedback activity from the frontal regions can modulate activity in the STG, refining sensory analysis to suppress irrelevant stimuli (Barbas, Medalla, Alade, Suski, Zikopoulos, & Lera, 2005). Specifically, forward pathways in the auditory STG relay feature-specific signals to higher-order areas, such as the prefrontal cortex, terminating in the deeper layers. In reciprocal fashion, axons from anterior lateral, medial prefrontal and orbitofrontal cortex (OFC) areas terminate in the STG, targeting mostly inhibitory neurons in the superficial layers. Disturbances in the temporo-frontal pathways affecting inhibitory interactions, perhaps through disconnection of robust

pathways, fits the findings from those patients with prefrontal damage who show decreased EEG activity over the dorsolateral prefrontal cortices and a concomitant increase of activity in auditory association cortices which is correlated with their impaired performance on tasks of auditory discrimination ability when irrelevant stimuli are introduced (Chao & Knight, 1998). Similar behavioural and neurophysiological correlates have been reported for aged humans, suggesting that neural changes in prefrontal cortices reduce inhibitory influences in auditory areas and impair the ability to ignore irrelevant sounds, thus impairing the ability to follow conversations in noisy environments (Chao & Knight, 1997).

Accumulating evidence shows regions in the frontal and temporal cortex to be active during the MMN but whether they actually interact within a functional network has yet to be directly demonstrated. Previous research in non-human primates with implanted electrode arrays has demonstrated, in the visual modality, changes in the oscillatory coherence between disparate brain regions depending on the ease of processing deviant stimuli. In a task requiring deliberate visual search selecting a target object among an array of similar objects, coherence in the beta frequency band (in that study defined as 22-34Hz) occurred between prefrontal and parietal cortical regions, whereas in a comparatively easier task when a target object is very different ('pop out') from distractors, synchronization in the gamma band (defined as 35-55 Hz) occurred between these same regions (Buschman & Miller, 2007). Gamma-band synchrony was thought to reflect more local processing serving to enhance stimulus representations. In contrast, top-down signals from frontal areas were thought to be more efficiently "broadcast" to the parietal region along the lower frequency beta-band where spike timing delays are less detrimental to long range communication (Engel, Fries, & Singer, 2001). This finding in the lower frequency range for top-down visual searches has also been found in scalp EEG with humans using similar

visual paradigms (Phillips & Takeda, 2009). In the latter study, however, gamma-band activity (GBA) was not correlated with bottom up 'pop-out' searches. Within the auditory modality, Debener and colleagues (Debener, Hermann, Kranczioch, Gembris, & Engel, 2003), employing a novelty-odd ball paradigm have shown evoked GBA around 60 ms post stimulus-onset to be related to top-down processing as it correlated with task-related target detection but not with the occurrence of task-irrelevant stimuli or with novel changes from the infrequent occurrence of novel stimuli. Others have found, however, that the sudden introduction of a salient auditory stimulus to an ongoing acoustic regularity did evoke GBA which then transitioned at 150 ms to beta-band activity (Haenschel, Baldeweg, Croft, Whittington, & Gruzelier, 2000)(Kisley & Cornwell, 2006), suggesting that certain features such as intensity, novelty or rarity, and degree of contrast may have induced later beta activity 'flagging' a stimulus as salient. It appears that top-down effects such as attention (Tiitinen, May, & Näätänen, 1997) and expectation of a task-relevant stimulus led to an enhancement of the early evoked GBA (Schadow, Lenz, Dettler, Fründ, & Herrmann, 2009). Beta-band activity does exhibit more widespread expression across the cortex and may likely serve as a mechanism for long range information transfer necessary for further stimulus monitoring. In summary, it appears that slower cortical oscillations affect larger areas of cortex and are poised to modulate faster oscillations occurring in more localized regions.

In order to study further local and global synchronization of the MMN sources, the first block of the experiment presented in the previous chapter (see Table 2.1) was used to compare performance during passive and active listening conditions. Our predictions for local synchrony, based on the MUM model, were that in the active condition where subjects respond to deviants as targets we should see increased local gamma-band power in the sources of the MMN

processing deviant targets. In contrast, in the passive listening oddball paradigm where the subject attends to a silent movie ignoring the auditory stimuli, we predicted within the STG and OFC regions increased local synchrony in the gamma-band for the standards relative to the deviants. Our reasoning is that if synaptic connections between neurons have already been strengthened by a stimulus that has been repeatedly presented, as in the case of the standards, then presentation of another standard stimulus should not further modify synaptic connections, but rather might lower the temporal variance among existing connections, increasing phase locking and resulting in increased local synchronization in the gamma-band (and thus an increase in gamma-band power).

Our predictions for global synchronization, based in part on Friston's predictive coding model, are increased long range synchrony between those neural regions of the STG and OFC during the latency of the MMN as these brain regions were shown in our previous study to be modulated by the MMN. According to Friston (Friston, 2009), when top-down predictions accurately encode the sensory input, the states of the brain generating those predictions become the representations of the corresponding bottom-up feature encodings of the stimulus, completing the process of perceptual inference. Top-down predictions may come in the form of feedback projections from PFC serving to enhance or prime neurons responsive to the expected pattern while suppressing neurons coding features not fitting that pattern. However, bottom-up processing of deviants would activate areas outside these primed neurons resulting in a mismatch signal specific to the changed features, alerting the perceptual system that inferences need to be adjusted or recalibrated.

Provided Friston's model is correct then extrinsic connections between the temporal and frontal generator are similar for deviants and standards. Both regions are needed to update

predictions given each incoming stimulus implying that long range synchronization would be occurring for both deviant and standard stimuli. It is, however, possible that larger prediction error could require longer periods of synchronization to refine the model, so that the deviant condition could display more temporally extended phase-locking increases.

During the passive listening paradigm sources in the ventral attention network were expected to emerge as found in the previous passive experiment. In the active listening paradigm with the same stimuli the ventral attention network is thought to be active during the reorienting of attention to a behaviourally relevant stimulus, should it be the case that attention to the rare but behaviourally relevant deviant tone wanes during the intervening standard tones, (Corbetta, Patel, & Shulman, 2008).

Materials and Methods

Participants

Fifteen right-handed volunteers participated in the study. One participant was excluded from data analysis because of low accuracy in the active listening task, resulting in a final sample of fourteen participants (7 women, 7 men, mean age 22, range 18 to 32 years, SD 3.8 years). All subjects provided written consent and were paid to participate. The experiments were approved by the Behavioural Research Ethics Board of the University of British Columbia. All participants were assessed by clinical audiometry and found to have hearing within normal range at the time of the EEG acquisition. No history of neurological disorders was reported during a prescreening interview. Handedness was assessed by The Edinburgh Inventory (Oldfield, 1971) completed by the participant and reviewed with the experimenter.

Stimuli and Procedure

Dichotic tonal stimuli from Block 1(see Table 2.1) were presented in pseudo random order (deviants to be separated by at least two standards) for two runs (total trials 4800). For the first run (~20 minutes) volunteers watched a silent video with closed captioning and ignored the sounds heard through insert earphones. Then after a short break, the block was presented again (although in a different pseudo random order) and the subjects were required to respond using their right hand to the deviant tones with a button press on the computer mouse. The EEG data from the passive and active blocks were appended and ICA conducted on the single 40 minute continuous dataset. The EEG recording and ICA decomposition have been described in the previous chapter and remained unchanged for the present experiment.

Results

Cluster Analysis

Narrow cluster analysis of all valid ICs (dipole fit within the head of RV <15%) was based on IC dipoles and ERSPs (0 - 350 ms, 5 - 55Hz). The algorithm finds the centers of a predetermined number (k=30) of natural clusters in the data by minimizing the total intra-cluster variance. A larger number (k=30) of clusters was chosen to group individual dipoles in this experiment resulting in less post hoc pruning within clusters. However, this resulted in fewer subjects contributing to each cluster. Even with fewer clusters (k=15) however, no cluster contained ICs from all subjects. The largest cluster contained data from only 71% of the subjects, or 11/14 subjects. This held for k = 15 up to k = 30. No cluster with fewer than 50% subject contribution is reported here. See Table 3.1 for details of cluster properties.

Regions of Interest (ROI) for the MMN

The regions of the STG (any of BA 41, 42 and 22) in the right and left hemispheres as well as the frontal orbital cortex (BA 11), in either the right, left or both hemispheres were expected to emerge from the cluster analysis as sources for the MMN as these regions were shown in the previous experiment to be the major contributors to the MMN scalp response. In addition, regions involved in the ventral attention network (R TPJ, R IFG) were expected to emerge as they did in the previous passive listening experiment. During the active listening paradigm sources in the ventral attention network were expected to emerge given the response requirement (button press) to the deviant target. Attention to the rare but behaviourally relevant deviant tone wanes during the intervening standard tones and the ventral attention network is thought to be active during the reorienting of attention to a behaviourally relevant stimulus (Corbetta, Patel, & Shulman, 2008).

Table 3. 1. Cluster properties with 50% subject contribution, ROI for the MMN in bold.

Cluster Brain Region *	% of Subjects Contributing	BA	Talairach x, y, z	RV % dipole fit
L PL	64	WM	-33, -35, 30	8.17
R IFG	**57**	**9**	**51, 13, 25**	**8.94**
R MFG	50	47	48, 41, -5	11.35
R OL	78	31	10, -58, 29	6.28
L MTG	64	37	-52, -64, 3	8.06
R CING	50	24	11, -3, 46	7.57
R OL	71	17	16, -90, 5	8.31
L PCG	50	9	-39, 6, 37	7.67
L IFG	**57**	**11**	**-21, 27, -21**	**11.01**
L STG	**64**	**42**	**-72, -14, 3**	**9.74**
R PCG	64	4	41, -17, 47	7.33
L CBL	64	NA	-17, -89, -21	7.58
R STG	**64**	**22**	**62, -34, 7**	**10.40**
R OG	**71**	**11**	**5, 42, -23**	**9.86**

BA Brodmann Area; **CBL** cerebellum; **CING** cingulate gyrus; **IFG** inferior frontal gyrus; **L** left; **MFG** middle frontal gyrus; **NA** not applicable, **OL** occipital lobe, **OG** orbital gyrus; **PCG** precentral gyrus; **PL** parietal lobe; **R** right; **STG** superior temporal gyrus, **WM** white matter. * Regional locations based on centroid mean, not all ICs within a cluster fall within a region.

Event Related Spectral Perturbation Analysis

Event-Related Spectral Perturbations (ERSPs) were computed by using EEGLAB v.7.1.4. (Delorme & Makeig, 2004) under 64-bit Matlab 7.4 (Mathworks, Inc). The spectral power changes (or perturbations) over time between post-stimulus and the pre-stimulus baseline activity are shown in Figures 3.1 and 3.2. ERSP are plotted as the log ratio of the two activities in decibel (dB) units with increased power represented in red and decreased power in blue. The frequencies were analyzed in 1.5 Hz increments using a sliding sinusoidal wavelet (Hanning-windowed) with linearly increasing cycles. The pre-stimulus baseline was limited to the period from -150 to -50 ms before sound onset to reduce overlap of pre-stimulus and post-stimulus activity due to windowing. Permutation statistical methods resample the data (in our experiment 400 resamplings), rearranging the condition labels on the observed data points during the prestimulus period to obtain a surrogate null distribution, which is then compared to the observations based on true condition assignment in the post stimulus period. This minimizes spurious findings by comparing effects from a time series of interest to those from a set of randomly generated surrogate time series with the same general properties. Significant differences between the ERSP of each condition are masked at $p < 0.005$ by permutations (see far right columns in Figures 3.1 and 3.2, differences in burgundy against a green background). For simplicity, we report all differences in terms of the condition showing the greater power (displayed in red or yellow in the first two columns). Significant differences lasting for less than a single frequency cycle (e.g., γ <25 ms, β <50ms, α <100 ms, θ <150 ms) were considered to be spurious and are not reported in Table 3.2 summarizing the ERSP results.

ERSP for Temporal Clusters

The R STG cluster shows the Active Deviant condition with significantly greater gamma-band power increase than Active Standard from -50 - 150 ms (see Figure 3.1, lower panels), which is consistent with our hypothesis and previous studies (Tiitinen, Sinkkonen, Reinikainen, Alho, Lavikainen, & Näätänen, 1993; Debener, Hermann, Kranczioch, Gembris, & Engel, 2003) that attention to deviant targets enhances gamma activity. Within the L STG cluster there is increased gamma-band power evident in the deviant and standard conditions for both the passive (top panels) and active (lower panels) paradigms but the overall difference between the stimulus types is significant for less than one gamma cycle. The Passive Deviant condition for the L STG cluster shows a significantly greater power increase in beta band activity at onset (-70 - 30 ms) and later (390 - 450 ms) compared to the Passive Standard condition. That beta-band activity within the L STG might serve to "flag" the deviant is not held during the active paradigm where the Standard displays significantly beta-band activity from 290 - 450 ms than does the Active Deviant.

The hypothesis for greater gamma-band power increases for the Standard condition in the passive paradigm was not supported. Indeed, significantly greater power increases in the Passive Standard do not occur in any frequency band when compared to the Passive Deviant for temporal or frontal clusters of interest (see Table 3.2).

ERSP for Frontal Clusters

The ERSP for the frontal sources did not confirm any of our hypotheses. Indeed, the R OG shows results completely contradictory to the predictions from the MUM (see Figure 3.2, middle columns) with the Passive Deviant condition displaying significantly greater gamma-band power increases than does the Passive Standard from 135 - 190 ms, 240 - 265 ms, and 310 - 380 ms. In

contrast, the Active Standard shows significantly greater gamma-band power increases than does the Active Deviant between 120 - 150 ms. The L IFG (Figure 3.2, left columns) shows no differences in power between the passive conditions, however the Active standard shows significantly greater gamma-band power increases from 390 - 450 ms compared to the Active Deviant. The R IFG (Figure 3.2, right columns) shows significantly greater power increases in gamma-band from 225 - 325 ms (and in alpha-band from 275 - 420 ms) in the Passive Deviant when compared to the Passive Standard. The Active Deviant shows greater theta-band power increases from 150-300 ms than for Active Standards.

Table 3. 2. Summary of ERSP results showing significantly greater ($p < 0.005$ by permutations) power increases by frequency band and time range (ms) for stimulus conditions within Passive and Active paradigms. The difference is listed for the stimulus condition with the greater amount of spectral power. **γ** gamma (30-55 Hz, 25ms), **β** beta (13-29 Hz, 50ms), **α** alpha (9-12, 100 ms), θ theta (≤8 HZ, 150 ms). Underlined entries overlap MMN time window for a frequency cycle.

Conditions		Temporal Clusters		Frontal Clusters		
Paradigm	Stimulus	L STG (BA42)	R STG (BA22)	L IFG(BA11)	R OG (BA11)	R IFG (BA9)
Passive	Deviant	**β, -70-30** **β, 390-450**		-	**γ, 135-190** **γ, 240-265** **γ, 310-380**	**γ, 230-310** **α, 275-420**
	Standard	-	-	-	-	-
Active	Deviant		**γ, -50-150**	-	-	**θ, 130-370**
	Standard	**β, 290-450** **α, 330-450**	-	**γ, 390-450**	**γ, 120-150**	-

IFG inferior frontal gyrus; **L** left, **OG** orbital gyrus; **R** right, **STG** superior temporal gyrus

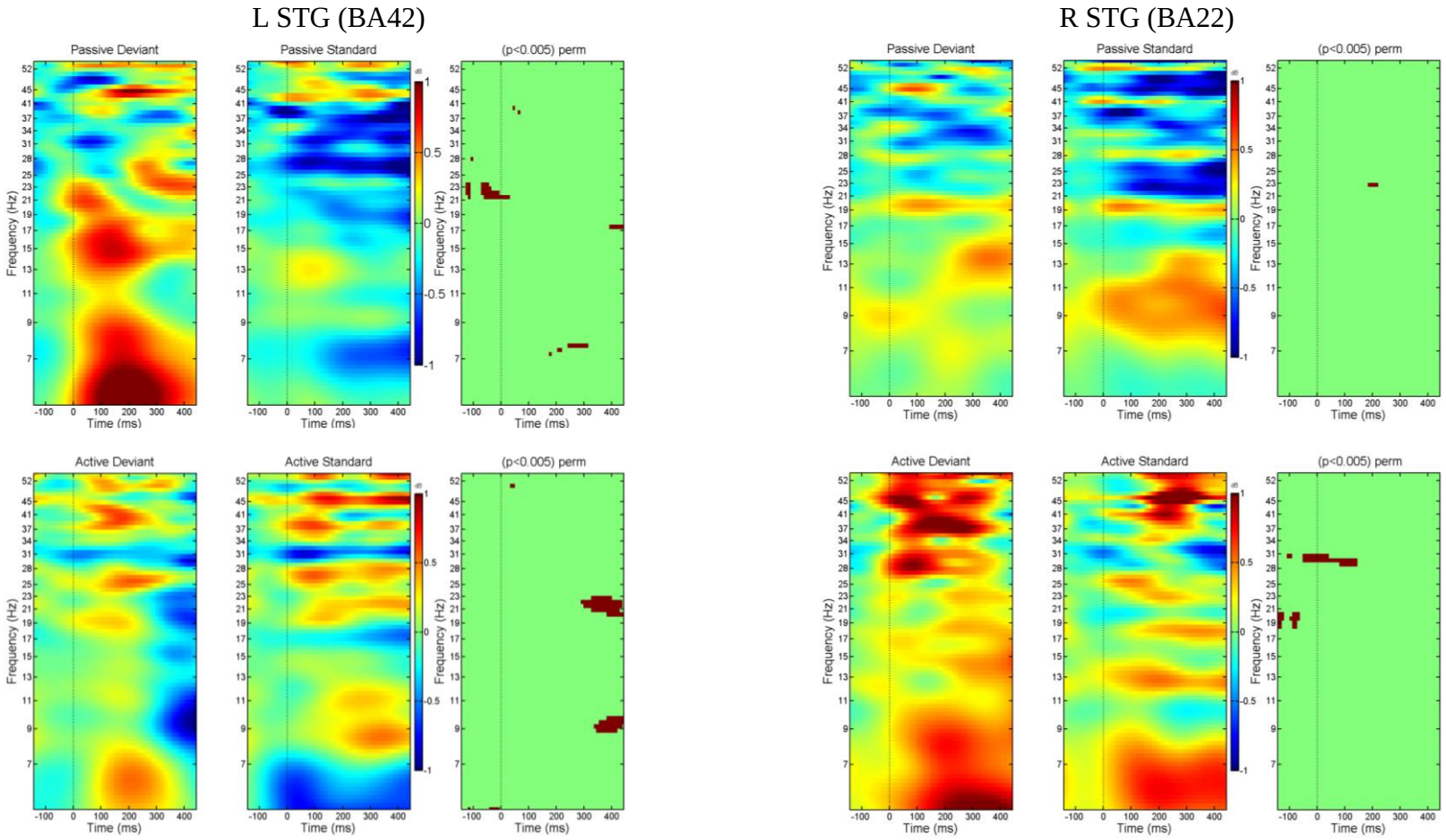

Figure 3. 1. Temporal clusters mean ERSP for Deviant and Standard conditions, significant differences are displayed in burgundy against a green background (masked $p < 0.005$ by permutations) in the far right column. Passive paradigm (top panels) and Active paradigm (lower panels). Power increase represented in red and power decrease in blue.

L STG (leftward 3 columns) Passive Deviant condition shows significantly greater increase in beta-band power from -70-30 ms and from 390-450 ms compared to Passive Standard. Differences in gamma-band and theta power are < 1 frequency cycle. For the Active Standard condition there is significantly greater power increase in beta-band from 290-450 ms and alpha-band from 330-450 ms compared to Active Deviant condition. Differences in gamma-band power are < 1frequency cycle.

R STG (rightward 3 columns) Power differences in beta-band from 180-215 ms between Passive conditions are < 1 frequency cycle. Active Deviant condition has significantly greater gamma-band power increase from -50-150 ms compared to Active Standard.

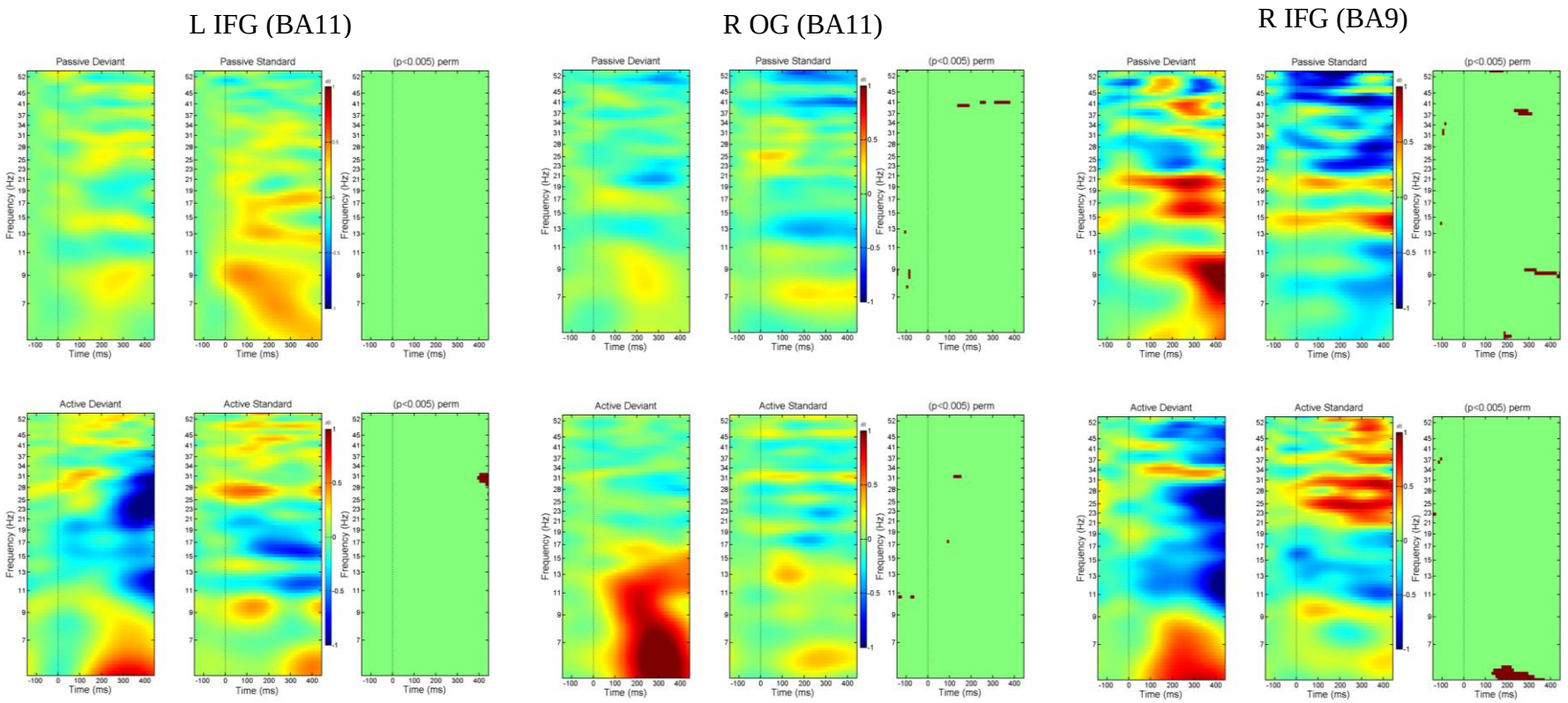

Figure 3. 2. Frontal clusters mean ERSP for Deviant and Standard conditions, significant differences are displayed in burgundy against a green background (masked $p < 0.005$ by permutations) in the far right column. Passive paradigm (top panels) and Active paradigm (lower panels). Power increase represented in red and power decrease in blue.

L IFG (leftward 3 columns) Passive paradigm shows no significant differences in power between deviant and standard. Active Standard condition shows significantly greater gamma-band power increase from 390-450 ms compared to Active Deviant.

R OG (middle 3 columns) Passive Deviant condition shows significantly greater gamma-band power increase from 135-190 ms, 240-265 ms, and 310-380 ms than Passive Standard. Active Standard condition shows significantly greater gamma-band power increase from 120-150 ms compared to Active Deviant. Beta-band power differences are < 1 frequency cycle

R IFG (rightward 3 columns) Passive Deviant shows significantly greater gamma-band power increase from 230-310 ms and alpha-band from 275-420 compared to Passive Standard condition. Theta band power differences from 185-220 ms are < 1 frequency cycle. Active Deviant condition shows significantly greater theta-band power increase from 130-370 ms compared to Active Standard.

Cross-coherence Analysis

One limitation of phase coherence measures on sensor data is that they might be contaminated by correlated amplitude. Correlated sensor amplitude can arise from volume conduction arising from anywhere in the EEG signal, not just between the two sensors compared. For this reason we chose to separate channel data into independent sources of EEG activity. ICA separates component time courses so that IC amplitude correlations as well as predictive relationships between all the higher-order moments of the IC signals approach zero. This process minimizes the effects of volume conduction on phase coherence measures. However, because ICA can only maximize the independence between sources, and that process is dominated by minimizing amplitude correlations, especially at higher frequencies, there can remain transient temporal dependencies in the phases between ICs that can be further investigated though cross-coherence analysis. Cross-coherence measures effective interactions between ICs based on only the phases of their narrow-band oscillations, that is, the extent to which two signals exhibit a consistent phase difference within a particular relatively narrow frequency band (as that is the only context in which the concept of phase has any coherent meaning). Cross-coherence values range from 0 (random phase relationship) to 1 (perfect phase locking), although within biological systems such as neural networks perfect phase locking relationships are not possible. See Figures C.1 – C.9 in Appendix C for the results of a mean cross-coherence analysis. All individual cross-coherences were masked at $p < 0.05$ in each time-frequency window. Masking for individual coherences was done with a surrogate method based on 200 shufflings of the epochs for each IC. For post hoc analysis to determine differences between stimulus types within the passive or active paradigms we used a permutation procedure to generate an unbiased empirical estimate of the Type I error rate ($p < 0.005$) based

on (Maris, Schoffelen, & Fries, 2007). First, we generated a 1000 different random samples of the experimental data by randomly swapping items designated as deviant and standard for each subject. Then we created a distribution of differences between the cross-coherences computed from these 1000 sets of sham conditions. From this distribution we could compare the magnitude of the difference we obtained from the actual conditions to those differences found in the distribution of differences between the sham conditions. As the cross-coherences were based on just a few pairs, at times as few as four pairs, we wanted to ensure the results of the permutations test were not skewed by large outliers but that most of even the small group showed synchrony within the MMN latency region. To identify consistent regions of increased cross-coherence for the group we used a binomial probability computation based on (Onton, Delorme, & Makeig, 2005). Here, the common *p*-value for the individuals, set at 0.05, was taken as the binomial probability of a "success," P(success), (with P(failure)=1-P(success)), and the probability of *k* or more of *n* individuals displaying a significant coherence at $p < 0.05$ was kept less than 0.001. When significant differences by the permutation test and consistent cross-coherence were shown by the binomial test, we considered the differences meaningful.

We examined cross-coherences between our temporal (L STG and R STG) and frontal sources (R OG, L IFG and R IFG) thought to be involved in the change detection process. Between the temporal regions theta-band synchrony across subjects was not sustained for more than a frequency cycle (~150 ms) so despite a burst of synchrony within the latency of the MMN (120-250) in the Active Deviant condition the effect was considered due to an outlier. Gamma-band synchrony was consistently found across subjects and was significantly increased in the Active Standard condition compared to the Active Deviant condition. We concluded therefore that there is interaction modulated by stimulus type between temporal sources for the active

oddball paradigm. See Figure C.1 for mean cross-coherences between R STG and L STG. Between the L STG and the L IFG we found increased alpha- and theta-band cross-coherence for the deviant condition compared to the standard condition across both paradigms (see Figure C. 2). Between the R STG and the L IFG we found increased gamma-band cross-coherence for the deviant condition compared to the standard condition in the active paradigm but the reverse contrast for the passive paradigm (see Figure C. 3). Between the L STG source and the R OG source we found the Passive Standard condition shows significantly increased gamma-band cross-coherence compared to the Passive Deviant condition. However, the Passive Deviant showed increased synchrony in the beta-band compared to the Standard condition. In the active paradigm, the Deviant condition showed significantly more cross-coherence compared to the Active Standard in alpha- and theta-bands within the latency period of the MMN (see Figure C. 4). These results suggest interaction between L STG and R OG along different frequency bands may serve a special purpose for the separate processing of deviants and standard stimuli.

Between the R OG and the R STG all conditions within a narrow band of gamma (>42 Hz, see Figure C.5) show consistent cross-coherence across subjects. The Active Standard condition we found significantly increased cross-coherence in the gamma-band within 120-250 ms post stimulus onset than did the Deviant condition, whereas no difference was found for the passive conditions ($p < 0.005$). Between the L STG and the R IFG we found no consistent cross-coherence among the IC pairs (see Figure C. 6). Between the R IFG and R STG all conditions showed consistent gamma, alpha and theta synchronization across subjects (see Figure C.7). These results across high and low frequency bands suggested a multi-functional interaction. The Passive Deviant condition displayed significantly increased cross-coherence in beta-band within the latency of the MMN relative to the Passive Standard condition, whereas the Active paradigm

a significant increase for the Deviant condition occurred in the theta-band for this period. The Passive Standard condition displayed significantly increased cross-coherence in theta-band within the latency of the MMN relative to the Passive Deviant condition, whereas the Active conditions show a significant increase for the Standard in alpha-band for this period. Between the right hemisphere frontal sources, R OG and R IFG, there was no significant difference between the gamma-band cross-coherence in conditions for active or passive paradigms. In the lower frequency bands there was no consistent synchrony across subjects (see Figure C. 9). The inter-hemisphere interactions between the R OG and L IFG showed increased cross-coherence for the Deviant condition in the theta-band for the passive paradigm and in the alpha- and gamma-band for the active paradigm. Gamma-band cross coherence was increased for the Standard condition in the passive paradigm only (see Figure C. 8).

In summary, the cross-coherence analysis reveals synchronous interactions during the MMN latency period between sources thought to be involved in generating the MMN response (L STG, R STG, R OG, and R IFG). These synchronous interactions are modulated by stimulus type and task demands, further suggesting that these interactions are indeed functional. Table 3.3 summarizes the significant cross-coherence differences between deviant and standard stimuli for the active and passive conditions for these regions of interest. The networks drawn from the cross-coherent results include only regional interactions that are significantly difference between deviant and standard conditions during the latency period of the MMN because the MMN response at the scalp is derived from difference between conditions. Figure 3.3 presents a MMN network model that is supported by these findings.

Table 3. 3. Significant cross-coherence differences (red: Deviant> Standard, green: Deviant< Standard, poc hoc comparisons $p < 0.005$) within the MMN latency period (120-250 ms) for Passive and Active paradigms. **γ** gamma-band (30-55 Hz) , **β** beta-band (13-29 Hz), **α** alpha- band (9-12 Hz) , **θ** theta-band (≤8 Hz).

		TEMPORAL	TEMPOROFRONTAL					FRONTAL
		L STG~R STG BA42~BA22	L STG~L IFG BA42~BA11	R STG~L IFG BA22~BA11	L STG~R OG BA42~BA11	R STG~R OG BA22~BA11	R STG~R IFG BA22~BA9	L IFG~R OG BA11~BA11
Passive D-S	**γ**							
	β							
	α							
	θ							
Active D-S	**γ**							
	β							
	α							
	θ							

* No consistent cross-coherence and/or significant differences for the temporo-frontal comparison: L STG~R IFG or the frontal comparison: R IFG~R OG .

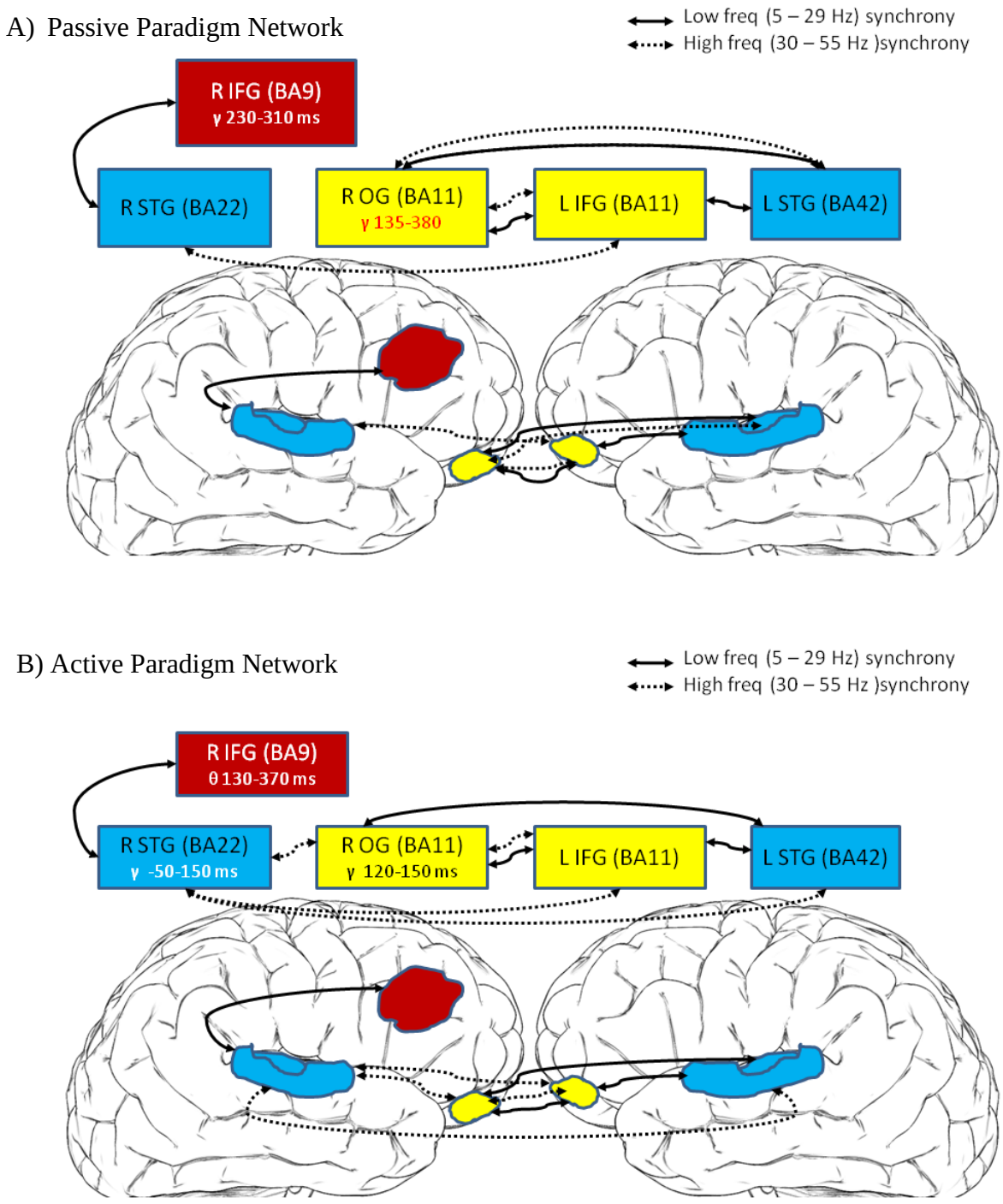

Figure 3. 3. MMN Network Model. A) Passive listening paradigm showed synchronous interactions differentiated by stimulus type ($p < 0.005$) during the MMN latency window among the bilateral STG (left BA42, R BA22), the L IFG and R OG (both BA11), and the R IFG (BA9). B) Active listening paradigm showed synchronous interactions differentiated by stimulus type ($p < 0.005$) during the MMN latency window among the bilateral STG (left BA42, R BA22), the L IFG and R OG (both part of BA11); and the R IFG (BA9). Local synchrony increases (from ERSP) are displayed in black for standard and in white or red for deviant within regions.

Discussion

The intrinsic activity (local synchrony) within the network nodes, as examined by the ERSP, shows for the R STG cluster significantly increased GBA for the Active Deviant condition shortly after stimulus onset compared to Active Standard condition. This result is consistent with our hypothesis and with previous studies (Tiitinen, Sinkkonen, Reinikainen, Alho, Lavikainen, & Näätänen, 1993; Debener, Hermann, Kranczioch, Gembris, & Engel, 2003) in that attention to deviant targets enhances GBA. Previous studies have localized most of the GBA to the auditory dipoles within the auditory temporal regions specialized for handling particular stimulus features, so this finding that tonal stimuli are evoking more gamma in the R STG is consistent with previous studies (Pantev, Makeig, Hoke, Galambos, Hampson, & Gallen, 1991). Within the active paradigm, it is reasonable that local computations within the R STG region would reflect the early sensory processing of stimulus features. Our hypothesis predicting increased GBA for the Standard condition in the passive paradigm, based on the MUM, was not supported for either of the temporal sources. In both temporal clusters (L STG and R STG) the absolute power of GBA is not so much different in magnitude between conditions as it is different in latency and in where in the gamma band (30-55 Hz) the activity occurs. Neither we nor any other researchers that we know of, however, have any hypotheses about how and why this activity could be divided among the frequencies within the gamma band.

The ERSP for the frontal sources did not confirm any of our hypotheses. Indeed, the R OG displayed very little increased activity in the gamma band and what increases occurred completely contradicted our hypothesis: the Standard condition in the passive paradigm and the Deviant condition in the active paradigm did not show greater gamma band activity compared to the respective stimulus condition. These findings in the active paradigm however are not

necessarily incompatible with the "match and utilization" model when considered in light of the recent findings from a study that examined the role of GBA in anticipation of musical sequences (Schadow, Lenz, Dettler, Fründ, & Herrmann, 2009). In that ERP study, six tone sequences served as the standards and deviants interrupted the anticipated sequence at the third and fifth position. Participants were asked to decide whether the presented tone sequence was predominantly ascending or descending, irrespective of a violation of the expected sequence. The standard tone that matched the continuation of a sequence elicited considerably more evoked GBA compared to deviant tones. These researchers concluded that the degree of anticipation during the task strongly biased the matching process between the incoming tone and the memory template, overriding the GBA generated by attentional processing to detect deviant. Interestingly, Schadow et al., source the GBA to the primary auditory cortex almost exclusively using a model of bilateral dipoles explaining that such gamma band enhancement is the result of a match of bottom up input with an internal prediction yet it is not clear where the internal prediction is computed. In our study, we interpret the role of the R OG in the active paradigm as largely matching incoming sensory data to predictions to explain our findings of more GBA to standards than to deviants within the R OG source. The greater increase power in the gamma band for the Active Standard condition compared to the Active Deviant condition indicates that gamma-band oscillations within this region are functionally more relevant for matching processes related to the regularity than for deviance detection, since regular tones that would match the listener's predictions evoked larger responses than did deviant tones that would violate them. In summary, the results of the ERSP analysis for the temporal and frontal clusters did not completely fit with general predictions from the MUM. However, now that the GBA can be analyzed within different brain regions, further refinements to the MUM need to be made to

describe how this activity may operate within temporal and frontal generators. According to MUM, GBA is enhanced when prior knowledge matches with the outcome of processing of the incoming stimulus. Regional specializations could bias processing of either standards or deviants to yield different matches. Thus enhanced GBA could provide some insight into the functional roles of local computation within brain regions participating in the acoustic analysis.

The perception of a changed stimulus as indexed by the MMN response at the scalp consistently coincides with changes in the long-range synchronous interactions among regions in the left and right STG (BA 22) with regions within the orbitofrontal cortex, (BA 11, the L IFG and R OG, in this study). Particularly consistent were increased long-range synchronous interactions for the deviant condition between the L STG and L IFG regions. This finding is in accordance with a recent MEG study of the MMN response to duration deviants among simple tonal stimuli that found low frequency (< 25 Hz) phase synchrony between left temporal and left frontal regions to be greater for the deviant condition than the standard condition (Hsiao, Cheng, Liao, & Lin, 2010). In our study network operations are modulated by stimulus condition with all nodes showing significant increases in synchronization for both the Deviant and the Standard conditions (relative to each other, not to baseline activity, see Figure 3.4). Network interactions common to both the passive and active paradigms are increased synchronization in the Deviant condition between the L STG and the ipsilateral L IFG (BA11), between the R STG and the ipsilateral R IFG (BA9),between the L STG and the contralateral R OG (BA11), and between the L IFG (BA11) and the homologue in the right hemisphere R OG (BA11) suggesting a stable functional core network for deviant processing (see Figure 3.4 A. and B. detailed schematics). The R STG maintains high frequency band synchronization with the L IFG across both the passive and active paradigms; however, this is increased for the Standard condition in the passive

paradigm but increased for the Deviant condition in the active paradigm. Friston's theoretical view is that the slower temporal dynamics are more appropriate for top-down effects, which tend to be modulatory and prolonged, while high frequency bands are appropriate for more transient sensory evoked responses (Friston, 2005). When viewed from this perspective the core network model of the MMN for both the passive and active paradigms portrays the orbitofrontal cortex as modulating the processing occurring in the L STG, the right inferior frontal cortex as modulating the processing occurring in the R STG whereas the R STG is feeding forward the more transient sensory information to the L IFG. In the passive paradigm, both left and right STG provide feed-forward input to sources in the orbitofrontal cortex (OFC) in the contralateral hemisphere, whereas in the active paradigm, just the R STG shows increased long-range synchrony for the Deviant condition in the high frequency band with the R OG, L IFG, and L STG. Overall, the active condition tends to have more long range interactions showing increased synchronization for the Deviant condition whereas the passive condition shows increased synchronization for the Standard condition (compare A and B in Figure 3.4). The finding that most network interactions in the active paradigm showed increased long range synchronization for the Deviant condition may reflect strengthening of coupling between task relevant areas to meet demands for attending to deviant targets. Our findings show long-range synchronization in gamma-band has a different role within the passive and active paradigms: significantly greater increases in long range synchrony for the Standard condition in the passive listening paradigm but greater for the Deviant condition in the active listening paradigm (see Figure 3.4 for increased synchrony by stimulus condition with passive and active paradigms). Interestingly, the long-range synchrony between network sources support our predictions from the MUM models (Hypothesis I b) more so than our predictions regarding the local synchrony within sources (Hypothesis I a). An

exception occurs between the R STG and R OG within the active paradigm: gamma-band increases are greater in the Standard condition. This exception may reflect the dynamic assignment of the R OG to the specific or exclusive role of processing the acoustic regularity while other resources are directed to processing the deviant or relaying prediction error.

Task demands of selective attention did modulate the character of these long-range synchronous interactions. The most notable was long-range gamma-band synchrony involving the R OG: in the passive paradigm synchrony was sustained across most of the analysis epoch, whereas in the active paradigm it was focused in periodic short bursts (see Figures C.4, C.5, C.8 in Appendix). Other studies have found attention, like the processes of working memory and perceptual organization, to be associated with gamma band oscillations modulated at theta band rhythms (Burgess & Ali, 2002; Schack, Varth, Petsche, Geissler, & Moller, 2002; Sauseng, Klimesch, Gruber, & Birbaumer, 2008). A recent study from our lab using a selective visuospatial cuing paradigm found that deploying attention to one visual hemifield yielded transient long-distance gamma-band synchronization between widespread brain regions that was modulated at a theta rate (Doesburg, Roggeveen, Kitajo, & Ward, 2008) and speculated this effect may arise from the influence of another network source, possibly the thalamus, using a lower frequency band as a means to interact with both sources, possibly to facilitate the long range gamma band interaction. Interestingly, within both paradigms, gamma-band synchrony within the latency of the MMN (120-250 ms) occurs during interhemisphere interactions (the longer cortico-cortical connections), but is absent for intrahemisphere interactions, the one exception is in the active paradigm between the R STG and R OG. Such facilitation might be necessary to maintain long range gamma band synchrony for extended periods when sources are separated by great distances. Although there is evidence that nature of the anatomical

connection is more relevant to the viability of long range gamma synchrony than to the distance between brain regions (Csicsvari et al., 2003), it is important to point out that functional connectivity as represented by long range synchrony of our models is not necessarily mediated by direct anatomical connections. Key elements of Friston's MMN model have been supported by our analysis, namely nodes in the L STG, R STG, and R IFG. These synchronous interactions may be a means of modulating the processing in the right hemisphere nodes should auditory stimuli become behaviourally relevant. During the behavioural discrimination task of our study, the R STG long-range interactions with R IFG were augmented by interactions with the R OG (compare Figure 3.3A with 3.3B). As well, the active paradigm showed temporal coordination between the left and right STG, not seen in the passive paradigm. The temporal coordination between bilateral homologous regions during the active paradigm may relate to increased task demands requiring more bilateral processing. Interestingly, the additional cross-coherent activity in the right hemisphere between the R STG and the R OG during the active task does complete a pattern of interactions which mirrors that of the left hemisphere, giving at least the appearance of symmetrical bilateral processing in the active paradigm.

Because our analysis did not uncover multiple independent sources in each auditory cortex, extrinsic interactions between intrahemispheric A1 and STG sources could not be assessed. Instead single sources in slightly different locations were found within each temporal cortex. This may reflect the different and possibly independent processing occurring in these regions. Friston's model may be too broad for this particular paradigm, in that perhaps processing here could be dominated by a subset of generators from Friston's model. More complicated stimuli or patterns of stimuli may require contributions from temporal generators that the present simple stimuli did not engage. The R OG and L IFG in this paradigm appear to

mediate between the L STG and the R STG. Consistent with graph theory this sparse linking between sources is an efficient means of relaying information with little redundancy. Another possibility is that the processing occurring in the respective primary auditory areas is not unique enough to be separated by ICA limited to 30 clusters and these sources get lumped with processing occurring in the neighboring STG. Or it may be that, for this particular paradigm, processing in the region of the R STG dominates primary sensory analysis, with refinements from the feedback loops between the orbital frontal cortex and L STG.

One caveat regarding our decision to perform ICA over concatenated passive and active paradigms is that this approach yields a core set of MMN network nodes operating during both listening conditions allowing us to observe increases or decreases in IC activations as a function of task. However, this approach may not reveal nodes that are unique to each condition. We speculate that in the active listening condition top-down control may also recruit additional prefrontal and parietal regions from the dorsal attention network, specialized for selecting and linking stimuli and responses. In the next experiments ICA was conducted separately for passive and active paradigms to show the different nodes of the network emerging from task demands.

A) Passive Paradigm Network

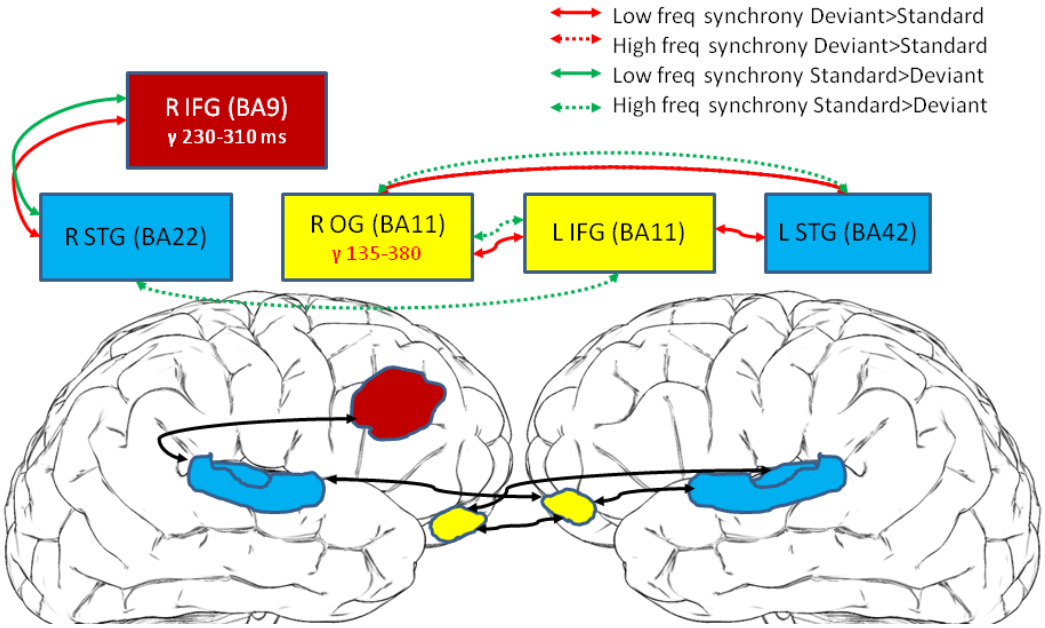

B) Active Paradigm Network

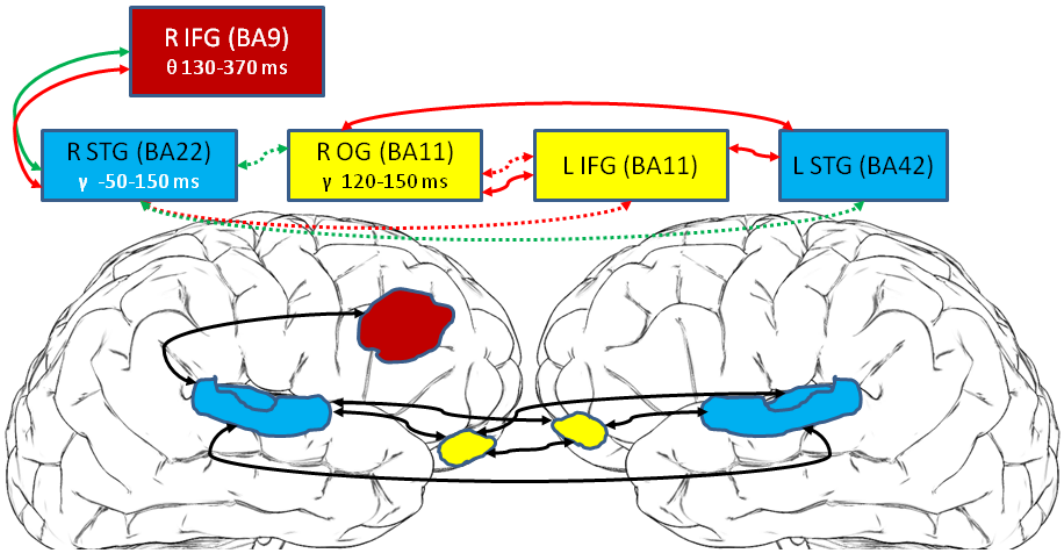

Figure 3. 4. MMN network as modulated by stimulus condition for passive and active paradigms. Regional interactions mapped in brain space by black double ended arrows provide broad view of MMN network, with a more detailed schematic provided above. Solid coloured arrows denote low frequency band (5-29 Hz), dotted coloured arrows denote high frequency band (30-55 Hz). Red: significantly greater synchrony for the AC Deviant condition. Green: significantly greater synchrony for the Standard condition.

CHAPTER 4: SPEECH STIMULI RECRUIT LTM REGIONS TO MMN NETWORK

Introduction

Previous research has found the MMN response to familiar and meaningful words is larger than to unfamiliar and meaningless pseudo words (Pulvermüller, et al., 2001). Similarly, the processing of speech segments relevant to one's own language evokes larger MMN responses than to non-native speech segments (Rivera-Gaxiola, Csibra, Johnson, & Karmiloff-Smith, 2000; Dehaene-Lambertz, 1997). As well, MMN responses to meaningful acoustic contrasts that cross a phoneme category boundary produce larger MMN responses than to meaningless acoustic contrasts which fall within a phoneme class (Phillips, et al., 2000). In summary, the MMN has been shown to index acoustic and phonological changes between linguistic units as well as semantic, lexical and syntactical information changes (Shtyrov et al., 2003; Pulvermüller and Shtyrov, 2006; Shtyrov, Hauk, & Pulvermüller, 2004; Shtyrov & Pulvemüller, 2007). The ability to assess complex familiar linguistic constructs within 200 ms of stimulus onset is unexplained by the predictive coding model of the MMN, a "tabula rasa" network endowed with inhibition and adaptation but lacking learning or long-term memory mechanisms. According to Pulvermüller the ability to automatically detect changes in complex sensory events depends on the ability to store meaningful aspects of the environment that occur regularly and with high frequency. Acoustic elements that are more relevant to one's experience such as meaningful language units are believed to be better developed in long term memory (LTM) as a consequence of repeated activation of specific sets of cells. These stimulus-specific memory circuits due to their strong internal connections effectively amplify sensory-elicited activity resulting in more robust automated responses to familiar or linguistically relevant stimuli (Pulvermüller, et al., 2001). Indeed, the MMN response to speech stimuli are larger over the left hemisphere (Alho, et

al., 1998), and generators for the MMN elicited from speech processing have been localized to the anterior regions of the left STG (Nääatänen, et al., 1997). Further support comes from aphasic patients with left hemisphere damage to the temporal regions have attenuated MMN responses to speech stimuli (Aaltonen, Tuomainen, Laine, & Niemi, 1993), but comparable responses to healthy adults for nonspeech stimuli (Ilvonen, et al., 2004).

Simulations with a neurobiologically-grounded model indicated that while neuronal adaptation and local inhibition of cortical activity can explain some aspects of change detection, the robust MMN response to meaningful linguistic elements cannot be explained on the basis of adaptation and inhibition alone. The larger MMN response to familiar and linguistically relevant stimuli is better explained by a neurocomputational model of change detection that includes adaptation, inhibition and LTM (Garagnani & Pulvermüller, 2010).

In the following experiments we use passive and active oddball paradigms with two types of acoustic contrasts, speech syllables that cross phonetic boundaries (across-category, AC) and those that do not (within-category, WC) to explore the effects of meaningful contrasts on the MMN network. We expect AC deviants to evoke a MMN response that lateralizes to the left hemisphere as previous studies have shown (Shtyrov, Kujala, Lyytinen, Ilmoniemi, & Näätänen, 2000; Näätänen, Jacobsen, & Winkler, 2005). Within category deviants are not expected to elicit the MMN response. If network interactions between sensory cortices and frontal sources included those in the left frontal regions specialized for processing certain types of linguistic information (Molholm, Matinez, Ritter, Javitt, & Foxe, 2005), we expect the MMN core network interactions between the orbitofrontal cortex regions and STG found in the previous experiments to expand to include regions of the left inferior frontal gyrus (L IFG or Broca's area) thought to be involved in the storage and retrieval of phonological and semantic information.

Materials and Methods

Participants

Eighteen right-handed (Oldfield, 1971) subjects participated in the passive listening paradigm (aged 19 - 31 years, mean age 23.1, SD 3.3, 7 men). Data from four of these participants were excluded from analysis, two for reasons of excessive movement during the recording session and two subjects were questionable native English speakers. All remaining participants were native English speakers born to English-speaking parents. Fifteen subjects from the original 18 were asked to return for the follow-up active listening session. Data from two subjects for the follow-up study were excluded from analysis, one for excessive muscle artifact (the same subject's data were excluded from the first session) and another due to a procedural error (the experiment debriefing summary was inadvertently read by the subject prior to the task and appeared to skew this subject's behavioural performance compared to other subjects with no such prior knowledge). All participants had no known history of neurological problems and passed a hearing screening (by tympanometry and otoacoustic emissions) at the time of the EEG acquisition. All provided written consent and were paid an honorarium for their time. The experiment was approved by the Behavioural Research Ethics Board of the University of British Columbia.

Stimuli and Procedure

The stimuli were three speech segments, naturally produced and then digitized, that have been used in previous studies (Werker & Lalonde, 1988; Rivera-Gaxiola, Csibra, Johnson, & Karmiloff-Smith, 2000). The three speech segments, approximately 400 ms in duration, contained the same neutral vowel /a/ but differed in the place of articulation for the initial consonant: labial plosive /b/, dental plosive /d/, and retroflex plosive /d/. The contrast between

the retroflex /d/ and dental /d/ plosives carries no meaning in English consequently native English speakers typically consider /d/ and /d/ to be the same phoneme, despite their acoustic differences. These alveolar plosives represent within-category (WC) contrasts. The acoustic difference between the bilabial plosive /b/ and either of the alveolar plosives (/d/, /d/) is meaningful in English and these represent across-category (AC) contrasts. Our oddball paradigm embedded both AC and WC contrast deviants among a series of alveolar standards (see Table 4.1 for the types and probabilities of stimuli in each block). Each block contained 660 stimuli, 86% of which were standards, 7% WC deviants, and 7% AC deviants. In one block the dental /d/ served as the standard, in another block the retroflex /d/ was the standard. Block 1 alternated with Block 2 for two runs (for a total of 4 blocks) and the initial block order was counterbalanced across subjects. A pseudo-random allocation of deviant stimuli was used so that no fewer than two standard stimuli preceded a deviant, and no two deviant stimuli appeared in succession. The total trials were 2640. ISI varied between 1500-1700 ms. Each block was approximately 22 minutes in length. Short breaks of 2-5 minutes were given between blocks.

Table 4. 1. Types and probabilities of stimuli in each block

p	**Type**	**Block 1**	**Block 2**
.86	Standard	dental /da/	retroflex /da/
.07	AC Deviant	labial /ba/	labial /ba/
.07	WC Deviant	retroflex /da/	dental /da/

The experiment was run twice, in two separate sessions. The first session involved passive listening followed a few weeks later by a second session involving an active listening task. Participants were unaware of a follow-up second session at the time of the first session. During the first session participants were instructed to watch a silent video with closed captioning and to ignore the sounds heard binaurally through insert earphones (E.A.R. 3A). For the second session participants were asked to discriminate between standard and deviant auditory stimuli and to ignore the video. Closed captioning during this second session was disabled because it was found during pilot testing to be too distracting for attending to auditory stimuli. Participants' behavioural and electrophysiological responses were monitored during each block. If mistakes responding to standards or AC deviants occurred successively, participants were informed and given a break. Participants were to begin the discrimination task after they heard enough examples of the frequently repeating sound (typically 3 – 5 presentations) to establish it as the standard tone and to press the corresponding "standard" button labeled on the computer mouse. They were instructed to note *any* changes to the standard stimuli by pressing a separate button pressed labeled "deviant". EEG recording and ICA decomposition have been described in previous the chapter and remained unchanged for the present experiments.

Results

Behavioural Analysis

All subjects easily selected the appropriate button in response to the AC deviant and to the standard, with a detection error lower than 4% for the group. However, for the WC deviant, detection error approached 100%. Since the WC deviant made up 7% of the task stimuli, the overall detection error for the task was 11%. No significant difference in performance was found

between blocks. However, there was more variability in incorrect responses when the retroflex /da/ served as the standard.

ERP Analysis

The stimulus conditions were collapsed across blocks as no significant differences were found responding to AC Deviants or WC Deviants against dental or retroflex Standards. Trials with activity exceeding 50 μV during the examined epoch were not included in any grand average. The WC Deviant, the AC Deviant, and the Standard (last standard stimulus to precede each AC Deviant) grand averages were computed for a subset of sensors (F3, FZ, F4, C3, CZ, C4, P3, PZ, P4, T7, and T8). We opted to calculate a single standard condition to avoid differences arising between the separate standard conditions (i.e., differences between a standard preceding a WC Deviant vs a standard preceding an AC deviant). The respective difference waves were calculated to confirm that the MMN response was evoked as expected by the AC Deviant condition but not by the WC Deviant condition in both passive and active paradigms (see difference waveform in Figure 4.1 – 4.4). For both paradigms the MMN response to the AC Deviant condition was largely absent at the frontal sites and the negative difference wave was maximal instead at the Cz sites from ~150 to 210 ms. Collapsing across blocks may have been the reason for the attenuated MMN response (~ 0.5 μV in our passive paradigm) as previous research (Rivera-Gaxiola, Csibra, Johnson, & Karmiloff-Smith, 2000) using the same stimuli found no MMN response to /ba/ deviants within a series of retroflex /da/ standards, only a MMN response for /ba/ deviants in a series of dental standards. For the passive paradigm the MMN response attenuates at lateral and posterior sites (see Figure 4.1). In the active paradigm, however, the MMN response is prominent at lateral and posterior sites (see Figure 4.3). Here the

MMN is likely summing with additional negativity from the N2b component (followed by the P3b positivity) from the attention and behavioural demands of the task.

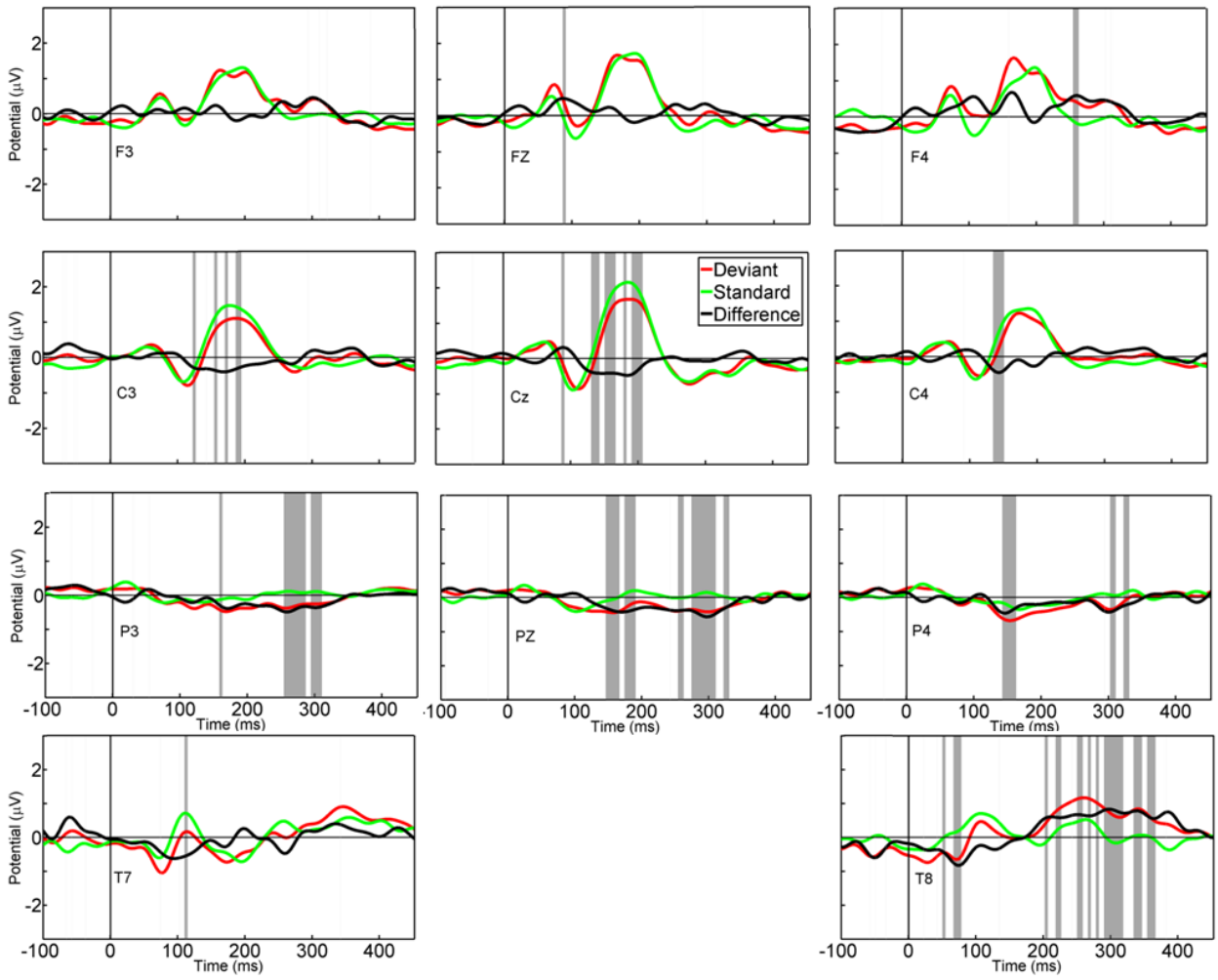

Figure 4. 1. Grand mean ERP AC Deviant – Standard for passive paradigm. Standard (green) and Ba Deviant (red) and their Difference (black, Deviant minus Standard) at F3, FZ, F4, CZ, C3, PZ, C4, T7 and T8 electrodes from -100 to 450 ms. Stimulus onset at 0 ms. Shaded regions are significantly different ($p < 0.05$). Negative is down. MMN response absent at frontal sites, but prominent at Cz from 150 to 210 ms and then attenuates at lateral and posterior sites.

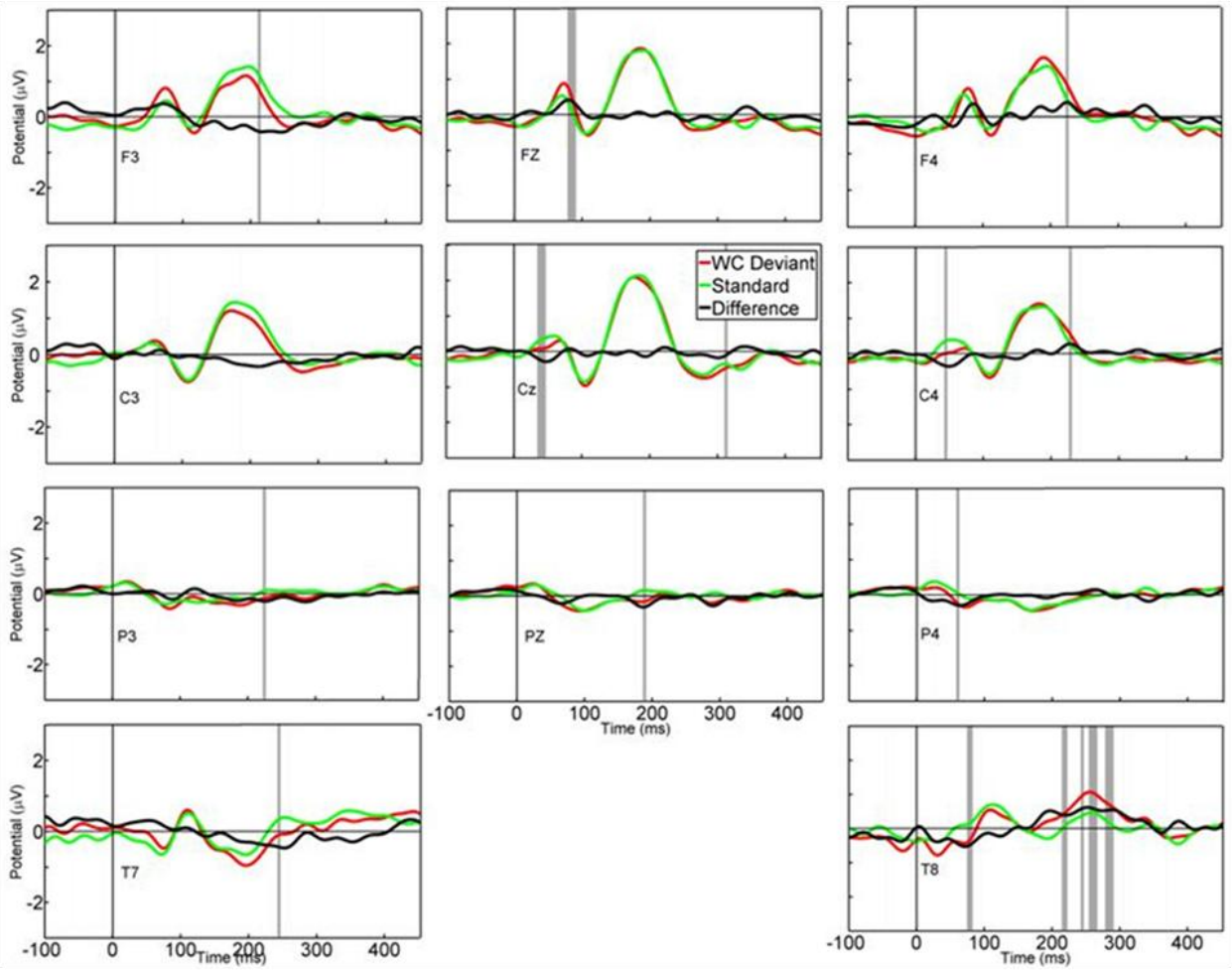

Figure 4. 2. Grand mean ERP WC Deviant – Standard for passive paradigm. Standard (green) and Within-category Deviant (red) and their Difference (black, Deviant minus Standard) at F3, FZ, F4, CZ, C3, PZ, C4, T7 and T8 electrodes from -100 to 450 ms. Stimulus onset set at 0 ms. Shaded regions are significantly different ($p < 0.05$). Negative is down. No MMN response at FZ or CZ sites. There is a negativity difference between conditions at Pz and the left lateral sites F3, P3, and T&, however the region of significance is not sustained across adjacent data points.

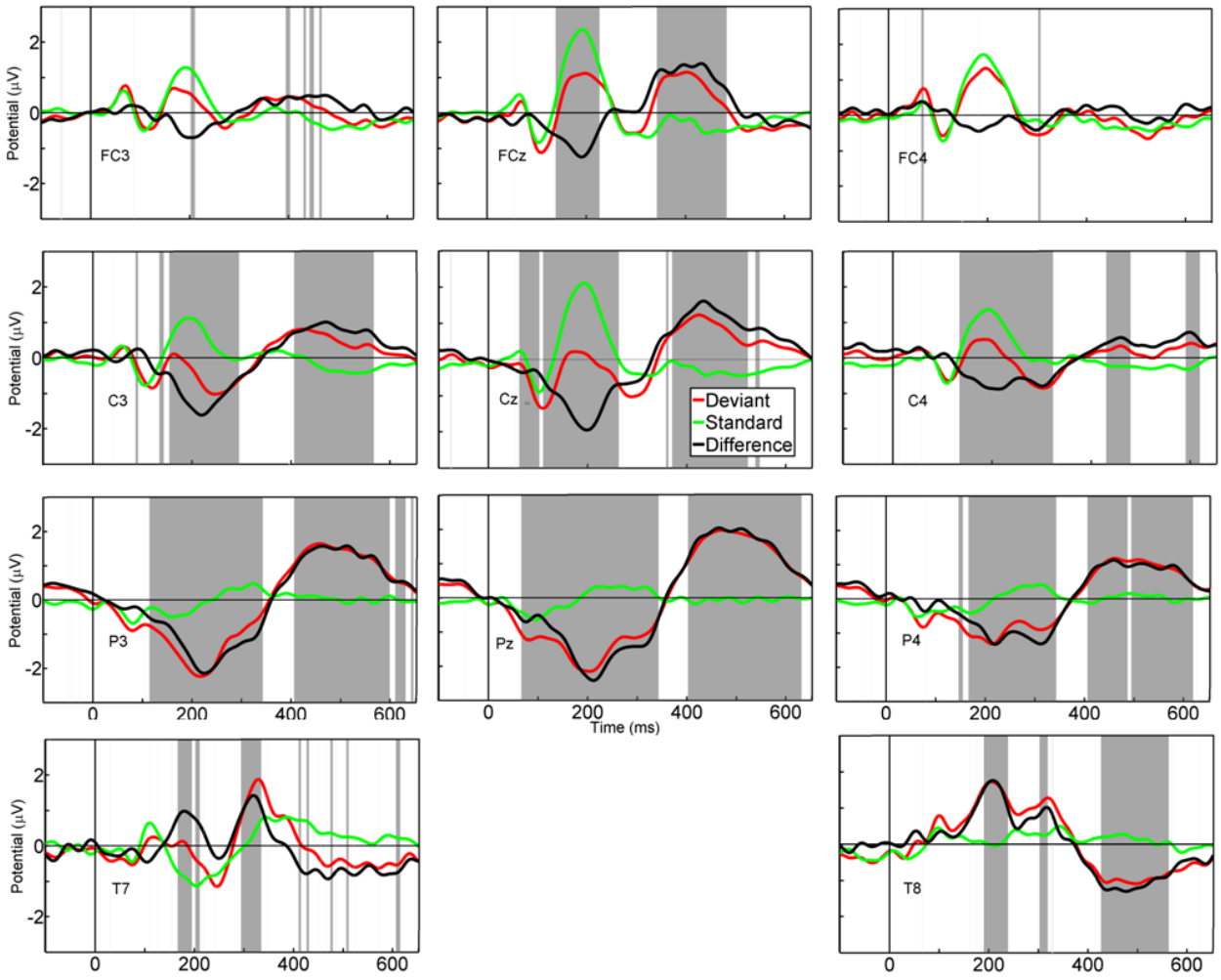

Figure 4. 3. Grand mean ERP AC Deviant – Standard for active paradigm. Standard (green) and Deviant (red) and their Difference (black, Deviant minus Standard) at F3, FZ, F4, C3, CZ, C4, P3, PZ, P4, , T7 and T8 electrodes from -100 to 650 ms. Stimulus onset set at 0 ms. Shaded regions are significantly different (*t*-test, $p < 0.05$). Negative is down. MMN response absent at frontal sites, but prominent at Cz and Pz and then attenuates more at right lateral sites. There may be addition negative contribution from N2b adding to the negativity at Pz.

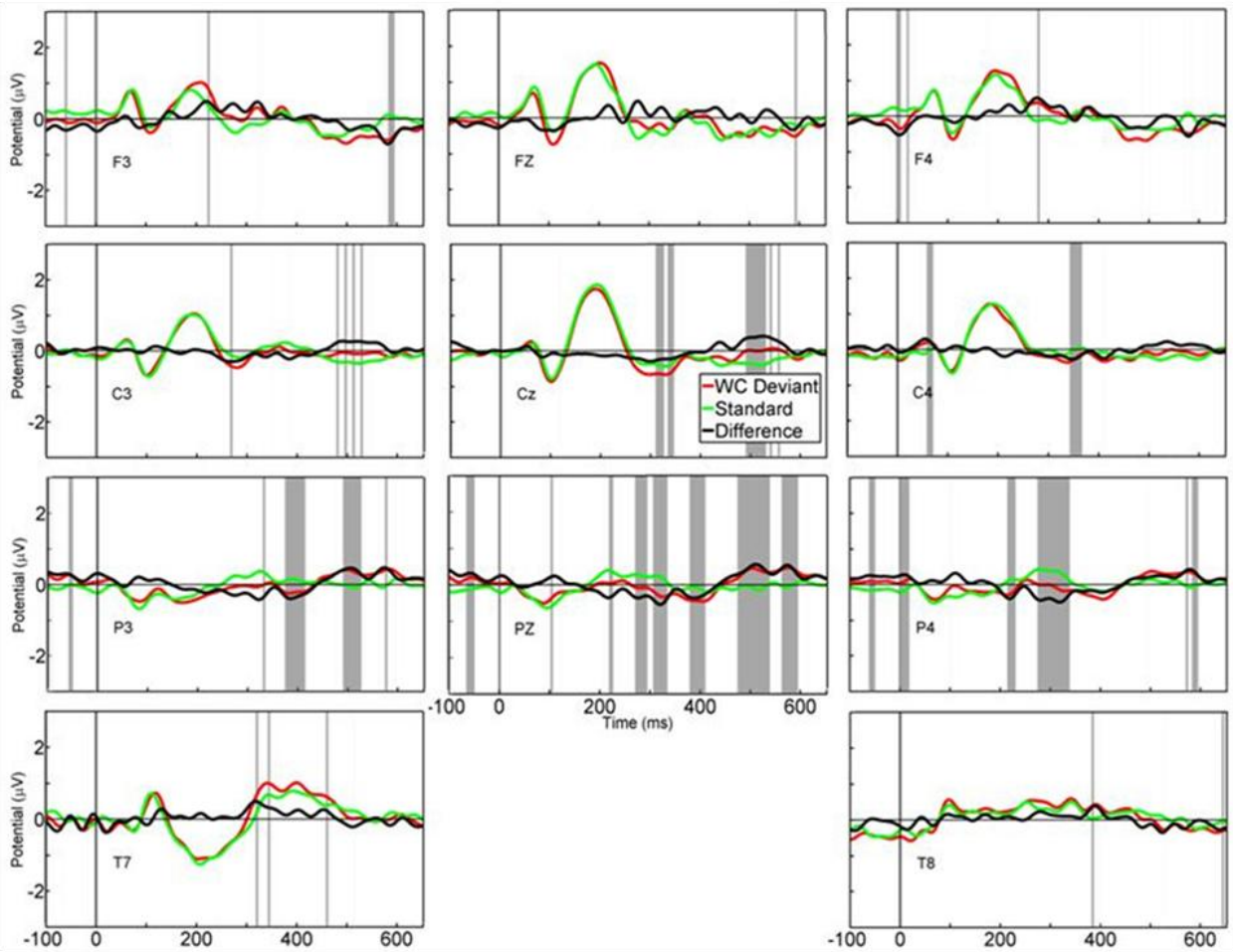

Figure 4. 4. Grand mean ERP WC Deviant – Standard for active paradigm. Standard (green) and Deviant (red) and their Difference (black, Deviant minus Standard) at F3, FZ, F4, C3, CZ, C4, P3, PZ, P4, T7 and T8 electrodes from -100 to 650 ms. Stimulus onset set at 0 ms. Shaded regions are significantly different (*t*-test, $p < 0.05$). Negative is down. There is a negativity difference between conditions at Fz at 120 ms however this did not reach significance.

Cluster Analysis

Cluster analysis of ICs was based on IC dipoles and ERSPs (0 - 550 ms, 5 - 55Hz). As in the previous experiment, a larger number (k=30) of clusters was chosen to group individual dipoles in this experiment resulting in less post hoc pruning within clusters. The largest cluster contained data from only 71% of subjects, or 11/14 subjects. No cluster with fewer than 50% subject contribution is reported here. See Table 4.2 and 4.3 for details of cluster properties.

Regions of Interest (ROI) for the MMN

The regions of the STG (any of BA 41, 42 and 22) in the right and left hemispheres as well as the orbital frontal cortex (BA 10 or 11), in either the right, left or both hemispheres were expected to emerge from the cluster analysis as sources for the MMN as these regions were shown in the previous experiments to be major contributors to the MMN network. In addition, regions involved in the linguistic processing (44, 45 and 47 in the left hemisphere) were expected to join the MMN network. For the active task components of the ventral attention network (R TPJ, R IFG) were expected to emerge as sources given the response requirement (button press) to the deviant and standard stimuli. The anterior cingulate (BA32) was also thought to be a possible source in the active task as it involved more monitoring to differentiate between appropriate responses.

Event Related Spectral Perturbation Analysis

The spectral power changes (or perturbations) over time between post-stimulus activity and the baseline (pre-stimulus) activity are shown for the passive paradigm in Figures E.1 – E.6, in the Appendix. Note when viewing the ERSP plots that the Standard condition is the same for both AC Deviant and WC Deviant conditions, however the plots for the Standard may appear slightly

Table 4. 2. Cluster properties for passive paradigm. ROI in bold.

Cluster Brain Region*	% of Subjects Contributing	BA	Talairach x, y, z	RV% dipole fit
L CBL	71	NA	-31, -80, -33	4.73
L CING	79	31	-11, -33, 41	5.44
R CBL	71	NA	16, -85, -21	8.35
L MTG	71	39	-40, -52, 10	10.31
L IFG	**57**	**47**	**-52, 44, -13**	**9.32**
L CING	57	32	-3, 12, 42	5.30
L CBL	64	NA	-34, -36, -47	9.54
L PCG	86	6	-38, -13, 30	5.83
L IFG	**64**	**45**	**-62, 16, 19**	**7.45**
R STG	**79**	**42**	**71, -11, 4**	**5.98**
L SFG	**57**	**10**	**-27, 73, 2**	**7.35**
L STG	**86**	**42**	**-73, -18, 1**	**4.84**
R SFG	**57**	**10**	**13, 57, -7**	**6.33**
L CAUDATE	50	NA	-7, 15, -7	8.99
L MOG	64	18	-32, -87, 3	7.33
R IFG	**64**	**45**	**52, 38, 7**	**9.03**
R MTG	71	37	53, -66, 5	8.11
R OL	71	17	8, -94, -3	6.55
R PCG	79	6	39, -1, 39	8.36
R OL	71	31	18, -67, 18	7.17
R IPL	79	40	33, -38, 37	6.89

BA Brodmann Area; **CBL** cerebellum, **CING** cingulate gyrus; **IFG** inferior frontal gyrus; **IOG** inferior occipital gyrus; **L** left; **MFG** middle frontal gyrus; **MOG** middle occipital gyrus; **MTG** middle temporal gyrus; **NA** not applicable; **OL** occipital lobe; **PCG** precentral gyrus; **R** right; **STG** superior temporal gyrus, **WM** white matter.
*Regional locations based on centroid mean, not all ICs within a cluster fall within a region.

Table 4. 3. Cluster properties for active paradigm. ROI in bold.

Cluster Brain Region*	% of Subjects Contributing	BA	Talairach x, y, z	RV% dipole fit
L PCG	54	3	-30, -20, 44	5.78
R IFG	**77**	**47**	**31, 33, -6**	**8.28**
L INSULA	62	13	-24, -36, 26	6.54
R MOG	85	18	32, -82, -9	3.91
L OL	69	7	-6, -69, 31	5.56
R STG	**85**	**22**	**69, -15, -1**	**8.06**
L MTG	54	37	-55, -63, 9	6.90
L STG	**92**	**22**	**-69, -18, -2**	**6.85**
R CING	**54**	**32**	**3, 14, 37**	**7.22**
R PCG	77	6	53, 0, 27	5.40
L IFG	**77**	**44**	**-59, 12, 17**	**7.23**
L IOG	62	17	-11, -90, -9	4.32
L IFG	**54**	**10**	**-45, 46, 0**	**9.05**
R CAUDATE	62	NA	24, -34, 14	4.36
R MOG	69	WM	35, -68, 16	7.29

BA Brodmann Area; **CING** cingulate; **IFG** inferior frontal gyrus; **IOG** inferior occipital gyrus; **L** left; **MFG** middle frontal gyrus; **MOG** middle occipital gyrus; **MTG** middle temporal gyrus; **NA** not applicable; **OL** occipital lobe; **PCG** precentral gyrus; **R** right; **STG** superior temporal gyrus, **WM** white matter. *Regional locations based on centroid mean, not all ICs within a cluster fall within a region.

different in absolute amplitude because comparisons within conditions share a common baseline. The results of the ERSP contrasts for the WC conditions are provided but will not be discussed further as this condition produced no MMN response at the scalp. The pre-stimulus baseline was limited to the period from -150 to -50 ms before sound onset to reduce overlap of pre-stimulus and post-stimulus activity due to wavelet temporal smearing. Significant differences between the ERSP of each condition are masked at $p < 0.05$ by permutations (see far right columns in Figures E.1 and E.6, differences in burgundy against a green background). For simplicity, we report all differences in terms of the condition showing the greater power (displayed in red or yellow in the first two columns). Finally, only differences that were significant by the permutation test for at least 1 frequency cycle were considered to be significant, again to reduce the possibility of making Type I errors. The ERSP results are summarized in Table 4.4.

ERSP for Temporal Clusters

The clusters in the region of the auditory cortex (L STG and R STG) show significant differences between standard and deviant conditions in gamma-band power for the passive paradigm (see Figure E.1. in the Appendix). Specifically, in the L STG the AC Deviant stimuli show a significantly greater power increase within a lower (~30 Hz) portion of the gamma-band during the latency of the MMN between 50-200 ms. In contrast, the Standard stimuli show a significantly greater power increase in a higher portion (~50 Hz) of the gamma band during the MMN latency from 0-220 ms. Thus both stimulus conditions in the passive paradigm display increases in gamma band power within the latency of the MMN but in different portions of the gamma band. This suggests that within an auditory area different parts of the gamma band might be allotted to the processing of different categorical aspects of the auditory stimuli.

For the R STG the AC Deviant stimuli show no significantly greater power increase during the MMN compared to the Standard stimuli. The Standard stimuli show a significantly greater power increase in the middle of the gamma band during the MMN latency from 160-220 ms and in the beta band between 130-190 and 200-270 ms compared to AC Deviant stimuli.

In the Active condition (see Figure E.4.) differences in gamma-band power occured only at stimulus onset: no gamma-band power differences occurred within the latency of the MMN. The L STG differences in power during the MMN period were limited to increased theta-band power for the AC Deviant stimuli between 120-290 ms. For the R STG no significant power differences occurred during the MMN period. These data are consistent with a model that speech processing occurs bilaterally in auditory cortex (Hickok & Poeppel, 2000; Poeppel, Guillemin, Thompson, Fritz, Bavelier, & Braun, 2004). Within the passive paradigm, differences in gamma power are apparent at stimulus onset for the L STG reflecting perhaps the proclivity for fast temporal analysis (e.g. formant transitions) whereas in the R STG the gamma power differences tended to occur later, consistent with analysis of 'slow' components (envelope of syllable, intonation contour) (Zatorre, Belin, & Penhune, 2002; Poeppel, 2003). The L STG shows more gamma-band power differences within the latency of the MMN suggesting that the left auditory cortex has a greater involvement in the processing of linguistic contrasts. Compared to the passive paradigm, the active conditions show very limited and restricted areas of increased power. Increases in power occurred in brief bursts near stimulus onset that may be indicative of increased inhibitory control from top down modulations.

ERSP for Frontal Clusters

In the active paradigms the left frontal sources show increases in gamma power during the latency of the MMN for the Standard compared to the Deviant stimuli suggesting perhaps that

this region is specialized for attending to the features or properties of the acoustic regularity (see Figure E.5.). In the L IFG (BA10) source the Standard shows significantly greater power increase in gamma-band from 80-600 ms and beta-band from 70-480 ms compared to the AC Deviant stimuli. The roughly corresponding region in the passive paradigm, L SFG (BA 10), shows no differences in power related to stimulus type. The L IFG (BA47) in the passive paradigm, however, is very similar in showing gamma-, alpha- and theta-band increases power during the latency of the MMN in just the Standard stimuli (see Figure E.2). No comparison with the active paradigm can be made as this region did not meet inclusion criteria for a valid cluster for that paradigm.

Different subregions of Broca's area, BA45 and BA44, emerged as valid clusters for the passive and active paradigms respectively. This anatomical split might be related to functional differences between the anterior and posterior regions of Broca's area. Area 44 may be more relevant to the processing of the phonological aspects of the stimuli when they are linked to a motor output. In the passive paradigm (see Figure E.2), the AC Deviant stimuli have greater theta-band power relative to the Standard stimuli between 0-240 ms. For Broca's area in the active paradigm, the Standard stimuli show significantly greater power increase in the gamma-band during the latency of the MMN. Specifically, gamma-band power increases are greater between -80-220, 150-220, and -80-520 ms in the Standard stimuli compared to AC Deviant stimuli (see Figure E.5.).

The R IFG (BA 45, right hemisphere homologue to Broca's area) for the passive paradigm only (no corresponding area in active paradigm) shows significantly greater power increases in the gamma band for both AC Deviant stimuli and the Standard stimuli, but never within the latency of the MMN (see Appendix D for significant power increases outside the

MMN latency region). This suggests that it may not be involved in the change detection processing but rather may contribute to subsequent attention switching should ay detected change prove relevant. The R SFG (BA10) in the passive paradigm shows significantly greater power increase in the gamma band for both AC Deviant stimuli and the Standard stimuli but never within the latency of the MMN. There is no corresponding region in the active paradigm. A previous study has shown that the frontopolar cortex (sub region of the FOC referring to BA10 exclusively) may be less active when attention is directed toward the auditory stream. (Salmi, Rinne, Koistinen, Salonen, & Alho, 2009). Selective attention may have some attenuating effect on the R SFG contribution to the task or possibly attention focuses or restricts activity to just the left frontopolar region (more on this in the discussion). In the active paradigm for the R IFG (BA47) the Standard stimuli show significantly greater power increase in the gamma band during the MMN latency compared to each deviant condition suggesting a role in the processing of the acoustic regularity. Specifically gamma-band power for the Standard stimuli increased between 160-390 ms and again later between 460-630ms, whereas power in the beta-band increased between -100-50 ms compared to AC Deviant stimuli.

The anterior cingulate (BA32) in the active paradigm also shows significantly greater power increase in the gamma band in the Standard stimuli compared to the AC Deviant stimuli but not within the latency of the MMN (see Appendix D). The Standard stimuli show significantly greater power increase in gamma band between 450-600 ms and in the beta-band between 0-100 ms compared to AC Deviant stimuli. The AC Deviant stimuli show significantly greater power increase in the beta band between -50-30 ms compared to the Standard stimuli.

Table 4. 4. ERSP results for stimulus conditions with the greater power (**γ** (30-55 Hz, 25ms) , **β** (13-29 Hz, 50 ms), **α** (9-12 Hz, 100 ms) , θ theta (≤8 Hz, 150 ms), $p < 0.05$) overlapping the MMN latency (120-250 ms) for a frequency cycle.

Conditions		**Temporal Clusters**		**Left Frontal Clusters**			**Right Frontal Clusters**	
Paradigm	**Stimulus**	**L STG (BA42)**	**R STG (BA42)**	**L SFG (BA 10)**	**L IFG (BA45)**	**L IFG (BA47)**	**R SFG (BA10)**	**R IFG (BA45)**
Passive	**AC Deviant**	**γ, 50-200**			**θ, 0-240**			
	Standard	**γ, 0-220**	**γ, 160-220** **β, 130-190** **β, 200-270**			**γ, 190-370** **α, 180-290** **θ, 110-360**		
	WC Deviant							
	Standard	**γ, -20-230** **θ, 160-350**	**γ, 60-150**	**γ, 0-190** **β, 0-180**	**γ, 50-170**	**γ, 120-340** **γ, 190-350** **γ, 430-650** **θ, 150-550**		**β, 190-440** **α, 60-230** **θ, 0-350**
Conditions		**Temporal Clusters**		**Left Frontal Clusters**			**Right Frontal Clusters**	
Paradigm	**Stimulus**	**L STG (BA22)**	**R STG (BA22)**	**L IFG (BA 10)**	**L IFG (BA44)**	*****	**R IFG (BA47)**	**R CING(BA32)**
Active	**AC Deviant**	**θ, 120-290**						
	Standard			**γ, 80-600** **β, 70-480**	**γ, -80-220** **γ, 150-220** **γ, -80-520**		**γ, 160-390**	
	WC Deviant							
	Standard			**γ, 150-230**	**γ, -20-220** **β, -100-180**		**γ, 100-150** **γ, 110-170**	

Cross-coherence Analysis

The cross coherence analysis described in Chapter 3 was applied similarly to these data: in brief, individual cross-coherences were masked at $p < 0.05$ to determine regions of synchrony significantly different from baseline for each stimulus condition. To determine group differences in cross-coherence between deviants and standard conditions during the MMN latency (120 – 250 ms) we used the permutation test, two-tailed, setting $p < 0.005$. This test contrasts the two conditions by subtracting the mean cross-coherence in one condition from the mean in the other, compared to a surrogate distribution of mean differences generated by random assignment of the scores to two groups, to determine the condition with the greater amount of cross-coherence in a predetermined frequency band within the MMN latency region. As the results of permutation test can be skewed by large differences from just a few subjects (a concern when cross-coherence is measured with just four to six subjects contributing pairs of ICs), we report significance differences only when they are supported by consistent non-zero cross-coherence for the group determined by the binomial probability computation with $p < 0.001$ (Onton, Delorme, & Makeig, 2005). For example, for those cross-coherences involving just four or five pairs, this requires all subjects to contribute cross-coherence significantly greater than zero at the .05 level within the MMN latency region for significant results of the permutation to be reported. The networks drawn from the cross-coherence results include only regional interactions that are significantly different between deviant and standard conditions during the latency period of the MMN because the MMN response at the scalp is derived from the difference between conditions. Tables 4.5 and 4.6 summarizes the significant cross-coherence differences in the passive and active paradigms respectively between AC Deviant and Standard stimuli and WC Deviant and Standard conditions for the temporal and frontal regions. As the AC Deviant

condition evokes the MMN response at the scalp only those interactions differentiated by the AC Deviant and Standard conditions (the top portion of the table) are included in the MMN network for the passive and active paradigms (Figures 4.5 and 4.6 respectively).

For the passive paradigm, cross-coherence analysis reveals a network consisting of the left and right STG (BA42), the right and left SFG (BA10), the left IFG (BA47), and the right IFG (BA45). The consistent wide band synchrony between the L STG and the anterior region of Broca's area (BA45) despite being only marginally differentiated by the stimulus type ($p < 0.05$) is a noteworthy interaction (See Figure 6 in Appendix F). Thus, it is included in the MMN network (see Figure 4.5, grey arrows). In the left hemisphere there was more synchronization for the Standard stimuli between the STG and two subregions of the IFG implicated in semantic and syntactical processing, BA45 and BA47 respectively. These results are consistent with Pulvermüller's view that a network model of MMN should include links to long-term stores of learned linguistic stimuli in order to explain the robust response to linguistically relevant stimuli. The L SFG (BA10, part of the OFC) is not directly synchronous with the L STG as seen in our previous experiment using complex tones; instead the L IFG (BA47) appears be an intermediating node, synchronized with the L SFG and L STG separately. The left SFG in turn is directly synchronous with the contralateral R IFG (BA45), unlike the passive network for tonal stimuli which had the R STG as mediator. Examining the local synchrony occurring with the nodes of each network provides some insight into the reasons for why these interactions may differ. The complex tonal stimuli evoke local power differences exclusively in the right hemisphere. The linguistic stimuli evoke local power differences in auditory cortex bilaterally and in most of the nodes in the left hemisphere, consistent with the view that linguistic stimuli are preferentially processed in the left hemisphere but involve both auditory cortices. It appears

the regional specializations for processing aspects of the stimuli necessarily impact on the long range synchronous interactions, evident in the differing links the R IFG maintains in the passive paradigms (compare Figure 3.3. A with Figure 4.5).

In the active paradigm, many of the network nodes are the similar to those of the passive paradigm. The left and right STG, the L IFG and R IFG (BA10 and BA47 respectively, regions of the OFC), Broca's area (posterior region, BA 44) and the right anterior cingulate (BA32) are synchronous during the MMN latency window. These interactions are different from the passive paradigm. Notably the interaction between the L STG and Broca's area (BA44) are significantly different by stimulus type at $p < 0.005$ and Broca's area now mediates interactions between the L STG and L IFG. The shift to the right hemisphere OFC source (R IFG, BA47) may occur in response the increased attention demands related to active listening and the R CING (BA 32) we speculate is recruited for response monitoring and control, respectively. Figure 4.5 and 4.6 present a MMN network model that reflects these findings.

Table 4. 5. Summary of significant cross-coherence differences for AC Deviant minus Standard and WC Deviant minus Standard within the MMN latency period (green box Standard > Deviant, red box Deviant > Standard, $p < 0.005$, except * $p < 0.05$) for passive paradigm.

		TEMPOROFRONTAL			FRONTAL			
		R STG~RSFG BA42~BA10	L STG~L IFG BA42~BA45	L STG~L IFG BA42~BA47	LSFG~R SFG BA10~BA10	L SFG~L IFG BA10~BA47	L SFG~R IFG BA10~BA45	L IFG~L IFG BA45~BA47
AC Dev-Standard	γ		*					
	β							
	α		*					
	θ							
WC Dev-Standard	γ							
	β							
	α							
	θ							

Note: No consistent cross-coherence differences for the temporal comparison L STG~R STG, or the following temporo-frontal comparisons: L STG~L SFG, R STG~L SFG, L STG~R SFG, R STG~L IFG(BA45), R STG~L IFG(BA47), L STG~R IFG, R STG~R IFG; or the following frontal comparisons: L SFG~L IFG(45), R SFG~L IFG(45), R SFG~L IFG(47), R SFG~R IFG, R IFG~L IFG(47), L IFG(BA45)~R IFG, L IFG(BA47)~R IFG.

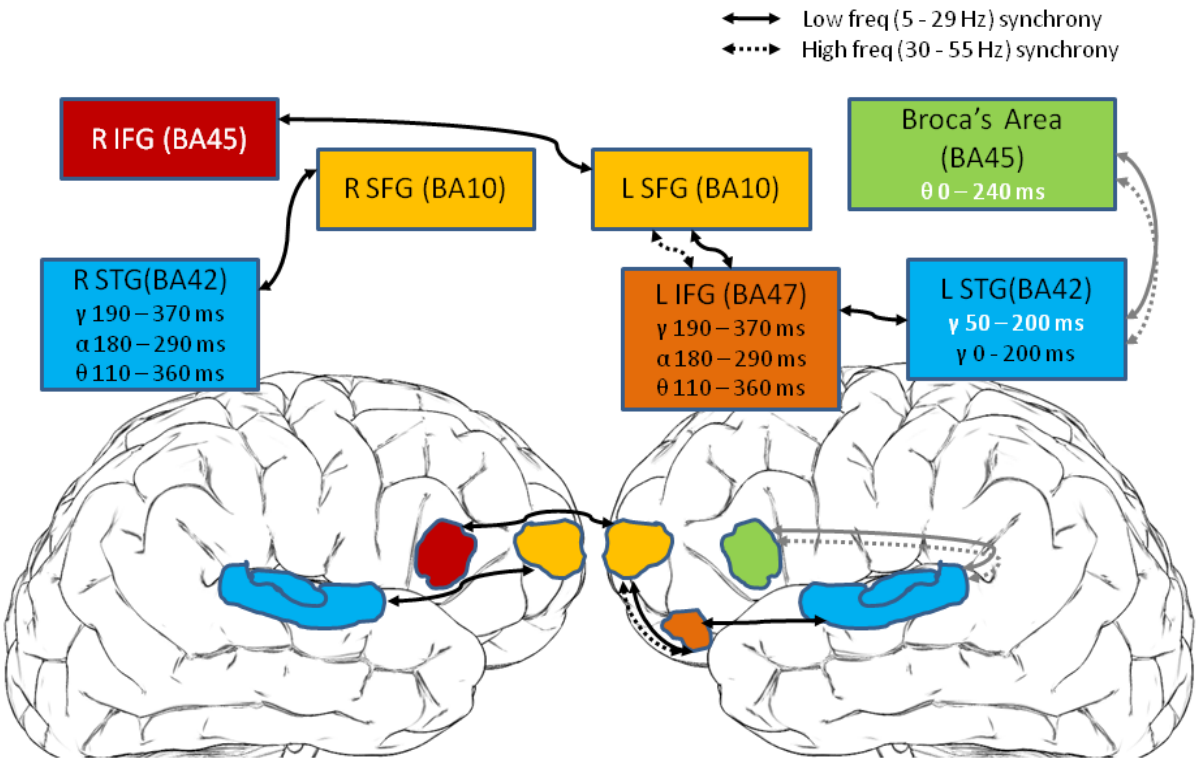

Figure 4. 5. MMN network model for passive oddball paradigm.

Cross-coherence analysis shows during the MMN latency window synchronous interactions differentiated by stimulus type ($p < 0.005$) within a network consisting of both left and right STG (BA42), both the left and right SFG (both BA10), R IFG (BA45), and the L IFG (BA47). Broca's area (BA45) maintains synchronous interactions with the L STG however these were weakly differentiated by condition ($p < 0.05$), represented by double-ended grey arrows. Long range (extrinsic) synchronous interactions ($p < 0.005$) are represented by double-ended black arrows (low frequency, 5-29 Hz, solid line; high frequency, 30-55 Hz, dotted line). Local synchrony increases (from ERSP) are displayed in black for standard and in white for deviant within regions.

Table 4. 6. Significant cross-coherence differences for active paradigm for AC Deviant minus Standard and WC Deviant minus Standard within the MMN latency period (green: Standard > Deviant, red: Deviant > Standard, post hoc comparison $p < 0.005$).

		TEMPORAL	TEMPOROFRONTAL			FRONTAL				
		LSTG~RSTG BA22~BA22	LSTG~L IFG BA22~BA10	L STG~L IFG BA22~BA44	R STG~R IFG BA22~BA47	L IFG~L IFG BA10~BA44	L IFG~R IFG BA10~BA47	L IFG~CING BA10~BA32	L IFG~R IFG BA44~BA47	R IFG~ CING BA47~BA32
AC Dev-Standard	γ									
	β									
	α									
	θ									
WC Dev-Standard	γ									
	β									
	α									
	θ									

*No consistent cross-coherence within MMN latency for the following temporofrontal comparisons: R STG~L IFG(BA10), R STG~L IFG(BA44), L STG~R IFG(BA47), L STG~CING, R STG~CING, or for the frontal comparisons : L IFG(BA44)~CING.

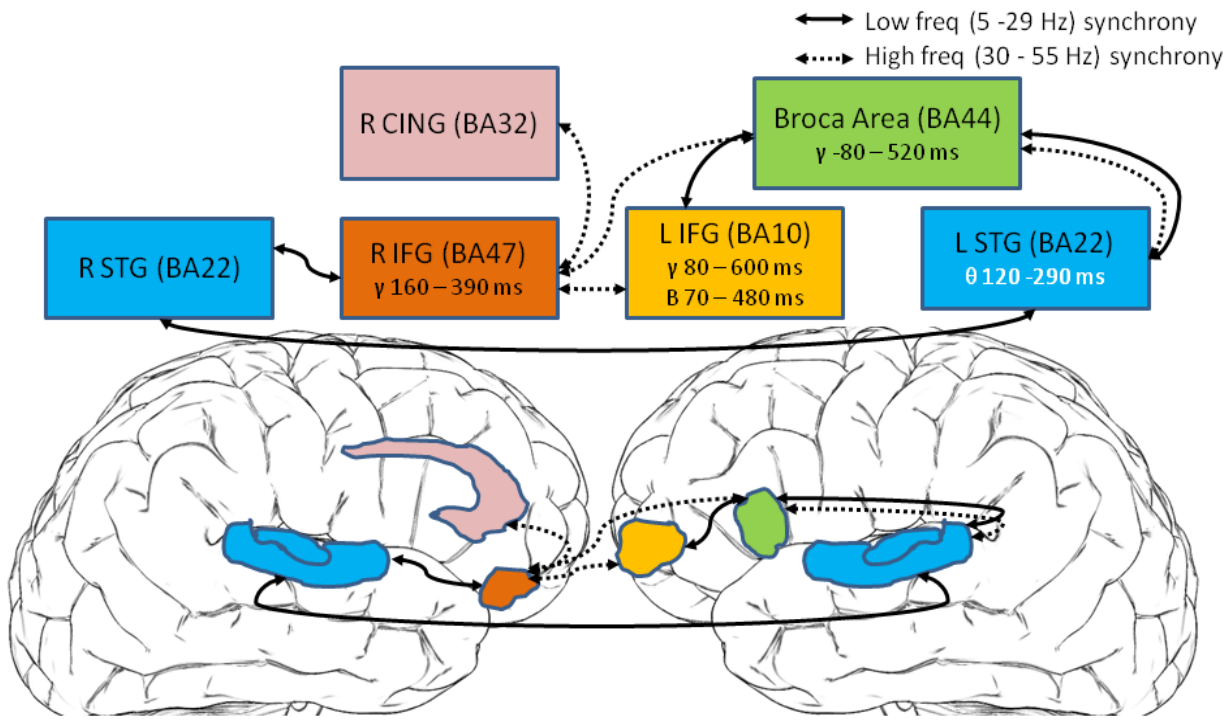

Figure 4. 6. MMN network model for active oddball paradigm.

Cross-coherence analysis shows synchronous interactions differentiated by stimulus type ($p <$ 0.005) within a network consisting of both left and right STG (BA22), the left IFG (BA10), Broca's area (BA44), the R IFG (BA47), and the R CING (BA32). Long range (extrinsic) synchronous interactions are represented by double-ended black arrows (low frequency, 5-29 Hz, solid line; high frequency,30-55 Hz, dotted line). Local synchrony increases (from ERSP) are displayed in black for standard and in red for deviant within regions.

Discussion

If we assume that increased local synchrony reflects a better match or coordination between processing related to prior knowledge (top-down) and the outcome of stimulus processing (bottom-up), then we can use the observed ERSP measurements to assess which brain regions have the more prominent role for processing standards and which for processing deviants. The L IFG (BA 10) exhibited increased local synchrony in the gamma band during the MMN latency for the Standard condition in both passive and active paradigms suggesting this region is routinely involved with processing the standard, and may be involved in computing the acoustic regularity. The L STG was found to have increased local synchrony in the gamma band for both stimulus conditions in the passive listening paradigm suggesting that this region participates in processing aspects common to both deviants and standards; however, in the active listening paradigm just the deviant condition showed increased local synchrony in the theta band suggesting an altered role. Broca's area also shows increased local synchrony which varied by stimulus condition and task: increased local synchrony in the theta band in the Deviant condition for the passive paradigm but increased local synchrony in the gamma band in the Standard condition for the active paradigm. Interestingly, increases in local power for the deviant condition occur only in the left hemisphere sources: L STG and Broca's are in the passive paradigm and just the L STG in the active paradigm suggesting that the left sources are more involved in the deviant processing. Rapid detection of changes in the initial phoneme, in the order of tens of milliseconds, is better handled by left auditory cortex which has been shown to have higher temporal resolution abilities compared to the right hemisphere counterpart (Zatorre, Belin, & Penhune, 2002). The R STG showed multi-frequency band power increases for the Standard condition in the passive paradigm but no increases for either stimulus condition in the

active paradigm. The R IFG was the only right hemisphere source in the active paradigm to show increased local synchronization and only for the Standard condition. Overall, more sources in the left hemisphere show local power modulated by stimulus conditions for both the passive and the active paradigms, portraying a network with a left hemisphere dominance for processing the linguistic stimuli. In general, our findings are consistent with previous studies of the left-hemisphere dominance in speech processing (Alho, et al., 1998).

Long range synchrony between the L STG and Broca's area occur along both low-frequency and high-frequency band EEG oscillations within MMN model for our passive and active paradigms. We interpret this as the L STG feeding forward sensory information (via high-frequency band) to Broca's area, and in turn, Broca's area providing feedback modulation (low-frequency band) to the L STG, or in the case of the active paradigm, to both the L STG and L IFG (BA10). It is important to note the Broca's areas are not homologous across the listening paradigms. In the passive paradigm the region is more anterior whereas in the active paradigm the region is more posterior. Functional imaging studies have suggested that within Broca's area there is a rostro-caudal division of labour for semantic and phonological processing. This claim has received considerable support from recent TMS studies that not only confirm the division of labour, but also clarify the specific regional contributions to semantic and phonological processing (Gough, Nobre, & Devlin, 2005). During the active paradigm the phonological processing may be more engaged as subjects may repeat the sound silently themselves to maintain involvement in the task. Another possibility is that the posterior region of Broca's area (BA44) has more robust connections with motor regions and may be activated with the assignment of a particular motor scheme (button selection) to a corresponding phonological unit.

Overall, during the active paradigm long range synchronization showed significant increases for the AC Deviant condition whereas during the passive paradigm long range synchronization tended to be increased for the Standard condition (see Figure 4.7. A and Figure 4.7.B). This same pattern was evident in MMN network for complex tones and likely for the same reasons: responding to the deviant target requires increased vigilance and likely recruits additional processing.

In both the passive and active paradigms sources in the left orbitofrontal cortex showed gamma-band power increases during the MMN latency for the Standard condition suggesting that this region is specialized for processing the acoustic regularities, possibly for the matching predictions to the incoming standard. In the active paradigm, the orbitofrontal region (R IFG, BA47) also showed increases in gamma-band power for the Standard condition suggesting a match of predictions to the outcome of processing the standard. In contrast, in the passive paradigm the right hemisphere frontal sources (R SFG & R IFG) had no gamma-band increases modulated by stimulus condition in the latency of the MMN. Low-frequency-band long range synchronization was shown to be greater than in deviant conditions suggesting these areas may communicate computed predictions to other downstream areas.

In conclusion, examination of the cross-coherences between the sources active during the MMN scalp response reveals a hierarchal network of both auditory cortices and several frontal sources that are temporally coordinated during the change detection process and differentiated by stimulus condition and by task demands (see Figure 4.7.) These functional connections may provide a mechanism for refining predictions about the stimulus through the iterative top-down/bottom-up integration process to resolve prediction error. The main functional elements common to both passive and active paradigms consist of the left and right STG (BA22), the left

frontopolar area (SFG/IFG, BA10), and Broca's area (L IFG, BA45/44). This finding supports longstanding notions of shared processing resources between automatic and active auditory deviant processing (Dittmann-Balcar, Thienel, & Schall, 1999; Sussman, Winkler, & Wang, 2003).

Specialized sub-domains of the orbitofrontal cortex such as the frontal polar cortex (FPC, BA10) have been shown to maintain distractor-resistant representations of postponed tasks during the performance of another task (Koechlin & Hyafil, 2007). It is reasonable that such a function is involved in automatic change detection during the passive listening paradigm. A recent fMRI study found that the activity in the ventromedial regions of the prefrontal cortex was enhanced to auditory stimuli in a to-be-ignored stream compared a to-be-attended stream, possibly related to evaluation of the distracting event (Salmi, Rinne, Koistinen, Salonen, & Alho, 2009). During our passive paradigm, the frontal polar cortex (BA10) may be more active as the deviants may transiently distract from the video watching. In the active paradigm, however, there is no pending state as attention is directed toward the auditory stream, so contribution from the R SFG (BA10) may be suppressed. We found also during active detection of target deviants that the L IFG (BA47) source is silenced and its anatomical homologue in the right hemisphere, the R IFG (BA47), is recruited, perhaps due to its proximity to the right cingulate, to assist in response monitoring. The active paradigm's node in the anterior cingulate (BA32) is believed to have been recruited possibly to monitor task performance or to resolve response conflict.

Our findings are consistent with previous fMRI research, which found MMN generators in parts of the medial frontal or anterior cingulate cortex (Molholm, Matinez, Ritter, Javitt, & Foxe, 2005), and the caudal or rostral inferior and middle frontal cortex on the right, often accompanied by a strong right superior temporal gyrus (STG) activation (Opitz, Rinne,

Mecklinger, von Cramon, & Schröger, 2002; Doeller, Opitz, Mecklinger, Krick, Reith, & Schröger, 2003; Molholm, Matinez, Ritter, Javitt, & Foxe, 2005; Restuccia, Della Marca, Rubino, & Valeriani, 2005; Schönwiesner, Novitski, Pakarinen, Carlson, Tervaniemi, & Näätänen, 2007). The MMN sources can also include the left inferior frontal cortex (Molholm, Matinez, Ritter, Javitt, & Foxe, 2005) with a corresponding left STG activation, or both left and right IFC ((Doeller, Opitz, Mecklinger, Krick, Reith, & Schröger, 2003)(Rinne, Degerman, & Alho, 2005), and bilateral superior frontal cortex (SFC), (Molholm, Matinez, Ritter, Javitt, & Foxe, 2005). Our analysis has provided evidence of phase synchrony between these regions further corroborating the view that these regions are working together and not simply incidental to one another's operations. This changes the view of the MMN as arising from an isolated processing centre and takes into consideration the dynamic network operations between temporal and frontal regions to bring about complex perceptions such as change detection.

A) Passive Paradigm Network

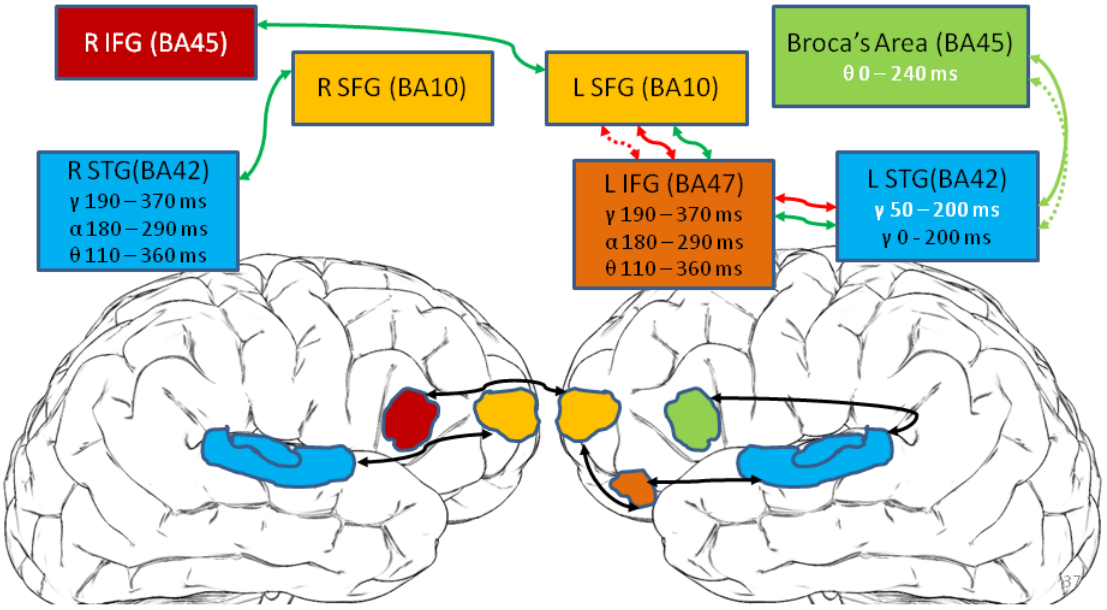

B) Active Paradigm Network

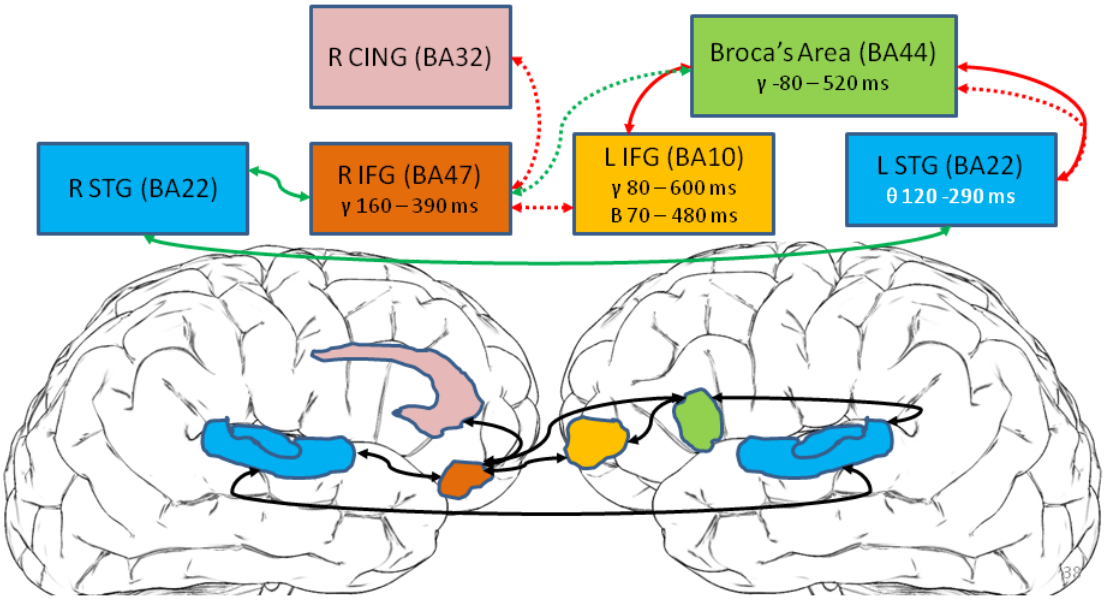

Figure 4. 7. MMN network as modulated by speech stimulus condition for passive and active paradigms. Regional interactions mapped in brain space by black double ended arrows provide broad view of MMN network, with a more detailed schematic provided above. Solid coloured arrows denote low frequency band (5-29 Hz), dotted coloured arrows denote high frequency band (30-55 Hz). Red: significantly greater synchrony for the AC Deviant condition. Green: significantly greater synchrony for the Standard condition. A) In the passive paradigm synchrony increases occur more often with Standard than with Deviant condition whereas in B) the active paradigm shows more interactions with significantly greater increases in synchrony for the Deviant condition.

CHAPTER 5: CONCLUSIONS

In both passive and active listening paradigms for linguistic and non-linguistic stimuli alike, the long-range synchronous interactions between the OFC regions (BA 10, 11, 47) and the auditory regions in the STG (BA 42, 22) were modulated by the deviant and standard stimulus conditions during the MMN scalp response, suggesting a functional cortical circuit for auditory change detection. Previous research relegated the role of deviance detection itself to the auditory cortex with a subsequent involuntary attention switch assigned to the right prefrontal cortex (Näätänen & Michie, 1979; Giard, Perrin, Pernier, & Peronnet, 1990; Opitz, Rinne, Mecklinger, von Cramon, & Schröger, 2002; Rinne et al, 2000). Our data support these roles for these regions. Coinciding with the MMN scalp response, regions in the STG showed greater increases in local synchrony for the deviant conditions corresponding to the respective hemispheric specializations for auditory features, in the right STG for oddball active paradigms involving complex tonal stimuli and the left STG in both passive and active paradigms with linguistic stimuli. For the frequency deviant oddball paradigms, sources in the right dorsal lateral prefrontal cortex (R IFG BA9) regions showed increased long-range synchrony with the OFC-STG nodes and are speculated to be recruited from the ventral attention network to transiently reorient attention. In the phoneme deviant oddball paradigms, however, the dorsal lateral PFC source (R IFG, BA45) found in the passive paradigm was not found in the active paradigm. The demands of the behavioral task requiring responses to both standards and deviants for nearly 90 minutes of sustained attention may have recruited the anterior cingulate, a region known to be involved in response monitoring and alertness. The consistent involvement of the OFC across tasks and stimuli implies however that this region plays a prominent role in the change detection process. Based on our current investigations, sources within the OFC region show 1) resistance

to habituation from repetitive stimuli resulting in a robust ERP, 2) increased local synchrony for processing standards (compared to deviants, with the exception of R OG in passive paradigm for complex tones (see Figure 3.4. A), and 3) consistent low-frequency long-range synchrony to modulate processing in other network nodes. These characteristics lead us to speculate that the function of the OFC in change detection is to distill abstract information, such as the relations between stimuli and their fit with the current regularities in the sensory environment, from the flow of sensory data. Relative information coding would facilitate quick decisions regarding changes without the lengthy process of computing every aspect of every object present in the environment. Recent work examining sources for the visual MMN with standardized low-resolution brain electromagnetic tomography (sLORETA) shows neural activations in the OFC regions, BA 11 and 47 in addition to the non-primary visual areas (Kimura, 2010). As well, invasive recordings in the macaque show that not only can neurons in the OFC represent an object, but they also can code the object's reward value and the degree to which it is expected in a given context (Schultz, Tremblay, & Hollerman, 2000).

Our results from the oddball paradigm with phoneme deviants showed synchronous interactions between the STG and two subregions of the IFG implicated in semantic and syntactical processing, BA45 and BA47 respectively. These results are consistent with Pulvermüller's view that a network model of MMN includes links to long term stores of learned linguistic stimuli to explain the robust response to linguistically relevant stimuli. The cortical dynamics of our MMN model for meaningful linguistic stimuli in the passive paradigm also fits with the dynamic causal modeling of fMRI data that found effective connectivity between the pars orbitalis (BA 47) in the left hemisphere with auditory association areas in Wernicke's area (BA 22 in the left temporal lobe) that were activated while listening to meaningful speech

utterances where subjects judged the gender of the speaker (Leff, Schofield, Stephan, Crinion, Friston, & Price, 2008).

Overall our MMN network models corroborate Friston's predictive coding model for the MMN network, which asserts that network interactions first create perceptual predictions and then through dynamic interactions quickly update these perceptual inferences based on available data. Coordinated activity between temporal and frontal regions serves as a viable mechanism for maintaining transient information for the short term. These dynamic interactions reflect ongoing processing within the network as it transiently shifts its configuration to accommodate to change in the acoustic environment and to refine predictions about that environment. The present model of change detection supported with electrophysiological data delineates a distributed network of coordinated temporal activity (long-range synchrony) coinciding with the generation of the MMN scalp response.

Although we could not predict how long-range synchrony between regional sources would be modulated by passive and active listening paradigms, the pattern of our findings resembled the "match to utilization" model in the general prediction that increased synchrony in the deviant condition predominates in active paradigms whereas increased synchrony in standard conditions predominates in passive paradigms. The MUM model proved to be too general to account for our findings of local synchrony within regional sources. Given that the MUM model was originally intended to explain GBA at the scalp, which is a mixture of source activity, it is not surprising to find that it falls short of explaining GBA occurring locally within largely independent neural sources. Now that the GBA can be analyzed within different brain regions, further refinements to the MUM need to be made to describe how this activity may operate within temporal and frontal generators. Perhaps the reason the general pattern of long-range

synchrony fits the 'match to utilization' model is because the MUM model is based more on global activities which are the result of network operations.

Limitations and Future Directions

This collective work provides the first detailed examination of the cortical dynamics coinciding with the MMN response based solely on electrophysiological data. To address the poor spatial resolution of EEG we decomposed the data into temporally independent components prior to source localization, assuming that physiologically distinct regions produce physiologically distinct temporal signatures. Although this approach has merit in easing the inverse problem by producing scalp maps that are arguably from single neural sources, the challenge remains of localizing those sources in brain space with reasonable precision using boundary element models in an average brain template. In addition to imprecise localization, sources localized to temporal and frontal regions often have spectral power peaks in gamma which makes them difficult to classify as neurogenic or artifactual in origin as these properties could arise from resonant neural activity known to characterize these areas or from muscular or ocular (i.e., micro saccades) activity. Further research is needed to explore these methodological issues. We tended to be conservative when faced with these equivocal options and may have removed valid neurogenic sources from the analysis. The loss of neurogenic sources has the most detrimental impact on the mean cross-coherence analysis, because this analysis requires IC pairs from the same subject (i.e., a subject must contribute an IC to each of the two clusters being compared). Unfortunately, the frequency with which we found the same subjects contributing ICs to each cluster under comparison was lower than we expected, although sufficient to make statistical inferences. Moreover, these interactions are only indexed by a subset of subject group, although statistically significant, cross-coherences, and there is still the danger that these

interactions are not specific to change detection but occur more generally from other causes. This is less likely when experimental conditions modulate the measure, as they do in these studies, but it remains a possibility. In future studies of cross-coherence we likely need to double the usual number (i.e., 12-14) of subjects run in MMN studies in order to ensure a larger number of IC pairs for each source comparison.

Measuring temporal dependencies that remain following segregation of EEG activities using a criterion of temporal independence seems to be inherently contradictory. ICA can only minimize, not eliminate, the higher order temporal dependencies between sources, meaning that there will remain some dependencies that can be further explored. Given that ICA is performed on individual datasets of continuous data collected from a 60-minute session (60,000 ms) and periods of phase synchrony are in the order of 25-100 ms, we do not believe such investigations are inconsistent with the segregation criterion. The limitation of segregating EEG activities using the criterion of temporal independence, however, is that we cannot fully examine the functional relationship between regions that are substantially interdependent for extended periods, nor can we examine temporal activities that are not spatially fixed. As well, the choice of the number of channels to record limits the number of independent components that can be separated, with the danger of over representing or under representing the number of sources. Further, the clustering of individual components for the purpose of group analysis is also limited by the number of clusters chosen. In summary both the number of channels and the number of clusters one chooses to use constrain the inferences that one can draw about the number and character of neurogenic sources contributing to the EEG data.

Long-range synchrony between regions, although implying a functional relationship, cannot determine if the activity in one region is caused by the activity in another. Although

measures such as Granger causality could be applied to the data to provide some indication of the direction of influence, this type of analysis still does not overcome the limitation of making inferences of causality based on time series rather than on direct manipulations of activity in one of the regions. Functional connectivity between regions is not necessarily mediated by direct anatomical coupling and could be brought about through the influence of mediating sources. Future studies using TMS in conjunction with an ICA approach to high-density EEG analysis is one means to directly manipulate regional interactions to better infer causality. Nonetheless, it was not the intent of this work to address the issue of causality but rather to lay the necessary groundwork for pursuing such questions by establishing convincing evidence for temporo-frontal interactions.

Despite these limitations, these novel findings provide preliminary evidence for the existence of a temporo-frontal hierarchical MMN network and demonstrate that high density EEG, with the help of ICA, can obtain information about the cortical dynamics of automatic auditory change detection. Ultimately such examinations of the MMN network properties have clinical applications in furthering our understanding of the nature of auditory processing difficulties in individuals following brain injury or in individuals with auditory impairments unexplained by peripheral hearing loss as well providing insight into the mechanisms of neuro-rehabilitation and assessing the efficacy of therapeutic interventions.

REFERENCES

Aaltonen, O., Tuomainen, J., Laine, M., & Niemi, P. (1993). Cortical differences in tonal versus vowel processing as revealed by an ERP component called mismatch negativity (MMN). *Brain and Language , 44*, 139-152.

Alain, C., Arnott, S. R., Hevenor, S., Graham, S., & Grady, C. L. (2001). "What" and "where" in the human auditory system. *Proceedings from the National Academy of Sciences USA, 9*, 12301-12306.

Alain, C., Woods, D. L., & Knight, R. T. (1998). A distributed cortical network for auditory sensory memory in humans. *Brain Research , 812*, 23-37.

Alho, K. (1995). Cerebral generators of mismatch negatvity (MMN) and its magnetic counterpart (MMNm) elecited by sound changes. *Ear & Hearing, 16(1)*, 38-51.

Alho, K., Connolly, J. F., Cheour, M., Lehtokoski, A., Huotilainen, M., Virtanen, J., et al. (1998). Hemispheric lateralization in preattentive processing of speech sounds. *Neuroscience Letters, 258*, 9-12.

Alho, K., Woods, D. L., Algazi, A., Knight, R. T., & Näätänen, R. (1998). Lesions of frontal cortex diminish the auditory mismatch negativity. *Electroencephalogra Clinical Neurophysiology , 91*, 353-362.

Anderson, L. A., Christianson, G. B., & Linden, J. F. (2009). Stimulus-specific adaptation occurs in the auditory thalamus. *Journal of Neuroscience, 29*, 7359-7363.

Atirnza, M., Cantero, J. L., & Dominguez-Marin, E. (2002). Mismatch negativity (MMN): An objective measure of sensory memory and long-lasting memories during sleep. *Interantional Journal of Psychophysiology, 46*, 215-225.

Barbas, H. (2000). Connections underlying the synthesis of cognition, memory, and emotion in primate prefrontal cortices. *Brain Research Bulletin, 52*, 319-330.

Barbas, H., Medalla, M., Alade, O., Suski, J., Zikopoulos, B., & Lera, P. (2005). Relationship of prefrontal connections to inhibitory systems in superior temporal areas in the rhesus monkey. *Cerebral Cortex, 15*, 1356-1370.

Bell, A. J., & Sejnowski, T. J. (1995). An information-maximization approach to blind separation and blind deconvolution. *Neural Computation, 7*, 1129-1159.

Bhattacharya, J., Petsche, H., & Pereda, E. (2001). Long range synchrony in the gamma band: role in music perception. *Journal of Neuroscience, 21*, 6329-6337.

Bignall, K. E., & Imbert, M. (1969). Polysensory and cortico-cortical projections to frontal lobe of squirrel and rhesus monkeys. *Electroencephalography Clinical Neurophysiology, 26*, 206-215.

Bregman, A. S. (1990). *Auditory scene analysis: The perceptual organization of sound.* Cambridge: MIT Press.

Brønnick, K. S., Nordby, H., Larsen, J. P., & Aarsland, D. (2010). Disturbance of automatic auditory change detection in dementia. *Neurobiology of Aging, 31*, 104-113.

Burgess AP, Ali L (2002) Functional connectivity of gamma EEG activity is modulated at low frequency during conscious recollection. *International Journal of Psychophysiology, 46*, 91–100.

Buschman, T. J., & Miller, E. K. (2007). Top-down versus bottom-up control of attention in the prefrontal and posterior parietal cortices. *Science, 315*, 1860-1862.

Buszaki, G. (2006). *Rhythms of the brain. Oxford University Press.* Oxford University Press.

Butler, R. A. (1968). Effect of changes in stimulus frequency and intensity on habituation of the human vertex potential. *Journal of the Acoustical Society of America, 44*, 945-50.

Chao, L. L., & Knight, R. T. (1998). Contribution of human prefrontal cortex to delay performance. *Journal of Cognitive Neuroscience, 10*, 167-177.

Corbetta, M., Patel, G., & Shulman, G. L. (2008). The reorienting system of the human brain: From environment to theory of mind. *Neuron, 58*, 306–324.

Cowan, N., Winkler, I., Teder, W., & Näätänen, R. (1993). Memory prerequisites of mismatch negativity in the auditory event related potential (ERP). *Journal of Experimental Psychology Learning Memory Cogntion, 19*, 909-921.

Csicsvari, J., Jamieson, B., Wise, K.D., & Buzsáki, G. (2003). Mechanisms of gamma oscillations in the hippocampus of the behaving rat. *Neuron, 37*, 311-22.

Curtis, C. E., & D'Esposito, M. (2003). Persistent activity in the prefrontal cortex during working memory. *Trends in Cogntive Science, 7*, 415-423.

Daltrozzo, J., Wioland, N., Mutschler, V., & Kotchoubey, B. (2007). Predicting coma and other low responsive patients outcome using event-related brain potentials: A meta-analysis. *Clinical Neurophysiology, 118*, 606-614.

Debener, S., Hermann, C. S., Kranczioch, C., Gembris, D., & Engel, A. K. (2003). Top-down attentional processing enhances auditory evoked gamma band activity. *NeuroReport, 14*, 683-686.

Dehaene-Lambertz, G. (1997). Electrophysiological correlates of categorical phoneme perception in adults. *Neuroreport, 8*, 919-924.

Delorme, A., & Makeig, S. (2004). EEGLAB: An open source toolbox for analysis of single trial EEG dynamics including independent component analysis. *Journal of Neuroscience Methods, 134*, 9-21.

Delorme, A., Westerfield, M., & Makeig, S. (2007). Medial prefrontal theta bursts precede rapid motor responses during visual selective attention. *Journal of Neuroscience, 27* (44), 11949-11959.

Deouell, L. Y. (2007). The frontal generator of the mismatch negativity revisited. *Journal of Psychophysiology, 21* (3-4), 188-203.

Deouell, L. Y., Bentin, S., & Giard, M. H. (1998). Mismatch negativity in dichotic listening: Evidence for interhemispheric differences and multiple generators. *Psychophysiology, 35*, 355-365.

Dittmann-Balcar, A., Thienel, R., & Schall, U. (1999). Attention dependent allocation of auditory processing resources as measured by mismatch negativity. *NeuroReport, 10*, 3749-3753.

Doeller, C. F., Opitz, B., Mecklinger, A., Krick, C., Reith, W., & Schröger, E. (2003). Prefrontal cortex involvement in preattentive auditory deviance detection: neuroimaging and electrophysiological evidence. *NeuroImage, 20*, 1270-1282.

Doesburg, S. M., Roggeveen, A. B., Kitajo, K., & Ward, L. M. (2008). Large-scale gamma-band phase synchronization and selective attention. *Cerebral Cortex, 18* (2), 386-96.

Engel, A. K., Fries, P., Koenig, P., Brecht, M., & Singer, W. (1999). Temporal Binding, Binocular Rivalry, and Consciousness. *Consciousness and Cognition, 8(2)*, 128-51.

Engel, A., Fries, P., & Singer, W. (2001). Dynamics predictions: Oscillations and synchrony in top-down processing. *Nature Reviews Neuroscience, 10*, 704-716.

Escera, C., Alho, K., Winkler, I., & Näätänen, R. (1998). Neural mechanisms of involuntary attention to acoustic novelty and change. *Journal of Cognitive Neuroscience, 10*, 590-604.

Ford, J. M., Gray, M., Faustman, W. O., Heinks, T. H., & Mathalon, D. H. (2005). Reduced gamma-band coherence to distorted feedback during speech when what you say is not what you hear. *International Journal of Psychophysiology, 57*, 143-150.

Fries, P. (2005). A mechanism for cognitive dynamics: neuronal communication through neuronal coherence. *Trends in Cognitive Neuroscience, 9(10)*, 474-480.

Fries, P., Reynolds, J., Rorie, A., & Desimone, R. (2001). Modulation of oscillatory neuronal synchronization by selective visual attention. *Science, 291*, 1560-1563.

Fries, P., Womeldorf, T., Oostenveld, R., & Desimone, R. (2008). The effects of visual stimulation and selective visual attention on rhythmic neuronal synchronization in macaque area v4. *The Journal of Neuroscience, 28*, 4823-4835.

Friston, K. J. (1997). Another neural code? *Neuroimage, 5*, 213–220.

Friston, K. J. (2009). Perception and hierarchical dynamics. *Frontiers in Neuroinformatics, 3*, 1-9.

Garagnani, M., & Pulvermüller, F. (2011). From sounds to words: A neurocomputational model of adaptation, inhibition and memory processes in auditory change detection. *NeuroImage, 54*,170-81.

Garrido, M. I., Friston, K. J., Kiebel, S. J., Stephan, K. E., Baldeweg, T., & Kilner, J. M. (2008). The functional anatomy of the MMN: A DCM study of the roving paradigm. *NeuroImage, 42*, 936-944.

Garrido, M. I., Kilner, J. M., Kiebel, S. J., Stephan, K. E., & Friston, K. J. (2007). Dynamic causal modelling of evoked potentials: a reproducibility study. *NeuroImage, 36*, 571-580.

Garrido, M. I., Kilner, J. M., Stephan, K. E., & Friston, K. J. (2009). The mismatch negativity: A review of the underlying mechanisms. *Clinical Neurophysiology, 120*, 453-463.

Giard, M. H., Lavikainen, J., Reinikainen, K., Perrin, F., Bertrand, O., Pernier, J., et al. (1995). Separate representation of stimulus frequency, intensity, and duration in auditory sensory memory: An event related potential and dipole-model analysis. *Journal of Cognitive Neuroscience, 7*, 133-143.

Giard, M. H., Perrin, F., Pernier, J., & Peronnet, F. (1990). Brain generators implicated in processing of auditory stimulus deviance: a topographic event-related potential study. *Psychophysiology, 27*, 627-640.

Gough, P.M., Nobre, A. C., & Devlin, J. T. (2005). Dissociating linguistic processes in the left inferior frontal cortex with transcranial magnetic stimulation. *The Journal of Neuroscience, 25*,8010–8016.

Gray, C. M., & Singer, W. (1989). Stimulus-specific neuronal oscillations in orientation columns of cat visual cortex. *Proceedings from the National Academy of Sciences USA, 86*, 1698-1702.

Gurtubay, I. G., Alegre, M., Valencia, M., & Artieda, J. (2006). Cortical gamma activity during auditory tone omission provides evidence for the involvement of oscillatory activity in top-down processing. *Experimental Brain Research, 175*, 463-470.

Haenschel, C., Baldeweg, T., Croft, R. J., Whittington, M., & Gruzelier, J. (2000). Gamma and beta frequency oscillations in response to novel auditory stimuli: a comparison of human electroencephalogram (EEG) data with in vitro models. *Proceedings from the National Academy of Sciences USA , 97*, 7645-7650.

Herdman, A. T., Pang, E. W., Ressel, V., Gaetz, W., & Cheyne, D. (2007). Task-related modulation of early cortical responses during language production: An event-related synthetic aperture magnetometry study. *Cerebral Cortex, 17*, 2536-2543.

Hermann, C. S., Munk, M. H., & Engel, A. K. (2004). Cognitive functions of gamma-band activity: memory match and utilization. *Trends in Congitive Science, 8(8)*, 347-355.

Herrmann, C. S., Fründ, I., & Lenz, D. (2010). Humangamm-band activity: A review on cognitive and behavioral correlated and network models. *Neuroscience and Behavioral Reviews, 34*, 981-992.

Hickok, G., & Poeppel, D. (2000). Towards a functional neuroanatomy of speech perception. *Trends in Cognitive Sciences, 4*, 131-138.

Hsiao, F.-J., Cheng, C.-H., Liao, K.-K., & Lin, Y.-Y. (2010). Cortico-cortical phase synchrony in auditory mismatch processing. *Biological Psychology, 84*,336-345.

Ilvonen, T., Kujala, T., Kozou, H., Kiesiläinen, A., Salonen, O., Alku, P., et al. (2004). The processing of speech and non-speech sounds in aphasic patients as reflected by the mismatch negativity (MMN). *Neuroscience Letters, 366*, 235-240.

Jääskeläinen, I. P., Ahveninen, J., Bonmassar, G., Dale, A. M., Ilmoniemi, R. J., Levänen, S., et al. (2004). Human posterior auditory cortex gates novel sounds to consciousness. *Proceeding of the National Academy of Science USA, 101*, 6809-14.

Javitt, D. C., Steinschneider, M., Schroeder, C. E., & Arezzo, J. C. (1996). Role of cortical N-methyl-D-aspartate receptors in auditory sensory memory and mismatch negativity generation: Implications for schizophenia. *Proceedings of the National Academy of Sciences of the United States of America, 93*, 11962-11967.

Jemel, B., Achenbach, C., Müller, B. W., Röpcke, B., & Oades, R. D. (2002). Mismatch negativity results from bilateral asymmetric dipole sources in the frontal and temporal lobes. *Brain Topography, 15*, 13-27.

Kaiser, J., Lutzenberger, W., Ackermann, H., & Birbaumer, N. (2002). Dynamicsof gamma-band activity induced by auditory pattern changes in humans. *Cerebal Cortex, 12*, 212-221.

Kaiser, J., Lutzenberger, W., Preissl, H., Ackermann, H., & Birbaumer, N. (2000). Right-hemisphere dominance for the processing of sound-source lateralization. *Journal of Neuroscience, 20*, 6631-6639.

Kalyakinai, I., Gonzálezb, N., & Kärkkäi, T. (2008). Independent component analysis on the mismatch negativity in an uninterrupted sound paradigm. *Journal of Neuroscience Methods, 174*, 301-312.

Kasai, K., Nakagome, K., Itoh, K., Koshida, I., Hata, A., Iwanami, A., et al. (1999). Multiple generators in the auditory discrimination process in humans. *NeuroReport, 10*, 2267-2271.

Kimura, M. (2010). Localizing sensory and cognitive systems for pre-attentive visual deviance detection: An sLORETA analysis of the data. *Neuroscience Letters, 485*, 198-203.

Kisley, M. A., & Cornwell, Z. M. (2006). Gamma and beta neural activity evoked during a sensory gating paradigm: effects of auditory, somatosensory and cross-modal stimulation. *Clinical Neurophysiology, 117*, 2549-2563.

Koechlin, E., & Hyafil, A. (2007). Anterior prefrontal function and the limits of human decision-making. *Science, 318*, 594-598.

Kohler, E., Keysers, C., Umilta, M. A., Fogassi, L., Gallese, V., & Rizzolatti, G. (2002). Hearing sounds, understanding actions: action representation in mirror neurons. *Science, 297(5582)*, 846-848.

Lamme, V. A., & Roelfsema, P. R. (2000). The distinct modes of vision offered by feedforward and recurrent processing. *Trends in Neuroscience, 23*, 571-579.

Leff, A. P., Schofield, T. M., Stephan, K. E., Crinion, J. T., Friston, K. J., & Price, C. J. (2008). The cortical dynamics of intelligible speech. *The Journal of Neuroscience, 28*, 13209-13215.

Leiberg, S., Lutzenberger, W., & Kaiser, J. (2006). Effects of memory load on cortical oscillatory activity during auditory pattern working memory. *Brain Research, 1120(1)*, 131-140.

Leitman, D. I., Sehatpour, P., Higgins, B. A., Foxe, J. J., Silipo, G., & Javitt, D. C. (2010). Sensory deficits and distributed hierarchical dysfunction in schizophrenia. *American journal of Psychiatry, 167*, 818-827.

Lenz, D., Schadow, J., Thaerig, S., Busch, N. A., & Herrmann, C. S. (2007). What's that sound? Matches with auditory long-term memory induce gamma activity in human EEG. *International Journal of Psychophysiology, 64* (1), 31-38.

Levänen, S., Ahonen, A., Hari, R., McEvoy, L., & Sams, M. (1996). Deviant auditory stimuli activate human left and right auditory cortex differently. *Cerebral Cortex, 6*, 288-296.

Makeig, S., Westerfield, M., Jung, T. P., Covington, J., Townsend, J., Sejnowski, T. J., et al. (1999). Functionally independent components of the late positive event-related potential during visual spatial attention. *Journal of Neuroscience, 19*, 2665-2680.

Makris, N., & Pandya, D. N. (2009). The extreme capsule in humans and rethinking of the language circuitry. *Brain Structure and Function, 213*, 343-358.

Malmierca, M. S., Cristaudo, S., & Covey, E. (2009). Stimulus-specific adaptation in the inferior colliculus of the anesthetized rat. *Journal of Neuroscience, 29*, 5483-5493.

Malmierca, M. S., Cristaudo, S., Pérez-González, D., & Covey, E. (2009). Stimulus-specific adaptation in the inferior colliculus of the anesthetized rat. *Journal of Neuroscience, 29*, 5483-5493.

Marco-Pallares, J., Grau, C., & Ruffini, G. (2005). Combined ICA-LORETA analysis of mismatch negativity. *NeuroImage, 25*, 471–477.

Maris, E., Schoffelen, J.-M., & Fries, P. (2007). Nonparametric statistical testing of coherence differences. *Journal of Neuroscience Methods, 163*, 161-175.

May, P. C., & Tiitinen, H. (2010). Mismatch negativity (MMN), the deviance-elicited auditory deflection explained. *Psychophysiology, 47*, 66-122.

Micheyl, C., Carlyon, R. P., Shtyrov, Y., Hauk, O., Dodson, T., & Pullvermüller, F. (2003). The neurophysiological basis of the auditory continuity illusion: a mismatch negativity study. *Journal of Cognitive Neuroscience, 15*, 747-758.

Molholm, S., Matinez, A., Ritter, W., Javitt, D. C., & Foxe, J. J. (2005). The neural circuitry of pre-attentive auditory change-detection: A fMRI study of pitch and duration mismatch negativity generators. *Cerebral Cortex, 15*, 545-551.

Mutschler, I., Wieckhorst, B., Specks, O., Schulze-Bonhage, A., Hennig, J., Seifritz, E., et al. (2010). Time Scales of Auditory Habituation in the Amygdala and Cerebral Cortex. *Cerebral Cortex, 20*, 531-2539.

Nääatänen, R., Lehtokoski, A., Lennes, M., Cheour, M., Huotilainen, M., Iivonen, A., et al. (1997). Language-specific phoneme representations revealed by electric and magnetic brain responses. *Nature, 385*, 432-434.

Näätänen, R., & Michie, P. T. (1979). Early selective-attention effects on the evoked potential: A critical review and reinterpretation. *Biological Psychology, 8*, 81-136.

Näätänen, R., Jacobsen, T., & Winkler, I. (2005). Memory-based or afferent processes in mismatch negativity (MMN): A review of the evidence. *Psychophysiology, 42*, 25-32.

Näätänen, R., Paavilainen, P., Rinne, T., & Alho, K. (2007). The mismatch negativity (MMN) in basic research of central auditory processing: A review. *Clinical Neurophysiology, 118*, 2544–2590.

Oldfield, R. C. (1971). The assessment and analysis of handedness: the Edinburgh inventory. *Neuropsychologia, 9*, 97-113.

Onton, J., Delorme, A., & Makeig, S. (2005). Frontal midline EEG dynamics during working memory. *NeuroImage, 27*, 341-356.

Onton, J., Westerfield, M., Townsend, J., & Makeig, S. (2006). Imaging human EEG dynamics using independent component analysis. *Neurosci Biobehav Rev., 30* (6), 808-22.

Opitz, B., Rinne, T., Mecklinger, A., von Cramon, D. Y., & Schröger, E. (2002). Differential contribution of frontal and temporal cortices to auditory change detection: fMRI and ERP results. *Neuroimage, 15*, 167-174.

Pantev, C., Makeig, S., Hoke, M., Galambos, R., Hampson, S., & Gallen, C. (1991). Human auditory evoked gamma-band magnetic fields. *Proceedings of the National Academy of Science USA , 88*, 8996-9000.

Pekkonen, E., Jousmaki, V., Kononen, M., Reinikainen, K., & Partanen, J. (1994). Auditory sensory memory impairment in Alzheimer's disease: an event-related potential study. *NeuroReport, 5*, 2537-2540.

Pekkonen, E., Rinne, T., Reinikainen, K., Kujala, T., Alho, K., & Näätänen, R. (1996). Aging effects on auditory processing: an event-related potential study. *Experimental Aging Research, 22*, 171-184.

Phillips, C., Pellathy, T., Marantz, A., Yellin, E., Wexler, K., Poeppel, D., et al. (2000). Auditory cortex accesses phonological categories: An MEG mismatch study. *Brain Research Cognition Brain Research, 4*, 231-242.

Phillips, S., & Takeda, Y. (2009). Greater frontal-parietal synchrony at low gamma-band frequencies for inefficient than efficient visual search in human EEG. *Journal of Psychophysiology, 73*, 350-354.

Poeppel, D. (2003). The analysis of speech in different temporal integration windows: Cerebral lateralization as 'asymmetric sampling in time. *Speech Communication, 41*, 245-255.

Poeppel, D., Guillemin, A., Thompson, J., Fritz, J., Bavelier, D., & Braun, A. R. (2004). Auditory lexical decision, categorical perception, and FM direction discrimination differentially engage left and right auditory cortex. *Neuropsychologia, 42*, 183-200.

Pulvermüller, F., & Shtyrov, Y. (2006). Language outside the focus of attention: The mismatch negativity as a tool for studying higher cognitive processes. *Progress in Neurobiology, 79*, 49-71.

Pulvermüller, F., Kujala, T., Shtyrov, Y., Simola, J., Tiitinen, H., Alku, P., et al. (2001). Memory traces for words as revealed by the mismatch negativity. *Neuroimage, 14(3),* 607-616.

Pulvermüller, F., Shtyrov, Y., & Ilmoniemi, R. (2005). Brain signatures of meaning access in action word recognition. *Journal of Cognitive Neuroscience, 17(6),* 884-892.

Ramnani, N., & Owen, A. M. (2004). Anterior prefrontal cortex: insights into function from anatomy and neuroimaging. *Nature Reviews Neuroscience, 5*, 184-194.

Rauschecker, J. P., & Tian, B. (2000). Mechanisms and streams for processing of "what" and "where" in audiotry cortex. *Proceedings of the National Academy of Sciences of the United States of America, 97*, 11800-11806.

Restuccia, D., Della Marca, G., Rubino, M., & Valeriani, M. (2005). Attentional load of the primary task influences the frontal but not the temporal generators of the mismatch negativity. *Cognitive Brain Research, 25*, 891-899.

Rinne, T., Alho, K., Ilmoniemi, R. J., Virtanen, J., & Näätänen, R. (2000). Separate time behaviors of the temporal and frontal mismatch negativity sources. *NeuroImage, 12*, 14-19.

Rinne, T., Degerman, A., & Alho, K. (2005). Superior temporal and inferior frontal cortices are activated by infrequent sound duration decrements: an fMRI study. *NeuroImag*e, *26(1),* 66-72.

Ritter, P., & Villringer, A. (2006). Simultaneous EEG-fMRI. *Neuroscience Biobehavior Reviews, 30*, 823-838.

Ritter, W., De Sanctis, P., Molholm, S., Javitt, D., & Foxe, J. (2006). Preattentively grouped tones do not elicit MMN with respect to each other. *Psychophysiology, 43* (5), 423-430.

Rivera-Gaxiola, M., Csibra, G., Johnson, M. H., & Karmiloff-Smith, A. (2000). Electrophysiological correlates of cross-linguistic speech perception in native English speakers. *Behavioural Brain Research, 111*, 13-23.

Romanski, L. M., & Goldman-Rakic, P. S. (2002). An auditory domain in primate prefrontal cortex. *Nature Neuroscience, 5* (1), 15-16.

Rosburg, T. (2003). Left hemispheric dipole locations of the neuromagnetic mismatch negativity to frequency, intensity and duration deviants. *Brain Research Cogntive Brain Research, 16*, 83-90.

Russ, B. E., Lee, Y.-S., & Cohen, Y. E. (2007). Neural and behavioral correlates of auditory categorization. *Hearing Research, 229*, 204-212.

Salinas, E., & Sejnowski, T. J. (2001). Correlated neuronal activity and the flow of neural information. *Nature Reviews Neuroscience, 2*, 539-550.

Salmi, J., Rinne, T., Koistinen, S., Salonen, O., & Alho, K. (2009). Brain networks of bottom-up triggered and top-down controlled shifting of auditory attention. *Brain Research, 1286*, 155-164.

Sams, M., Alho, K., & Näätänen, R. (1993). Sequential effects on the ERP in disciminating to stimuli. *Biological Pyschology, 17*, 41-58.

Sandmann, P., Eichele, T., Buechler, M., Debener, S., Jäncke, L., Dillier, N., et al. (2009). Evaluation of evoked potentials to dyadic tones after cochlear implantation. *Brain, 132*, 1967-1979.

Sandmann, P., Kegel, A., Eichele, T., Dillier, N., Lai, W., Bendixen, A., et al. (2010). Neurophysiological evidence of impaired musical sound perception in cochlear-implant users. *Clinical Neurophysiology, 121*, 2070-82.

Sauseng P, Klimesch W, Gruber WR, Birbaumer N (2008). Cross-frequency phase synchronization: a brain mechanism of memory and attention. *Neuroimage, 40*, 308-317.

Schack B, Vath N, Petsche H, Geissler HG, Moller E (2002) Phase-coupling of theta-gamma EEG rhythms during short-term memory processing. *International Journal of Psychophysiology, 44*, 143-163.

Schadow, J., Lenz, D., Dettler, N., Fründ, I., & Herrmann, C. S. (2009). Early gamma-band responses reflect anticipatory top-down modulation in the auditory cortex. *Neuroimage, 47*, 651-658.

Schönwiesner, M., Novitski, N., Pakarinen, S., Carlson, S., Tervaniemi, M., & Näätänen, R. (2007). Heschl's gyrus, posterior superior temporal gyrus, and mid-ventrolateral prefrontal cortex have different roles in thedetection of acoustic changes. *Journal of Neurophysiology, 97*, 2075-2082.

Schultz, W., Tremblay, L., & Hollerman, J. R. (2000). Reward processing in primate orbitofrontal cortex and basal ganglia. *Cerebral Cortex, 10*, 272-284.

Sederberg, P. B., Schulze-Bonhage, A., Madsen, J. R., Bromfield, E. B., McCarthy, D. C., Brandt, A., et al. (2007). Hippocampal and neocortical gamma oscillations predict memory formation in humans. *Cerebral Cortex, 17*, 1190-1196.

Shalgi, S., & Deouell, L. Y. (2007). Direct evidence for differential roles of temporal and frontal components of auditory change detection. *Neuropsychologia, 45*, 1878-1888.

Shtyrov, Y., & Pulvemüller, F. (2007). Early MEG activation dynamics in the left temporal and inferior frontal cortex reflect semantic context integration. *Journal of Cognitive Neuroscience, 19* (10), 1633-1642.

Shtyrov, Y., Hauk, O., & Pulvermüller, F. (2004). Distributed neuronal networks for encoding category-specific semantic information: the mismatch negativity to action words. *European Journal of Neuroscience, 19*, 1083-1092.

Shtyrov, Y., Kujala, T., Lyytinen, H., Ilmoniemi, R. J., & Näätänen, R. (2000). Lateralization of speech processing in the brain as indicated by the mismatch negativity and dichotic listening. *Brain Cognition, 43*, 392-398.

Sirota, A., Montgomery, S., Fujisawa, S., Isomura, Y., Zugaro, M., & Buzsáki, G. (2008). Entrainment of neocortical neurons and gamma oscillations by the hippocampal theta rhythm. *Neuron, 60*, 683-697.

Stone, J. V. (2004). *Independent component analysis: a tutorial introduction.* Cambridge, Massachusetts: The MIT Press.

Sussman, E., Winkler, I., & Wang, W. (2003). MMN and attention: Competition for deviance detection. *Psychophysiology, 40*, 430-435.

Tata, M. S., & Ward, L. M. (2005). Early phase of spatial mismatch negativity is localized to a posterior "where" auditory pathway. *Experimental Brain Research, 167*, 481-486.

Tiitinen, H., May, P., & Näätänen, R. (1997). The transient 40-Hz response, mismatch negativity, and attentional processes in humans. *Progress in Neuro-Psychopharmacology and Biological Psychiatry, 21*, 751-771.

Tiitinen, H., Sinkkonen, J., Reinikainen, K., Alho, K., Lavikainen, J., & Näätänen, R. (1993). Selective attention enhances the auditory 40-Hz transient response in humans. *Nature, 364*, 59-60.

Tse, C. Y., & Penney, T. B. (2008). On the functional role of temporal and frontal cortex activation in passive detection of auditory deviance. *Neuroimage, 41*, 1462-1470.

Umbricht, D., Schmid, L., Koller, R., Vollenweider, F. X., Hell, D., & Javitt, D. C. (2000). Ketamine-induced deficits in auditory and visual context-dependent processing in healthy volunteers: implications for models of cognitive deficits in schizophrenia. *Archives of General Psychiatry, 57*, 1139-47.

Urakawa, T., Inui, K., Yamashiro, K., & Kakigi, R. (2010). Cortical dynamics of the visual change detection process. *Psychophysiology, 47*, 905-912.

van Zuijen, T. L., Simoens, V. L., Paavilainen, P., Näätänen, R., & Tervaniemi, M. (2006). Implicit, intuitive, and explicit knowledge of abstract regularities in a sound sequence: an event-related brain potential study. *Journal of Cognitive Neuroscience, 18*, 1292-1303.

Varela, F., Lachaux, J. P., Rodriguez, E., & Martinerie, J. (2001). The brainweb: phase synchronization and large-scale integration. *Nature Reviews Neuroscience, 2 (4)*, 229–239.

Verhoef, B. E., Kayaert, G., Franko, E., Vaneneugden, J., & Vogels, R. (2008). Stimulus simularity-contingent neural adaptation can be time and cortica area dependent. *Journal of Neuroscience, 28*, 10631-10640.

Viola, F. C., Thorne, J., Edmonds, B., Schneider, T., Eichele, T., & Debener, S. (2009). Semi-automatic identification of independent components representing EEG artifact. *Clinical Neurophysiology, 120*, 868-877.

Vuust, P., Pallesen, K. J., Bailey, C., van Zuijen, T. L., Gjedde, A., Roepstorff, A., et al. (2005). To musicians, the message is in the meter pre-attentive neuronal responses to incongruent rhythm are left-lateralized in musicians. *Neuroimage, 24*, 560-564.

Werker, J. F., & Lalonde, C. (1988). Cross-language speech perception: initial capabilities and developmental change. *Developmental Psychology, 24(5)*, 672-683.

Winkler, I., Karmos, G., & Näätänen, R. (1996). Adaptive modelling of the unattended acoustic environment reflected in the mismatch negativity event-related potential. *Brain Research, 742*, 239-252.

Winkler, I., Kujala, T., Tiitinen, H., Sivonen, P., Alku, P., Lehtokiski, A., et al. (1999). Brain responses reveal the learning of foreign language phonemes. *Psychophysiology, 36*, 638-642.

Wolff, C., & Schröger, E. (2001). Human preattentive auditory change detection with single, double, and triple deviations as revealed by mismatch negativity additivity. *Neuroscience Letters, 311*, 37-40.

Womelsdorf, T., Fries, P., Mitra, P. P., & Desimone, R. (2006). Gamma-band synchonization in visual cortex predicts speed of change detection. *Nature, 439*, 733-736.

Womelsdorf, T., Schoffelen, J.-M., Oostenveld, R., Singer, W., Desimone, R., Engel, A. K., et al. (2007). Modulation of neuronal interactions through neuronal synchronization. *Science, 316*, 1609-1612.

Yabe, H., Tervaniemi, M., Reinikainen, K., & Näätänen, R. (1997). Temporal window of integration revealed by MMN to sound omission. *NeuroReport, 8*, 1971-74.

Yago, E., Escera, C., Alho, K., & Giard, M. H. (2001). Cerebral mechanisms underlying orienting of attention towards auditory frequency changes. *NeuroReport, 12*, 2583-2587.

Yucel, G., McCarthy, G., & Belger, A. (2007). fMRI reveals that involuntary visual deviance processing is resource limited. *NeuroImage, 34*, 1245-1252.

Zatorre, R. J., Belin, P., & Penhune, V. B. (2002). Structure and function of auditory cortex: music and speech. *Trends in Cognitive Science, 6*, 37-46.

Appendix A. Table A. 1. Relevant clusters with all contributing ICs. (Chapter Two)

OFG Cluster		R STG Cluster		L STG Cluster	
10 Subjects, 23 ICs (PVAF)		7 Subjects, 20 ICs (PVAF)		6 Subjects, 15 ICs (PVAF)	
S01 IC1 (34.18)	S06 IC10 (0.94)	S02 IC7 (11.59)	S08 IC26 (-1.31)	S01 IC15 (0.77)	**S11 IC17 (0.62)**
S01 IC16 (1.80)	S06 IC14 (1.51)	S02 IC8 (0.69)	S08 IC27(4.49)	S01 IC20 (0.32)	S11 IC20 (2.31)
S02 IC1 (58.66)	S06 IC16 (-4.34)	S02 IC16 (0.21)	S08 IC28 (1.03)	**S02 IC22 (0.15)**	S11 IC28 (1.57)
S02 IC3 (30.51)	**S07 IC1 (30.29)**	S02 IC17 (-0.20)	S08 IC29 (2.10)	S02 IC24 (4.33)	
S02 IC12 (12.54)	**S08 IC11 (16.97)**	**S02 IC21 (0.20)**	S11 IC7 (0.75)	S02 IC26 (0.43)	
S02 IC15 (7.23)	S08 IC30 (3.74)	S04 IC23 (0.37)	S11 IC19 (1.66)	S04 IC4 (3.19)	
S03 IC1 (59.09)	**S09 IC1 (48.38)**	**S05 IC7 (12.07)**	**S11 IC24 (0.84)**	**S04 IC15 (3.12)**	
S03 IC12 (0.82)	S11 IC4 (13.43)	S05 IC10 (0.82)	S11 IC27 (1.06)	S04 IC22 (0.58)	
S04 IC2 (35.39)	S11 IC8 (30.43)	S06 IC8 (6.66)		**S08 IC6 (6.35)**	
S04 IC14 (-3.09)	**S11 IC12 (57.38)**	S07 IC5 (8.08)		S08 IC16 (1.25)	
S04 IC21 (1.50)	S11 IC22 (0.51)	**S07 IC8 (2.05)**		S09 IC13 (1.20)	
S05 IC6 (21.18)		**S08 IC15 (0.60)**		**S09 IC17 (-0.90)**	
Mean (20.38)		**Mean (2.68)**		**Mean (1.68)**	

Note: ICs in bold were retained in the pruned clusters.

Appendix B. Unpruned task relevant clusters. (Chapter Two)

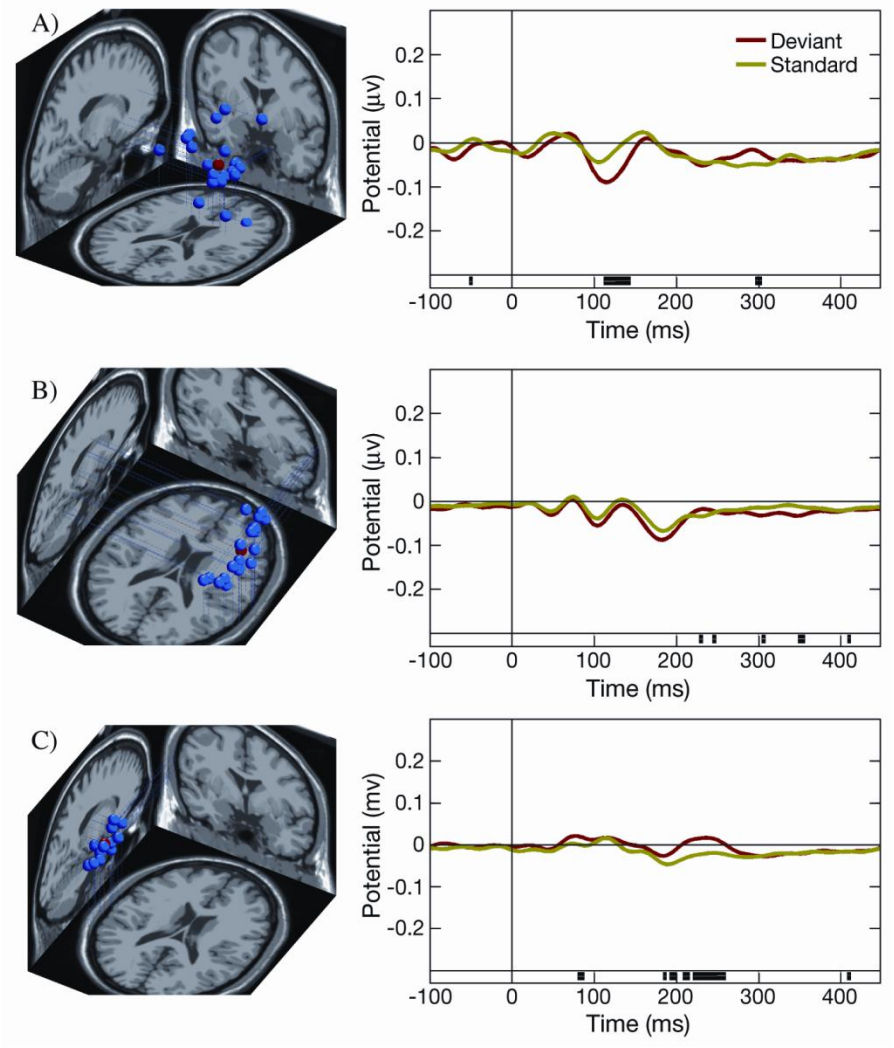

Figure B. 1. Unpruned task relevant clusters. (Chapter Two)

Appendix C: Mean cross-coherence plots. (Chapter Three)

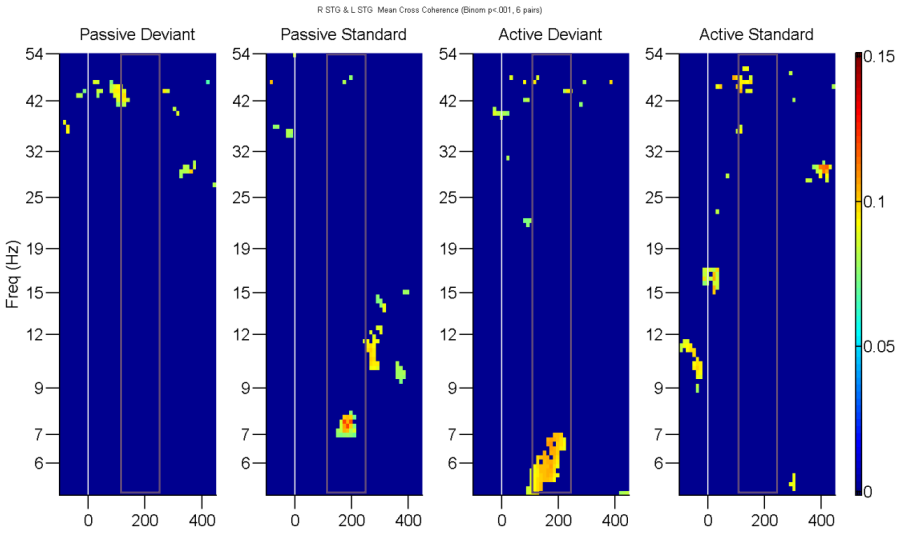

Figure C. 1. Mean cross-coherence between L STG and R STG (Binom $p < 0.001$, 6 pairs). ROI is MMN latency region 120 -250 ms, within mauve box. Consistent gamma-band cross-coherence for the Active Standard condition is significantly > the Active Deviant condition ($p < 0.005$). No other consistent cross-coherence ≥1 frequency cycle across subjects.

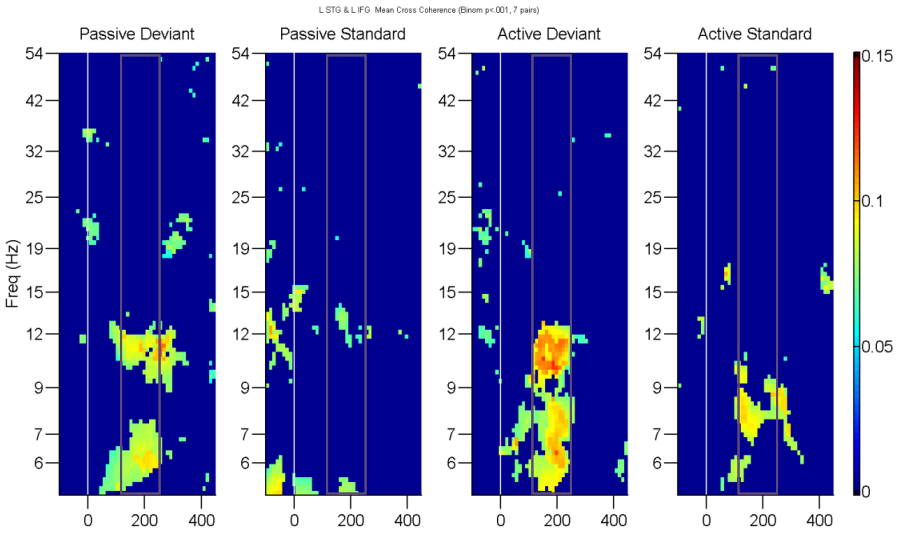

Figure C. 2. Mean cross-coherence between L STG and L IFG (Binom $p < 0.001$, 7 pairs). ROI is MMN latency region 120 - 250 ms, within mauve box. Consistent theta- and alpha-band cross-coherence for the Passive and Active Deviant conditions are significantly > the Standard conditions ($p < 0.005$). No other consistent cross-coherences ≥ 1 frequency cycle across subjects.

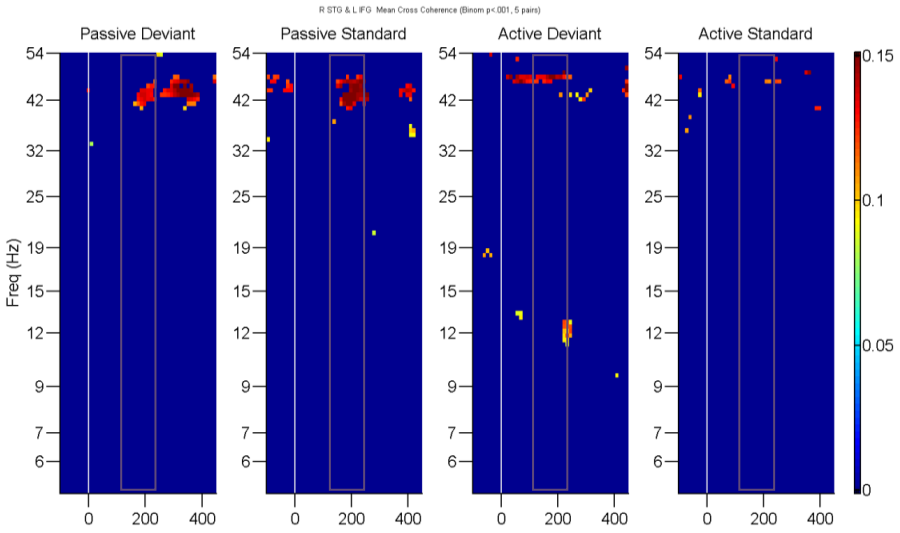

Figure C. 3. Mean cross-coherence between R STG and L IFG (Binom $p < 0.001$, 5 pairs). ROI is MMN latency region 120 -250 ms, within mauve box. Consistent gamma-band cross-coherence for the Passive Standard condition is significantly > the Passive Deviant condition ($p < 0.005$). Consistent gamma-band cross-coherence for the Active Deviant condition is significantly > the Active Standard condition ($p < 0.005$).

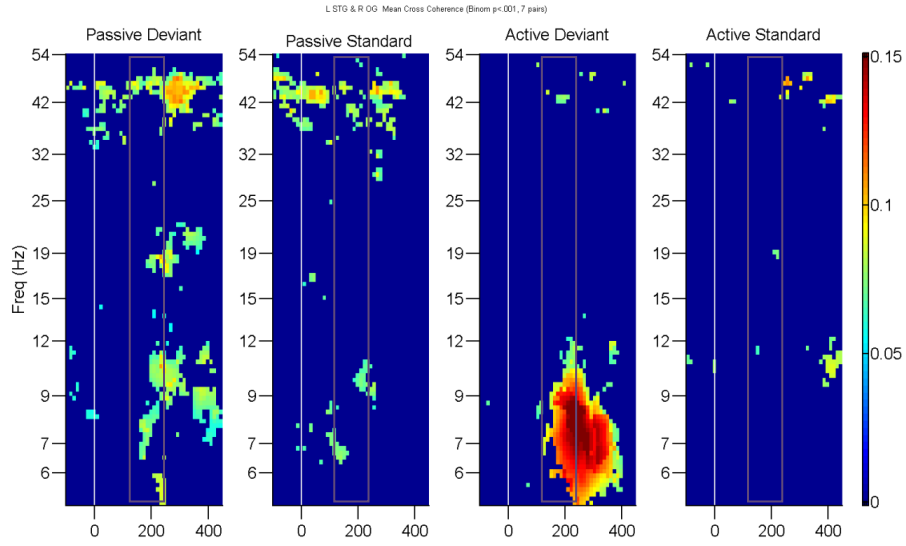

Figure C. 4. Mean cross-coherence between L STG and R OG (Binom $p < 0.001$, 7 pairs). ROI is MMN latency region 120 - 250 ms, within mauve box. Consistent gamma-band cross-coherence for the Passive Standard condition is significantly > the Passive Deviant condition ($p < 0.005$). Consistent beta-band cross-coherence for the Passive Deviant condition is significantly > the Passive Standard condition ($p < 0.005$). Consistent theta- and alpha-band cross-coherence for the Active Deviant condition are significantly > the Active Standard condition ($p < 0.005$).

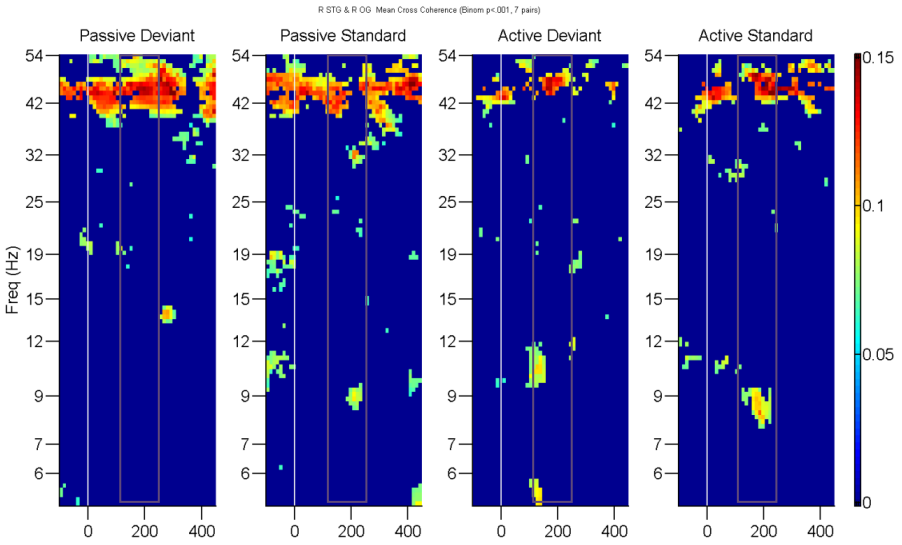

Figure C. 5. Mean cross-coherence between for R STG and R OG (Binom $p < 0.001$, 7 pairs). ROI is MMN latency region 120 - 250 ms, within mauve box. Consistent gamma-band cross-coherence for the Active Standard condition is significantly > the Active Deviant condition ($p < 0.005$). No significant difference exits for the Passive conditions ($p < 0.005$) despite the plot display to the contrary. No other consistent cross-coherence > 1 frequency cycle.

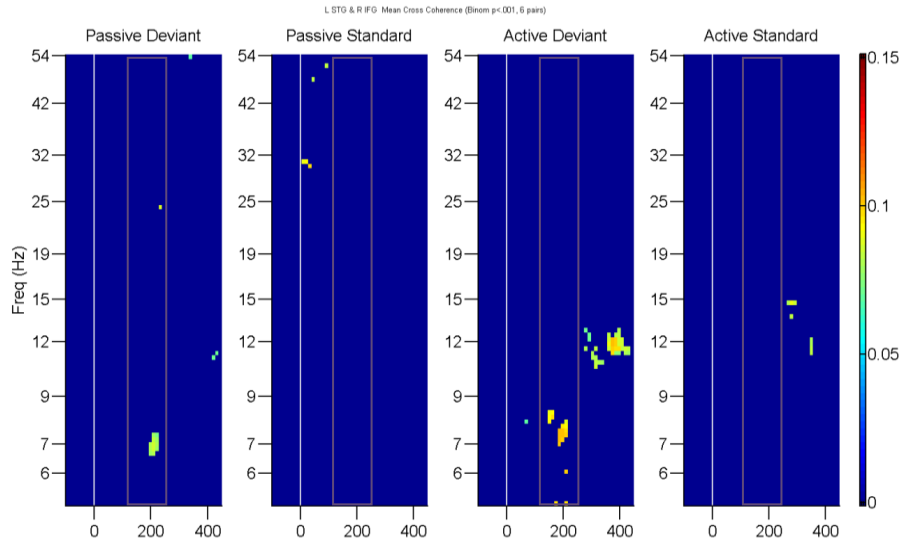

Figure C. 6. Mean cross-coherence between L STG and R IFG (Binom $p < 0.001$, 6 pairs). ROI is MMN latency region 120 - 250 ms, within mauve box. No consistent cross-coherences across subjects.

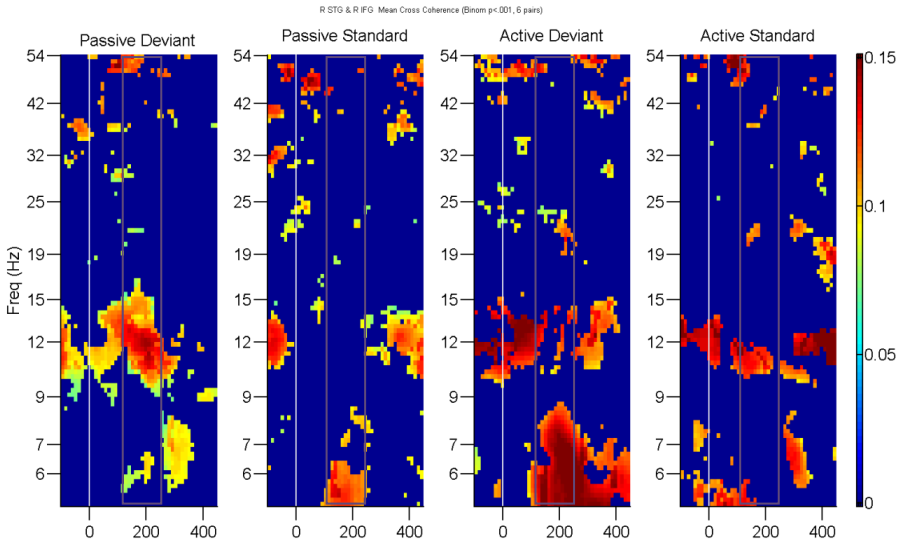

Figure C. 7. Mean cross-coherence between R STG and R IFG (Binom $p < 0.001$, 6 pairs). ROI is MMN latency region 120 - 250 ms, within mauve box. Consistent beta-band cross-coherence for the Passive Deviant condition is significantly > the Passive Standard condition ($p < 0.005$). Consistent theta-band cross-coherence for the Passive Standard condition is significantly different from the Passive Deviant condition ($p < 0.005$). Consistent theta-band cross-coherence for the Active Deviant condition is significantly > the Active Standard condition ($p < 0.005$). Consistent alpha-band cross-coherence for the Active Standard condition is significantly different from the Active Deviant condition ($p < 0.005$).

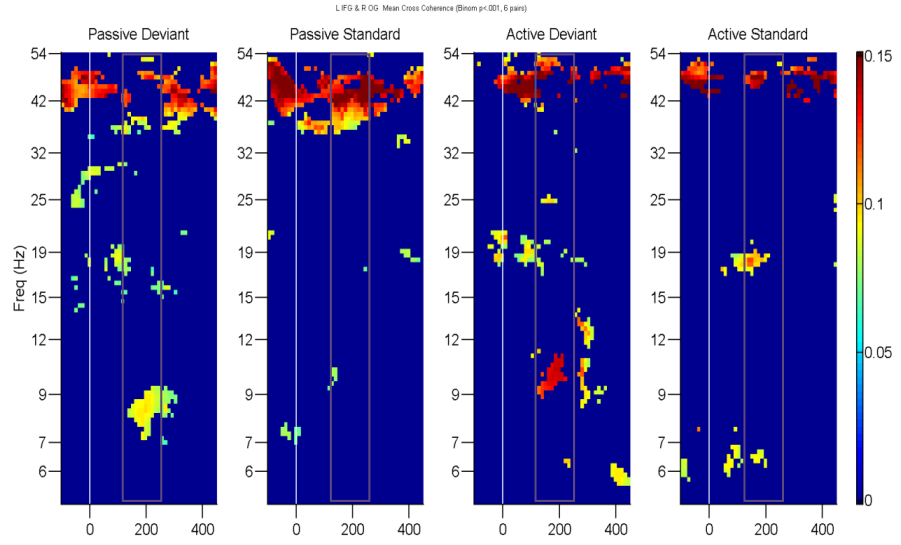

Figure C. 8. Mean cross-coherence between L IFG and R OG (Binom $p < 0.001$, 6 pairs). ROI is MMN latency region 120 - 250 ms, within mauve box. Consistent theta-band cross-coherence for the Passive Deviant condition is significantly > the Passive Standard condition ($p < 0.005$). Consistent gamma-band cross-coherence for the Passive Standard condition is significantly > the Passive Deviant condition ($p < 0.005$). Consistent gamma-band and alpha-band cross-coherence for the Active Deviant condition is significantly > the Active Standard condition ($p < 0.005$).

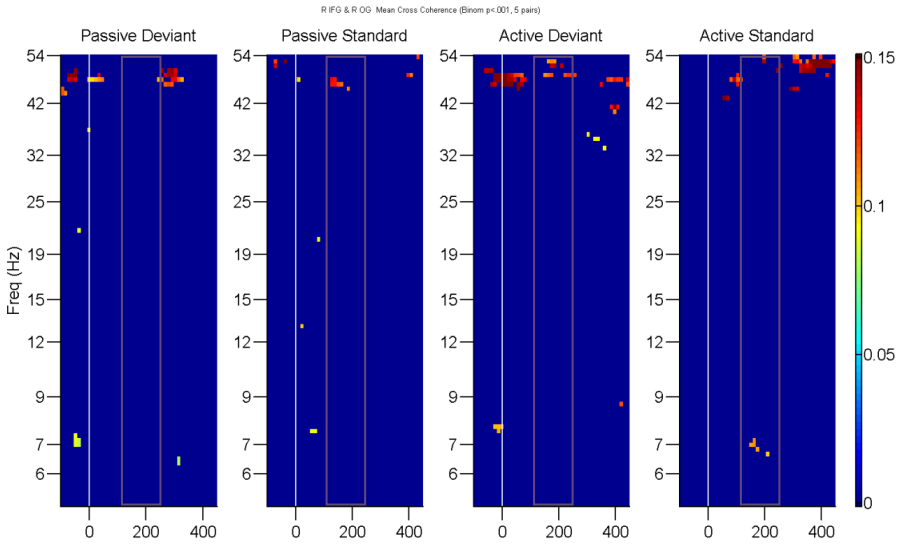

Figure C. 9. Mean cross-coherence between R IFG and R OG (Binom $p < 0.001$, 5 pairs). ROI is MMN latency region 120 -250 ms, within mauve box. Consistent gamma-band cross-coherence for the Passive Standard condition is not significantly different from the Passive Deviant condition ($p < 0.005$). Consistent gamma-band cross-coherence for the Active Deviant condition is not significantly different from the Active Standard condition ($p < 0.005$). No consistent cross-coherence > 1 frequency cycle in the lower frequency bands.

.

Appendix D: Table D. 1. Complete ERSP results for stimulus condition with the greater power within the two paradigms. Underlined for MMN latency window.

Conditions		Temporal Clusters		Left Frontal Clusters			Right Frontal Clusters	
Paradigm	Stimulus	L STG (BA42)	R STG (BA42)	L SFG (BA 10)	L IFG (BA45)	L IFG (BA47)	R SFG (BA10)	R IFG (BA45)
Passive	AC Deviant	γ, 0-70 γ, 450-600 γ, 50-200 β, 0-70 β, 350-400	γ, 460-550 β, 460-570		γ, 320-440 θ, 0-240	β, 360-460	γ, 280-350 β, 340-400	γ, 280-310 α, 350-540
	Standard	γ, 0-220	γ, 160-220 β, 130-190 β, 200-270	γ, -50-60 β, 360-480		γ, 190-370 α, 180-290 θ, 110-360	γ, 60-120 γ, 250-330 θ, 510-650	γ, 550-650 β, 540-650
	WC Deviant	γ, 50-100	γ, 0-40 γ, 400-450		β, 490-650			β, 490-610
	Standard	γ, -20-230 γ, 340-420 θ, 160-350	γ, 60-150 γ, 570-620 α, -20-80	γ, 0-190 γ, 320-390 β, 0-180	γ, 50-170 θ, 290-500	γ, 120-340 γ, 190-350 γ, 430-650 α, 60-280 α, 440-650 θ, 150-550	γ, 450-550 β, 330-650 α, 350-550 θ, -50-110 θ, 350-650	γ, 20-120 γ, 430-600 β, 190-440 β, 510-650 α, 60-230 θ, 0-350 θ, 460-650
Conditions		**Temporal Clusters**		**Left Frontal Clusters**			**Right Frontal Clusters**	
Paradigm	Stimulus	L STG (BA22)	R STG (BA 22)	L IFG (BA 10)	L IFG (BA44)	*	R IFG (BA47)	R CING(BA32)
Active	AC Deviant	γ, 20-80 θ, 120-290						β, -50-30
	Standard		γ, -30-10	γ, 360-460 γ, 80-600 β, 70-480	γ, 450-620 γ, -80-220 γ, 150-220 γ, -80-520 β, -20-160 β, 280-550 α, 420-520		γ, 460-630 γ, 160-390 β, -100-50	γ, 450-600 β, 0-100
	WC Deviant		β, 230-320				β, 300-520 β, 570-620	β, -30-150 α, -60-150
	Standard			γ, 150-230 γ, 500-560	γ, -70-10 γ, -20-220 β, -100-180		γ, 100-150 γ, 110-170	β, 0-150 α, 200-460 θ, 220-400

Appendix E: ERSP for Speech MMN

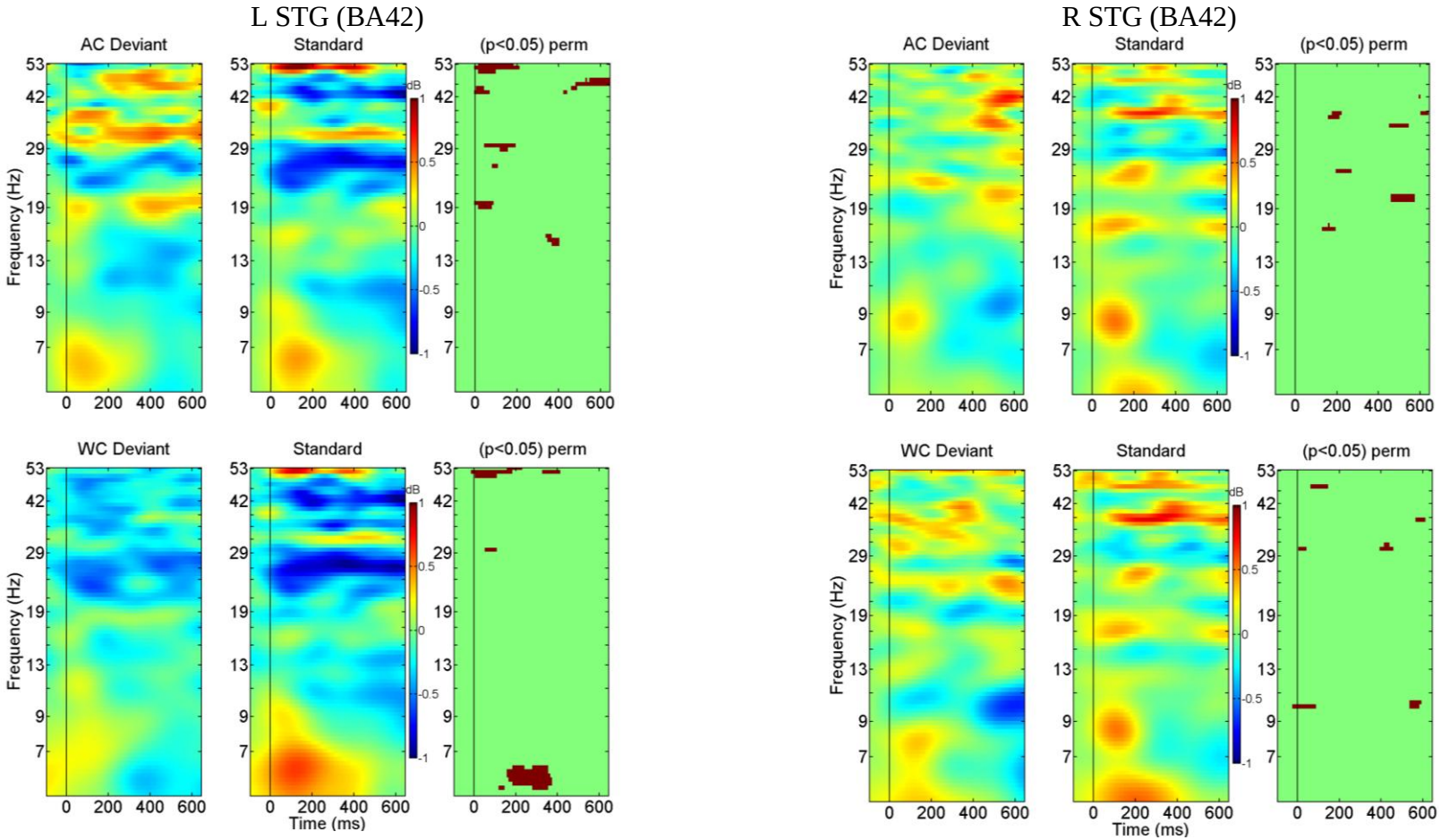

Figure E. 1. Passive paradigm temporal clusters mean ERSP for Deviant and Standard conditions, significant differences are displayed in burgundy against a green background (masked $p < 0.05$ by permutations) in the far right column. AC Deviant and Standard (top panels) and WC Deviant and Standard (lower panels). Power increase represented in red and power decrease in blue.

L STG - AC Deviant shows significant power increase in gamma-band (0-70, 450-600, and 50-200 ms) and beta-band (0-70, 350-400 ms) compared to the Standard. Standard shows significant power increase in gamma band from 0-220 ms compared to AC Deviant. WC Deviant shows significant power increase in gamma-band from 50-100 ms compared to the Standard. Standard shows more increased power in gamma (-20-230 and 340-420 ms) and theta from 160-350 ms than WC Deviant.

R STG- AC Deviant shows significant power increase in gamma-band (460-550 ms) and beta-band (460-570 ms) compared to the Standard. Standard shows significant power increase in gamma band from 160-220 ms and beta-band (130-190, 200-270 ms) compared to AC Deviant. WC Deviant shows significant power increase in gamma-band (0-40, 400-450 ms) compared to the Standard. Standard shows significant power increase in gamma (60-150 and 570-620 ms) and alpha from -20-80 ms than WC Deviant.

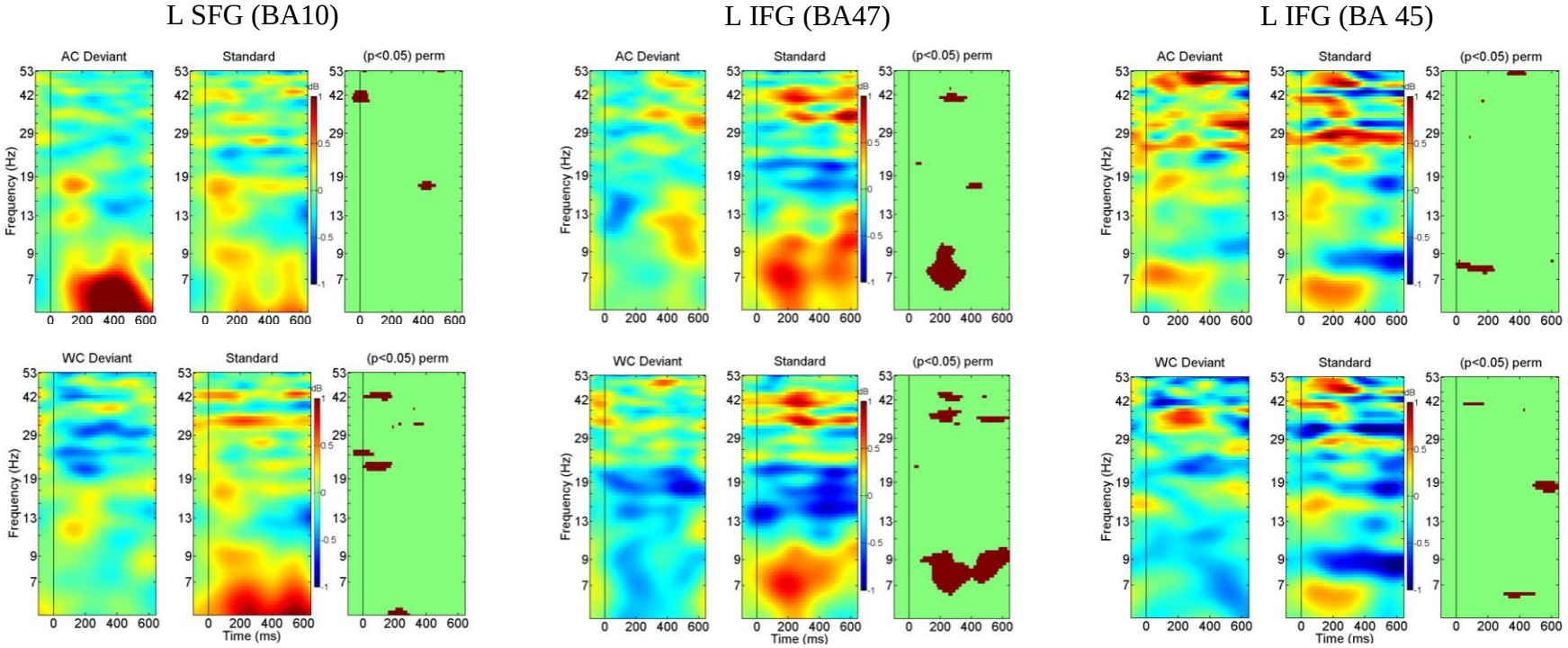

Figure E. 2. Passive paradigm left frontal clusters mean ERSP for Deviant and Standard conditions, significant differences are displayed in burgundy against a green background (masked $p < 0.05$ by permutations) in the far right column. AC Deviant and Standard (top panels) and WC Deviant and Standard (lower panels). Power increase represented in red and power decrease in blue.

L SFG (BA10) - Standard shows significant power increase in gamma-band (-50-60 ms) and beta-band (360-480 ms) than AC Deviant. Standard shows significant power increase in gamma-band (0-190, 320-390 ms) and beta-band (0-180 ms) than WC Deviant.

L IFG (BA47) - AC Deviant shows significant power increase in beta-band (360-460 ms) compared to the Standard. Standard shows significant power increase in gamma-band (190-370), alpha-band (180-290 ms) and theta-band (110-360) than AC Deviant. Standard shows significant power increase in gamma-band (120-340, 190-350, 430-650 ms), alpha-band (60-280, 440-650 ms), and theta-band (150-550 ms) than WC Deviant.

L IFG (BA45) - AC Deviant shows significant power increase in gamma-band (320-440 ms) and theta-band (0-240 ms) than Standard. WC Deviant shows significant power increase in beta-band (490-650 ms) than Standard. Standard shows significant power increase in gamma-band (50-170 ms) and theta-band (290-500 ms) than WC Deviant.

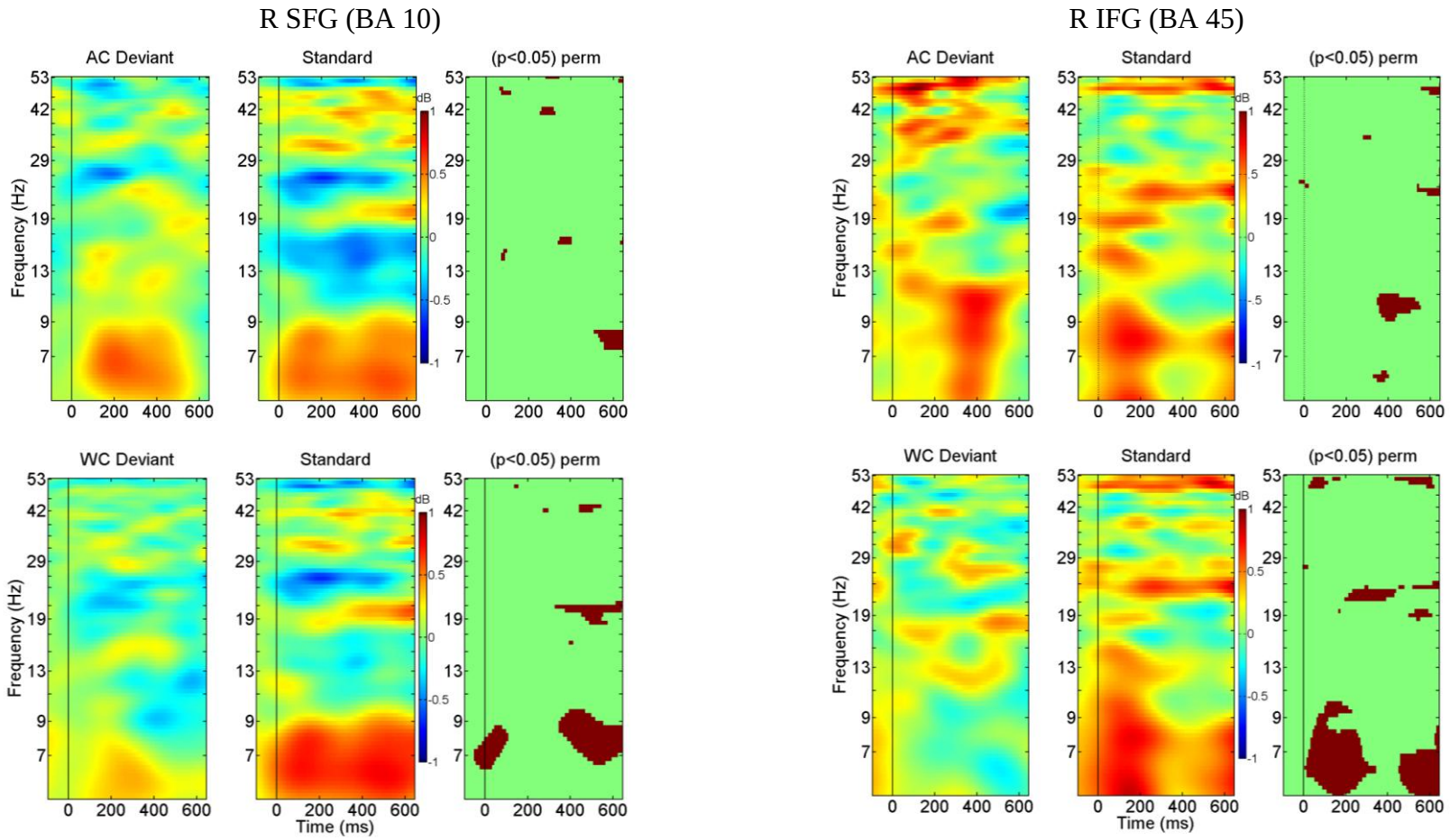

Figure E. 3. Passive paradigm right frontal clusters mean ERSP for Deviant and Standard conditions, significant differences are displayed in burgundy against a green background (masked $p < 0.05$ by permutations) in the far right column. AC Deviant and Standard (top panels) and WC Deviant and Standard (lower panels). Power increase represented in red and power decrease in blue.

R SFG (BA10) - AC Deviant shows significant power increase in gamma-band (280-350 ms) and beta-band (340-400 ms) compared to the Standard. Standard shows significant power increase in gamma band (60-120, 250-330 ms) and theta-band (510-650) compared to AC Deviant. Standard shows significant power increase in gamma (450-550 ms), beta-band (330-650 ms), alpha-band (350-550 ms) and theta (-50-110, 350-650 ms) than WC Deviant.

R IFG (BA45) - AC Deviant shows significant power increase in gamma-band (280-310 ms) and alpha-band (350-540 ms) compared to the Standard. Standard shows significant power increase in gamma band (550-650 ms) and beta-band (540-650 ms) compared to AC Deviant. WC Deviant shows significant power increase in beta-band (490-610 ms) compared to the Standard. Standard shows significant power increase in gamma-band (20-120, 430-600 ms), beta-band (190-440, 510-650 ms), alpha-band (60-230 ms), and theta-band (0-350, 460-650 ms) than WC Deviant.

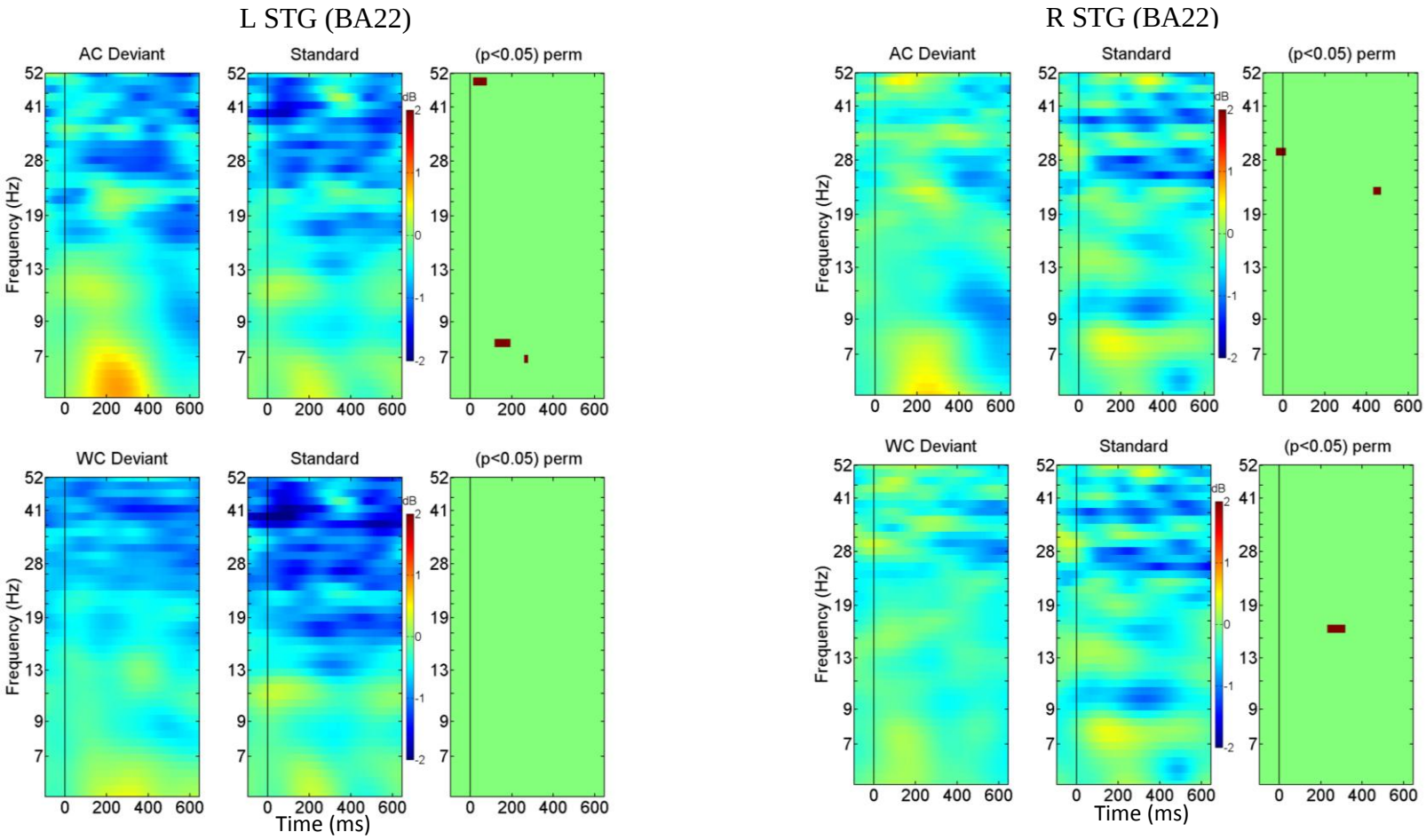

Figure E. 4. Active paradigm temporal clusters mean ERSP for Deviant and Standard conditions, significant differences are displayed in burgundy against a green background (masked $p < 0.05$ by permutations) in the far right column. AC Deviant and Standard (top panels) and WC Deviant and Standard (lower panels). Power increase represented in red/yellow and power decrease in blue.

L STG - AC Deviant shows significantly increased power in gamma-band (20-80 ms) and theta-band (120-290). No power differences between WC Deviant and Standard.

R STG - Standard shows significant power increase in gamma-band (-30-10 ms) than AC Deviant. WC Deviant shows significant power increase in beta-band (230-320 ms) than Standard.

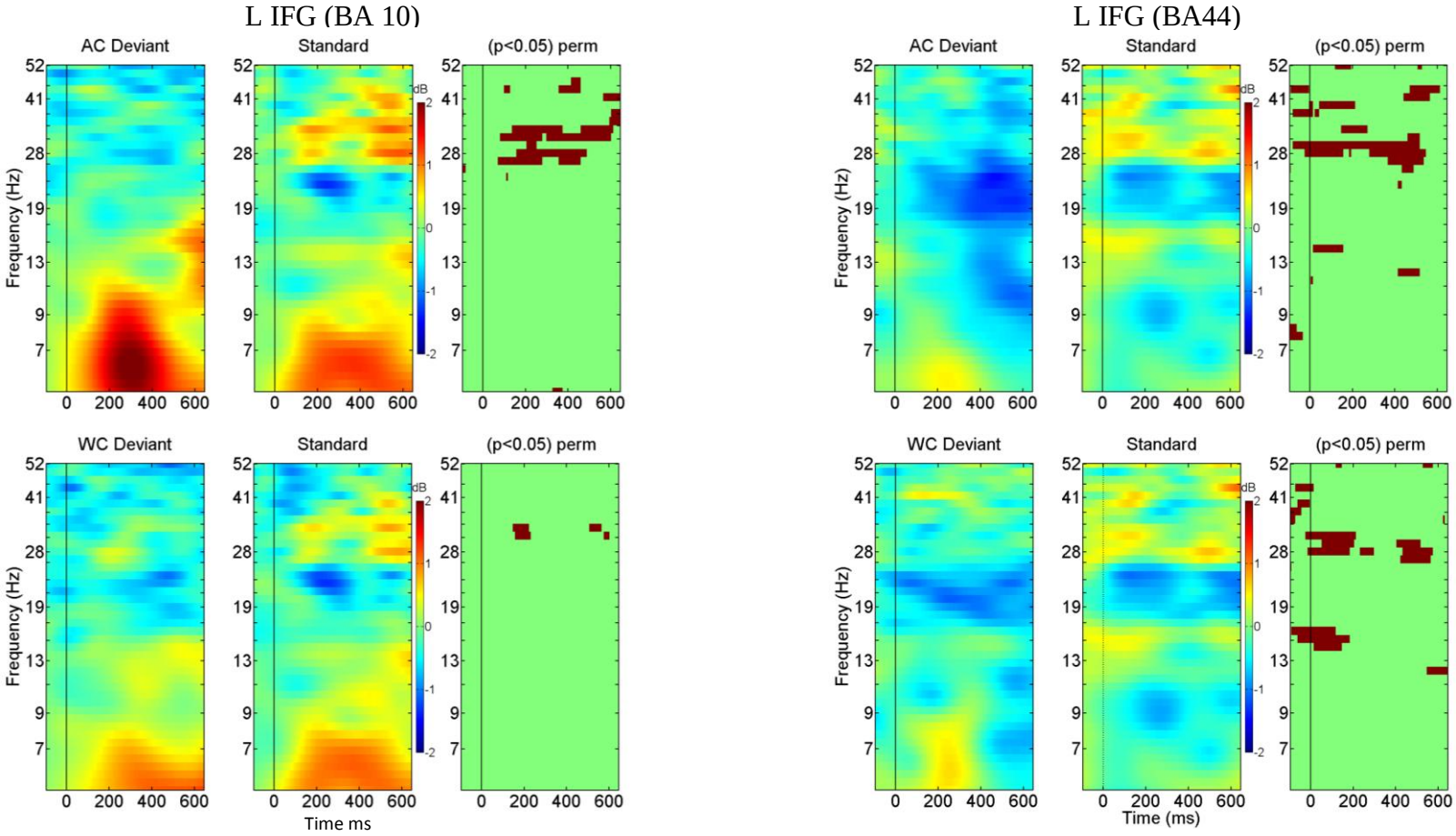

Figure E. 5. Active paradigm left frontal clusters mean ERSP for Deviant and Standard conditions, significant differences are displayed in burgundy against a green background (masked $p < 0.05$ by permutations) in the far right column. AC Deviant and Standard (top panels) and WC Deviant and Standard (lower panels). Power increase represented in red/yellow and power decrease in blue.

L IFG (BA10) - Standard shows significant power increase in gamma band (360-460, 80-600 ms) and beta-band (70-480 ms) compared to AC Deviant. Standard shows significant power increase in gamma-band (150-230, 500-560 ms) compared to WC Deviant.

L IFG (BA44) - Standard shows significant power increase in gamma band (450-620, -80-220, 150-220, -80-520 ms), beta-band (-20-160, 280-550 ms) and alpha-band (420-520) compared to AC Deviant. Standard shows significant power increase in gamma-band (-70-10, -20-220 ms), beta-band (-100-180 ms), and alpha-band (550-650) compared to WC Deviant.

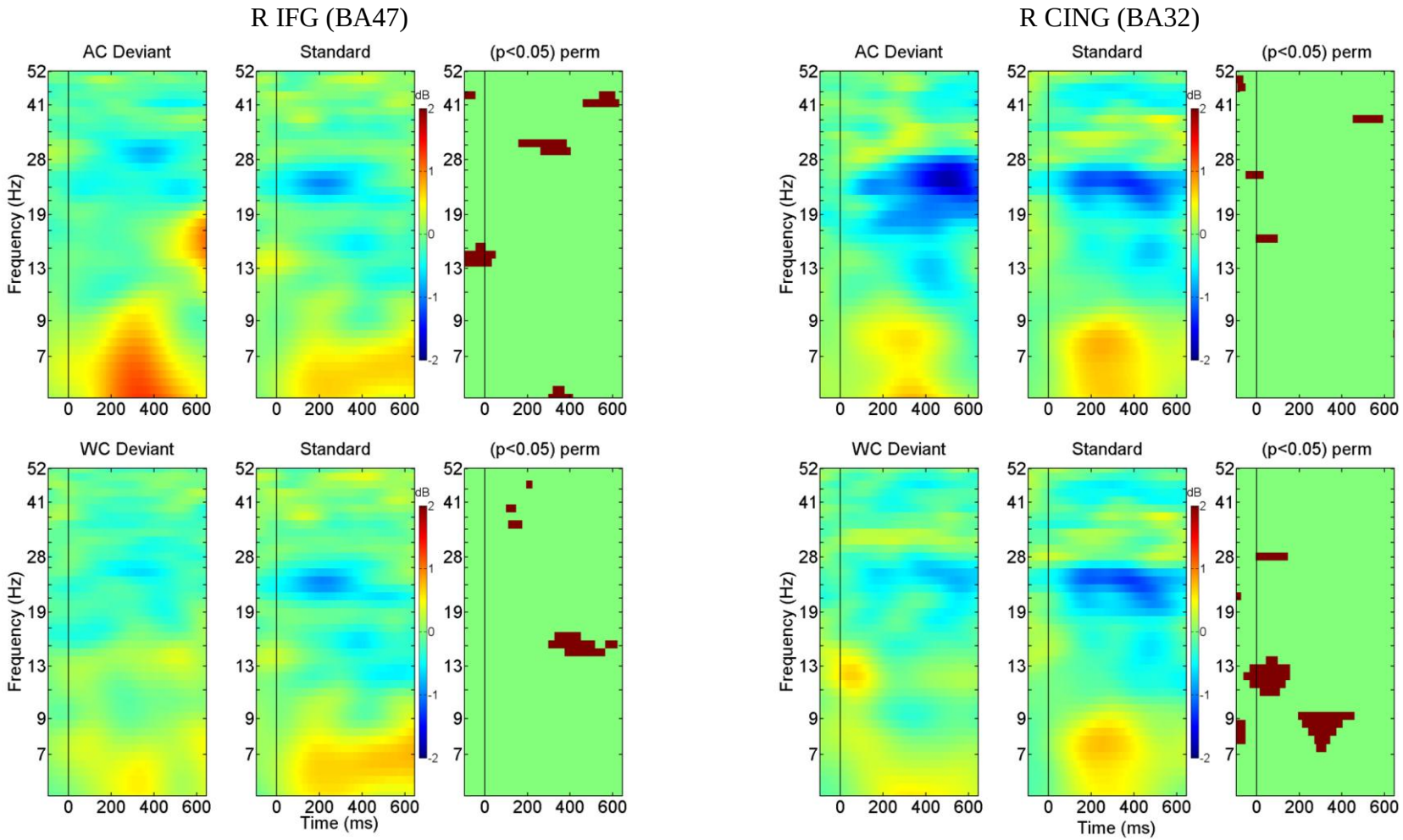

Figure E. 6. Active paradigm right frontal clusters mean ERSP for Deviant and Standard conditions, significant differences are displayed in burgundy against a green background (masked $p < 0.05$ by permutations) in the far right column. AC Deviant and Standard (top panels) and WC Deviant and Standard (lower panels). Power increase represented in red/yellow and power decrease in blue.

R IFG (BA47) – Standard shows significant power increase in gamma band (460-630, 160-390 ms), beta-band (-100-50 ms) compared to AC Deviant. WC Deviant shows significant power increase in beta-band (300-520, 570-620 ms) than Standard. Standard shows significant power increase in gamma-band (100-150, 110-170 ms) compared to WC Deviant.

R CING (BA32) – AC Deviant shows significant power increase in beta-band (-50-30 ms) than Standard. Standard shows significant power increase in gamma band (450-600 ms), and beta-band (0-100 ms) compared to AC Deviant. WC Deviant shows significant power increase in beta-band (-30-150 ms) and alpha-band (-60-150 ms) than Standard. Standard shows significant power increase in beta-band (0-150 ms), alpha-band (200-460 ms), and theta-band (220-400 ms) compared to WC Deviant.

Appendix F: Mean cross-coherence plots for speech MMN passive paradigm

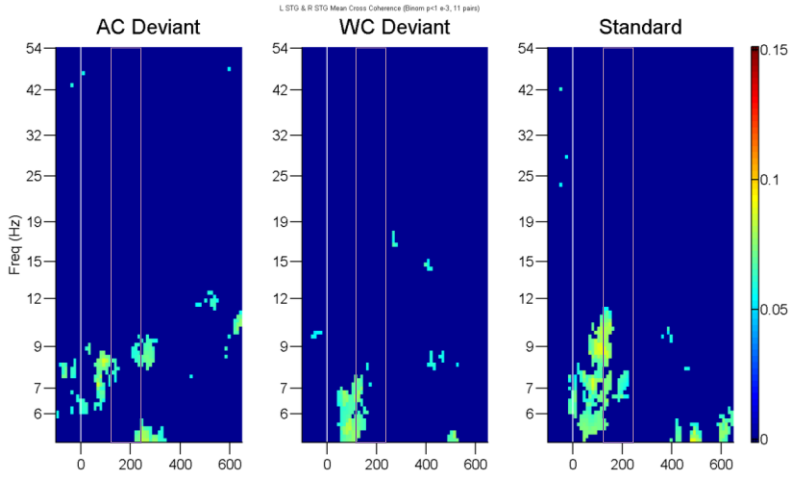

Figure F. 1. Mean cross-coherence between L STG and R STG for passive paradigm (binomial $p < 0.001$, 11pairs). ROI is MMN latency region 120 - 250 ms, within mauve box. No consistent frequency cross-coherence ≥ 1 frequency cycle within the latency of the MMN.

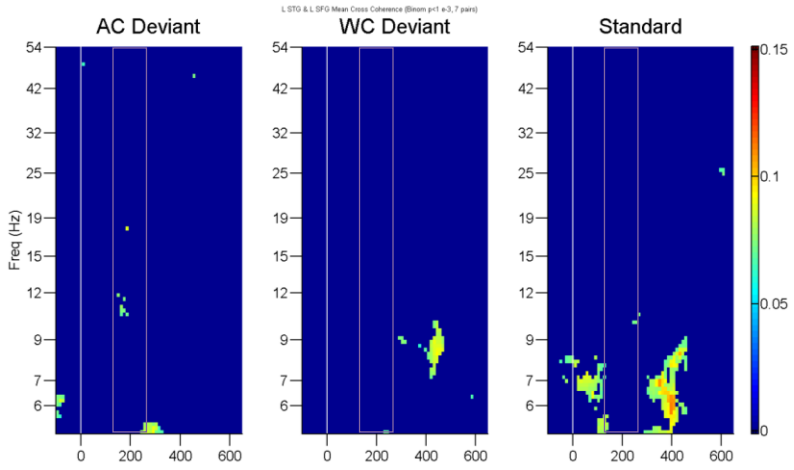

Figure F. 2. Mean cross-coherence between L STG and L SFG for passive paradigm (binomial $p < 0.001$, 7 pairs). ROI is MMN latency region 120 - 250 ms, within mauve box. No consistent frequency cross-coherence ≥ 1 frequency cycle within the latency of the MMN.

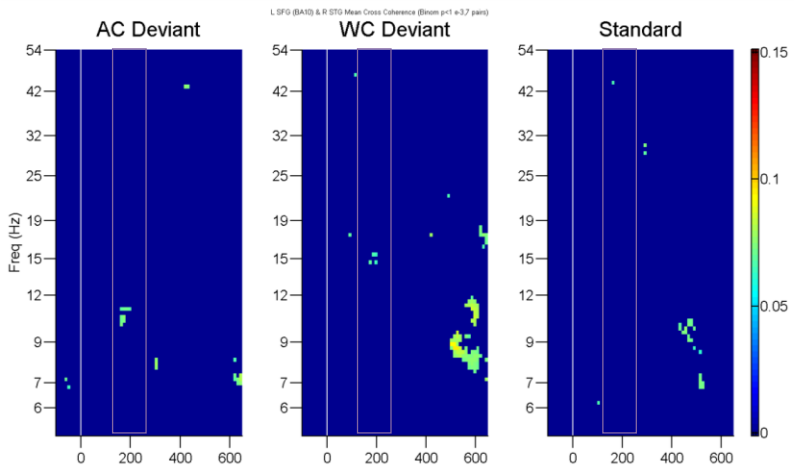

Figure F. 3. Mean cross-coherence between R STG and L SFG for passive paradigm (binomial $p < 0.001$, 7 pairs). ROI is MMN latency region 120 - 250 ms, within mauve box. No consistent frequency cross-coherence ≥ 1 frequency cycle within the latency of the MMN.

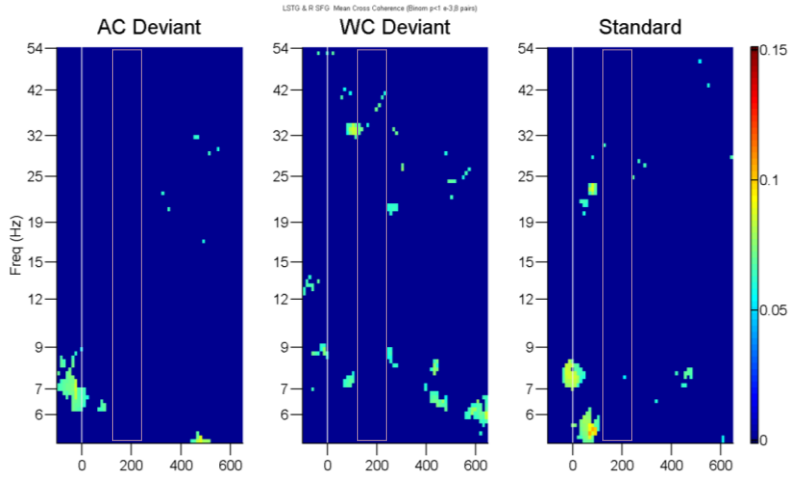

Figure F. 4. Mean cross-coherence between L STG and R SFG for passive paradigm (binomial $p < 0.001$, 8 pairs). ROI is MMN latency region 120 - 250 ms, within mauve box. No consistent frequency cross-coherence ≥ 1 frequency cycle within the latency of the MMN.

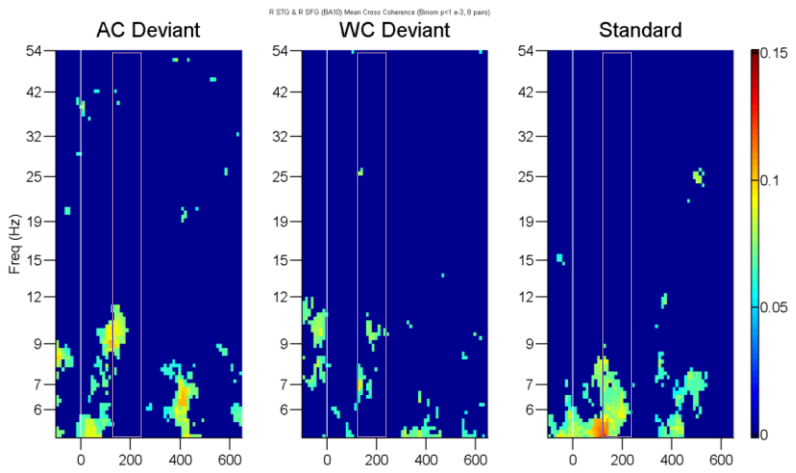

Figure F. 5. Mean cross-coherence between R STG and R SFG for passive paradigm (binomial $p < 0.001$, 8 pairs). ROI is MMN latency region 120 - 250 ms, within mauve box. Consistent theta-band cross-coherence in Standard condition is significantly > AC Deviant and WC Deviant conditions within latency of the MMN ($p < 0.005$).

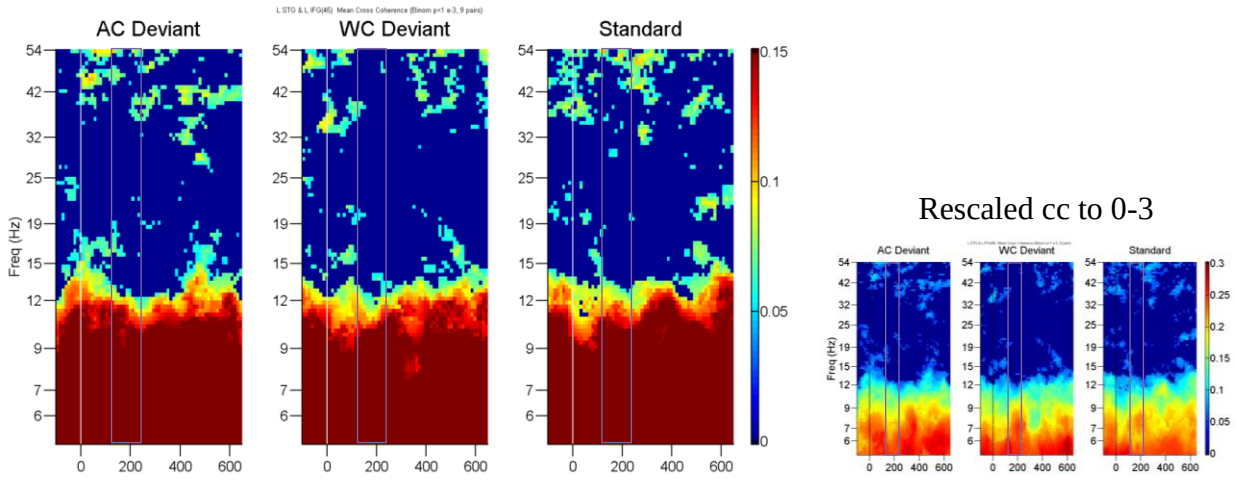

Figure F. 6. Mean cross-coherence between L STG and L IFG (BA45) for passive paradigm (binomial $p < 0.001$, 9 pairs). ROI is MMN latency region 120 - 250 ms, within mauve box. Inset provides expanded cross-coherence scale from 0-3 for better visualization. Consistent gamma- and alpha-band cross-coherence for the Standard condition were significantly > the AC Deviant condition ($p < 0.05$*). Consistent gamma- and beta-band cross-coherence for the Standard condition are significantly > the WC Deviant condition ($p < 0.005$). Consistent theta-band cross-coherence for the WC Deviant condition is significantly > the Standard condition ($p < 0.005$).

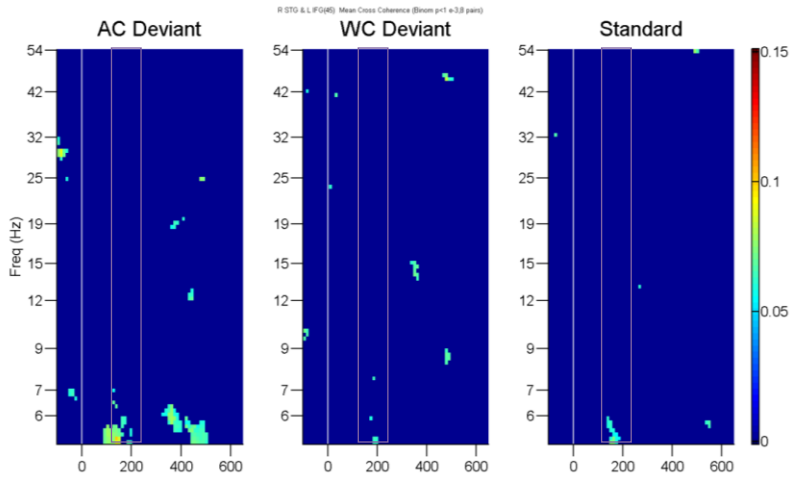

Figure F. 7. Mean cross-coherence between R STG and L IFG (BA45) for passive paradigm (binomial $p < 0.001$, 8 pairs). ROI is MMN latency region 120 - 250 ms, within mauve box. No consistent frequency cross-coherence ≥ 1 frequency cycle within the latency of the MMN.

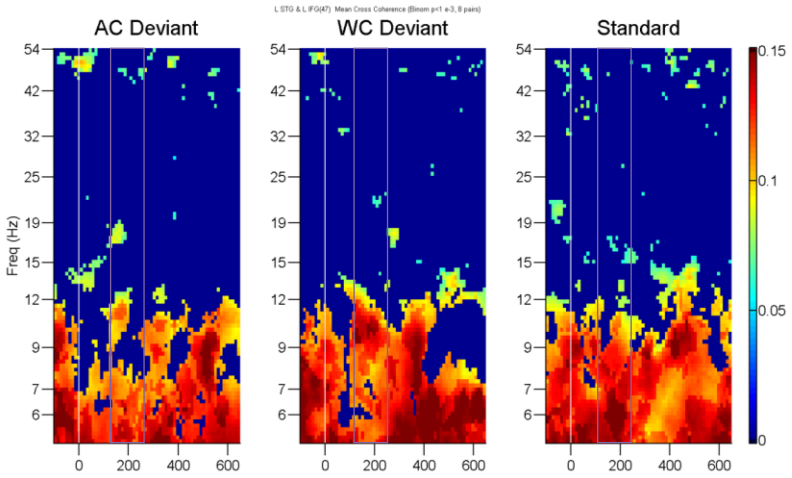

Figure F. 8. Mean cross-coherence between L STG and L IFG (BA47) for passive paradigm (binomial $p < 0.001$, 8 pairs). ROI is MMN latency region 120 - 250 ms, within mauve box. Consistent beta-band cross-coherence for AC Deviant condition is significantly > the Standard condition ($p < 0.005$). Consistent alpha-band cross-coherence for WC Deviant condition is significantly > the Standard condition ($p < 0.005$). Consistent theta-band cross-coherence for the Standard condition is significantly > the AC Deviant and WC Deviant conditions ($p < 0.005$).

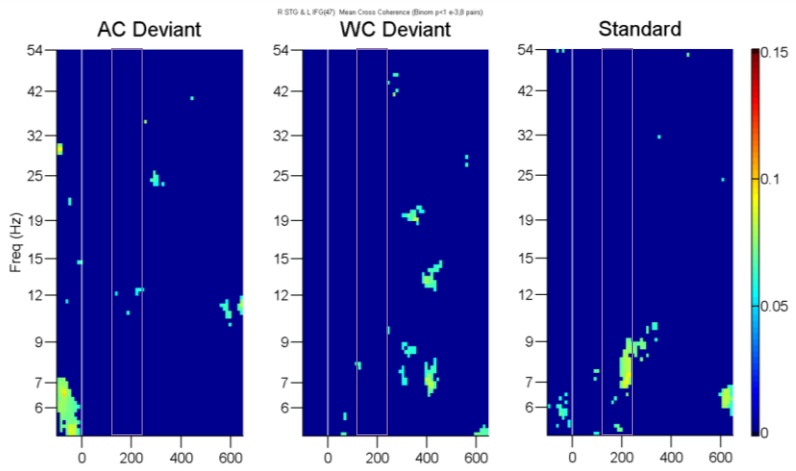

Figure F. 9. Mean cross-coherence between R STG and L IFG (BA47) for passive paradigm (binomial $p < 0.001$, 8 pairs). ROI is MMN latency region 120 - 250 ms, within mauve box. . No consistent frequency cross-coherence ≥ 1 frequency cycle within the latency of the MMN.

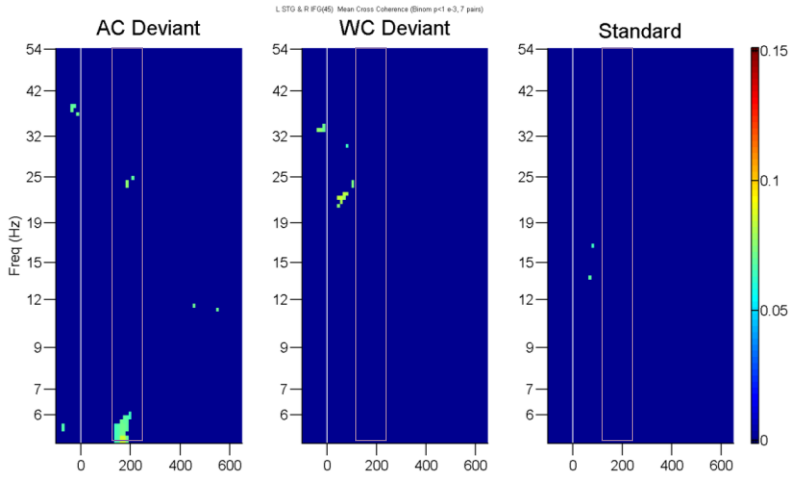

Figure F. 10. Mean cross-coherence between L STG and R IFG for passive paradigm (binomial $p < 0.001$, 7 pairs). ROI is MMN latency region 120 - 250 ms, within mauve box. No consistent frequency cross-coherence ≥ 1 frequency cycle within the latency of the MMN.

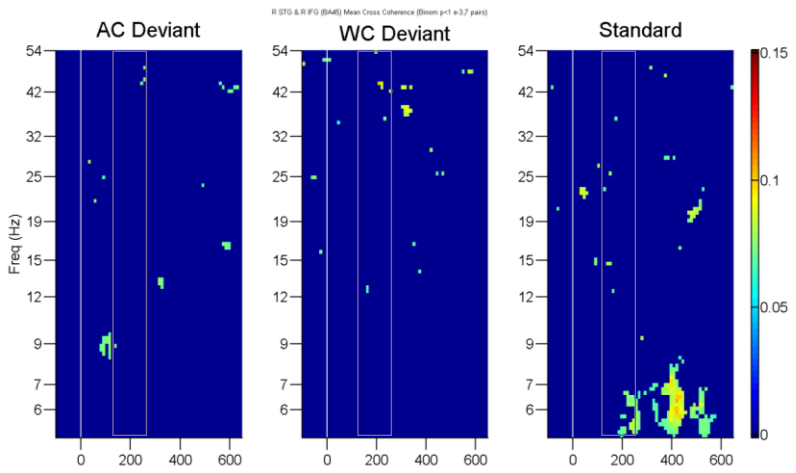

Figure F. 11. Mean cross-coherence between R STG and R IFG for passive paradigm (binomial $p < 0.001$, 7 pairs). ROI is MMN latency region 120 - 250 ms, within mauve box. No consistent frequency cross-coherence ≥ 1 frequency cycle within the latency of the MMN.

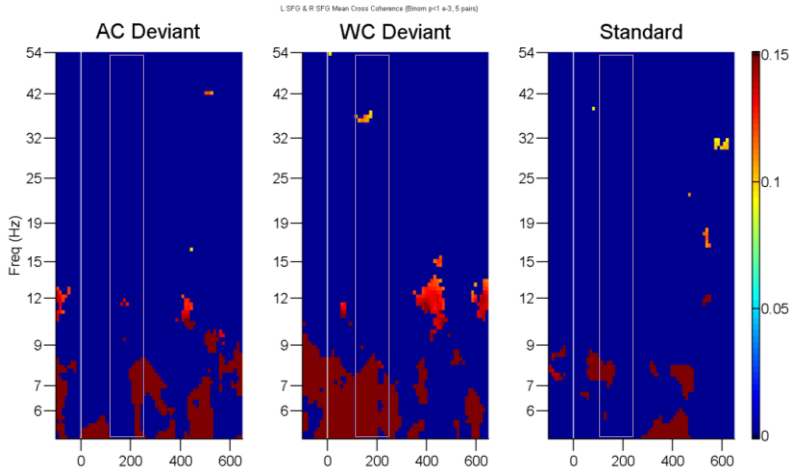

Figure F. 12. Mean cross-coherence between L SFG and R SFG for passive paradigm (binomial $p < 0.001$, 5 pairs). ROI is MMN latency region 120 - 250 ms, within mauve box. Consistent gamma-band cross-coherence for WC Deviant condition is significantly > the Standard ($p < 0.005$), however consistent theta-band cross-coherence for WC Deviant condition is not significantly different from the Standard condition within the latency of the MMN ($p < 0.005$).

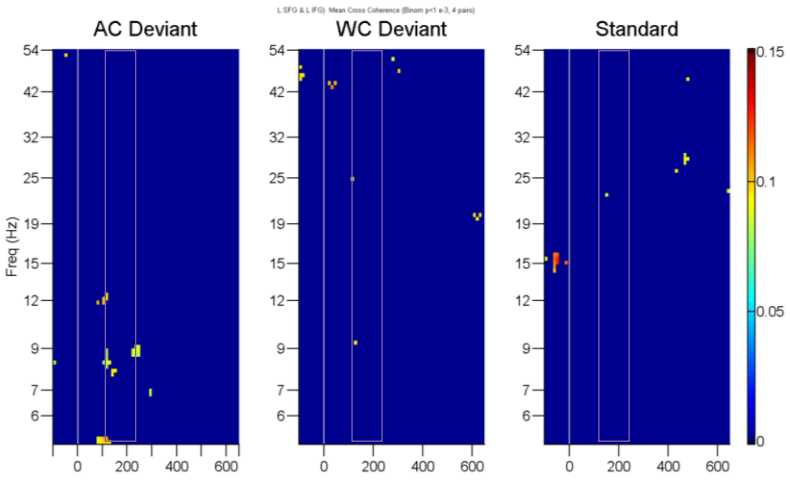

Figure F. 13. Mean cross-coherence between L SFG and L IFG (BA45) for passive paradigm (binomial $p < 0.001$, 4 pairs). ROI is MMN latency region 120 - 250 ms, within mauve box. No consistent frequency cross-coherence ≥ 1 frequency cycle within the latency of the MMN.

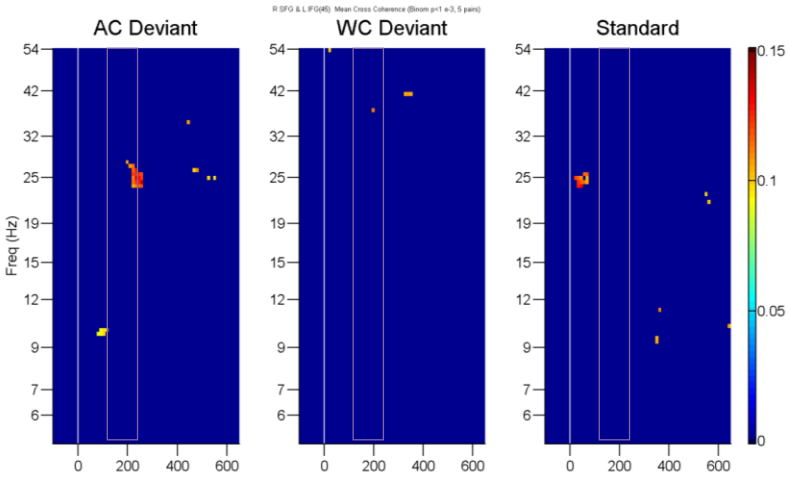

Figure F. 14. Mean cross-coherence between R SFG and L IFG (BA45) for passive paradigm (binomial $p < 0.001$, 5 pairs). ROI is MMN latency region 120 - 250 ms, within mauve box. No consistent frequency cross-coherence ≥ 1 frequency cycle within the latency of the MMN.

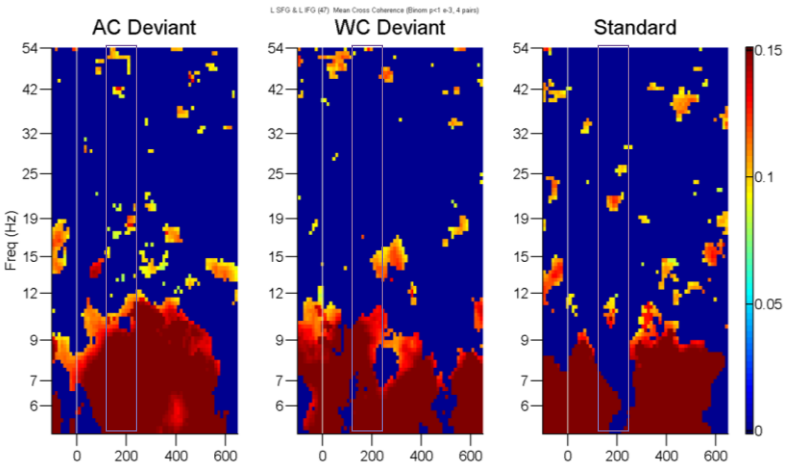

Figure F. 15. Mean cross-coherence between L SFG and L IFG (BA47) for passive paradigm (binomial $p < 0.001$, 4 pairs). ROI is MMN latency region 120 - 250 ms, within mauve box. Consistent gamma-, alpha-, and theta-band cross-coherence for AC Deviant condition is significantly > the Standard condition ($p < 0.005$). Consistent beta-band cross-coherence for the Standard condition is significantly > the AC Deviant condition ($p < 0.005$). Consistent gamma- and alpha-band cross-coherence for the WC Deviant condition is significantly > the Standard condition ($p < 0.005$).

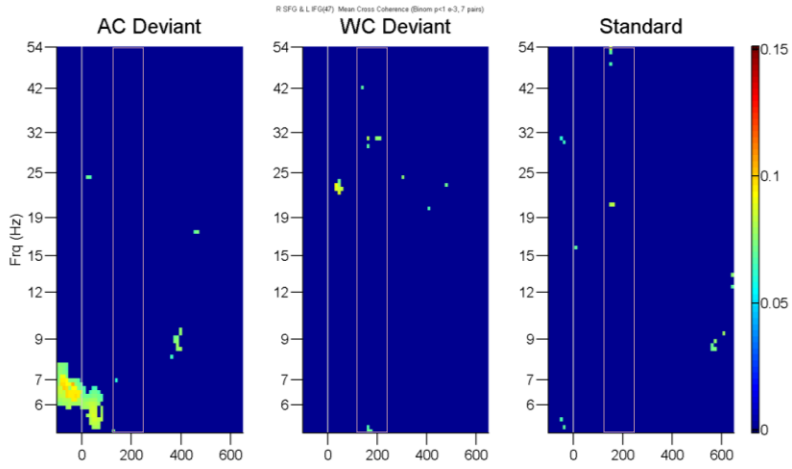

Figure F. 16. Mean cross-coherence between R SFG and L IFG (BA47) for passive paradigm (binomial $p < 0.001$, 7 pairs). ROI is MMN latency region 120 - 250 ms, within mauve box. No consistent frequency cross-coherence ≥ 1 frequency cycle within the latency of the MMN.

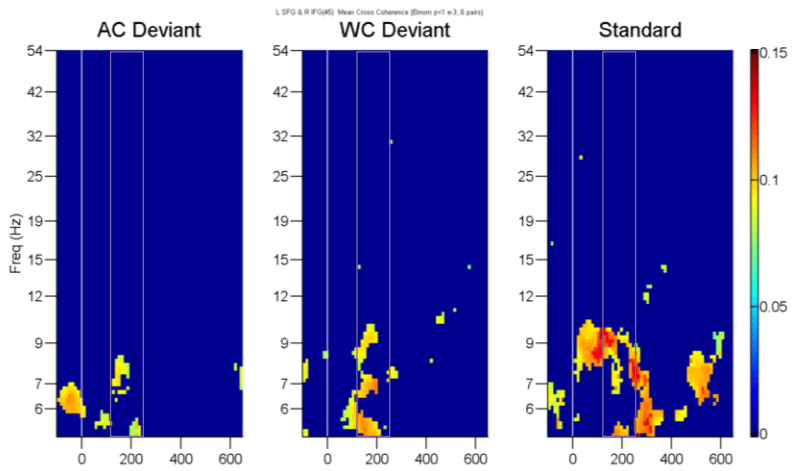

Figure F. 17. Mean cross-coherence between L SFG and R IFG for passive paradigm (binomial $p < 0.001$, 6 pairs). ROI is MMN latency region 120 - 250 ms, within mauve box. Consistent alpha-band cross-coherence for Standard condition is significantly > the AC Deviant and WC Deviant conditions within latency of the MMN ($p < 0.005$). No other consistent frequency cross-coherence ≥ 1 frequency cycle within the latency of the MMN.

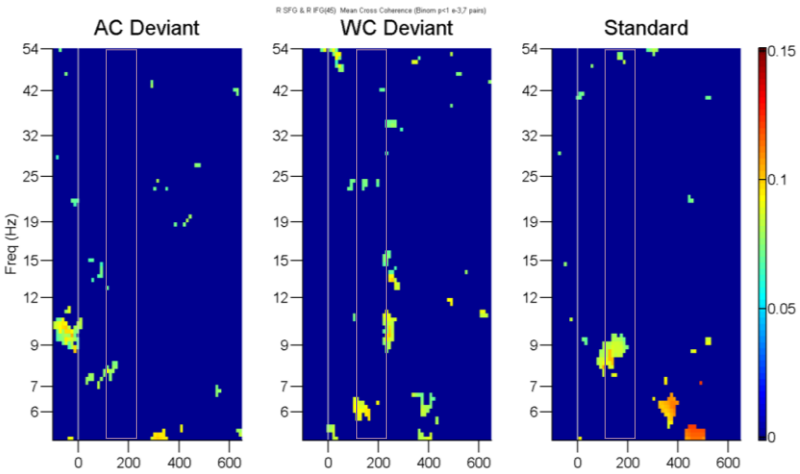

Figure F. 18. Mean cross-coherence between R SFG and R IFG for passive paradigm (binomial $p < 0.001$, 7 pairs). ROI is MMN latency region 120 - 250 ms, within mauve box. Consistent alpha-band cross coherence in the Standard is not significantly different from AC Deviant or WC Deviant conditions ($p < 0.005$).

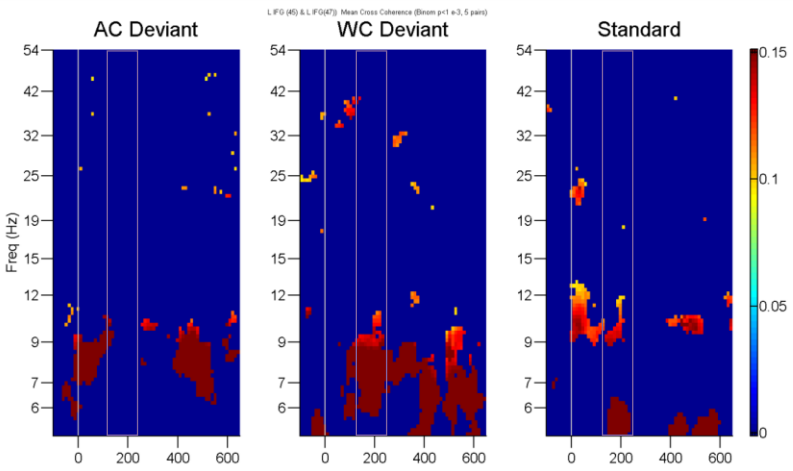

Figure F. 19. Mean cross-coherence between L IFG (BA45) and L IFG (BA47) for passive paradigm (binomial $p < 0.001$, 5 pairs). ROI is MMN latency region 120 - 250 ms, within mauve box. Consistent theta and alpha-band cross-coherence for the Standard condition are not significantly different from the AC Deviant condition ($p < 0.005$). Consistent theta-band cross-coherence for the WC Deviant condition is significantly > the Standard condition ($p < 0.005$).

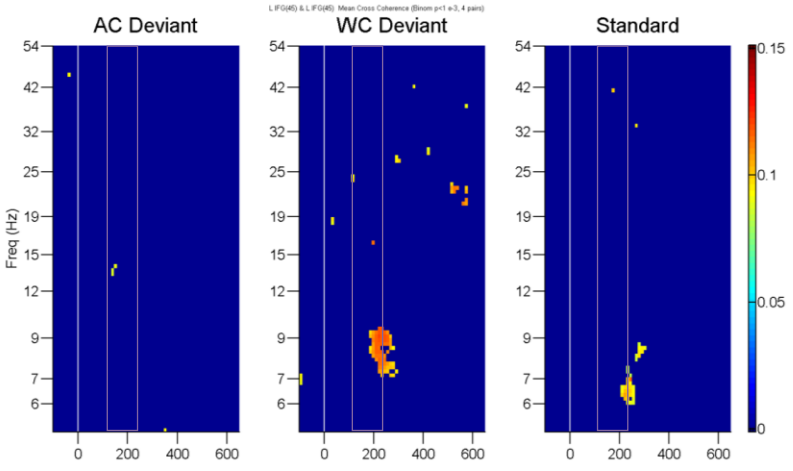

Figure F. 20. Mean cross-coherence between L IFG (BA45) and R IFG and for passive paradigm (binomial $p < 0.001$, 4 pairs). ROI is MMN latency region 120 - 250 ms, within mauve box. No consistent frequency cross-coherence ≥ 1 frequency cycle within the latency of the MMN.

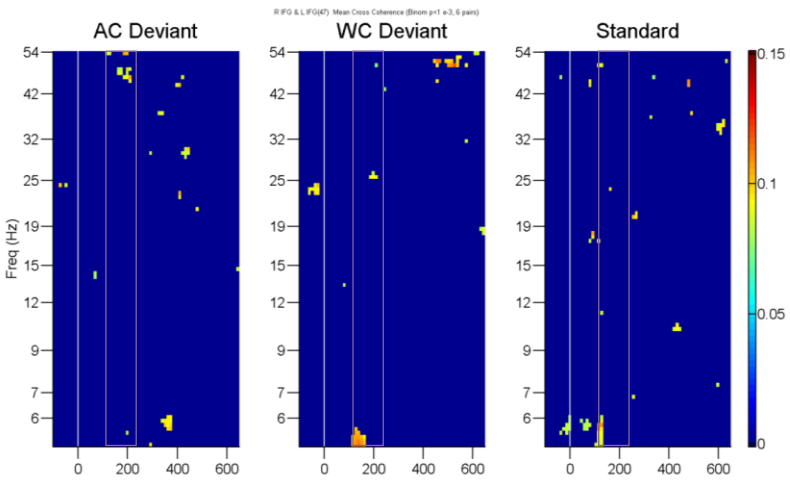

Figure F. 21. Mean cross-coherence between L IFG (BA47) and R IFG and for passive paradigm (binomial $p < 0.001$, 6 pairs). ROI is MMN latency region 120 - 250 ms, within mauve box. Consistent gamma-band cross-coherence in the AC Deviant condition was not significantly different from the Standard condition. No other consistent frequency cross-coherence ≥ 1 frequency cycle within the latency of the MMN.

Appendix G: Mean cross-coherence plots for speech MMN active paradigm

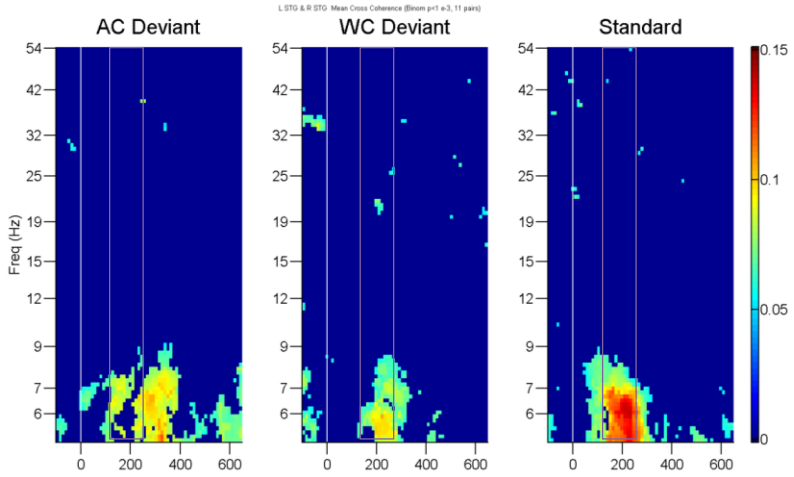

Figure G. 1. Mean cross-coherence between L STG and R STG for active paradigm (binomial $p < 0.001$, 11pairs). ROI is MMN latency region 120 - 250 ms, within mauve box. Consistent theta-band cross-coherence for the Standard condition is significantly > AC Deviant and WC Deviant conditions ($p < 0.005$). No other consistent frequency cross-coherence ≥1 frequency cycle within the latency of the MMN.

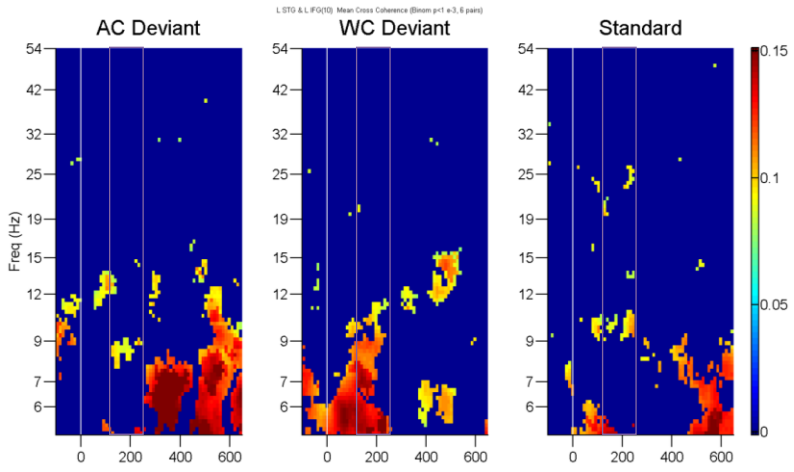

Figure G. 2. Mean cross-coherence between L STG and L IFG (BA10) for active paradigm (binomial $p < 0.001$, 11pairs). ROI is MMN latency region 120 - 250 ms, within mauve box. Consistent theta- and alpha-band cross-coherence for WC Deviant condition are significantly > the Standard condition ($p < 0.005$). No other consistent frequency cross-coherence ≥ 1 frequency cycle within the latency of the MMN.

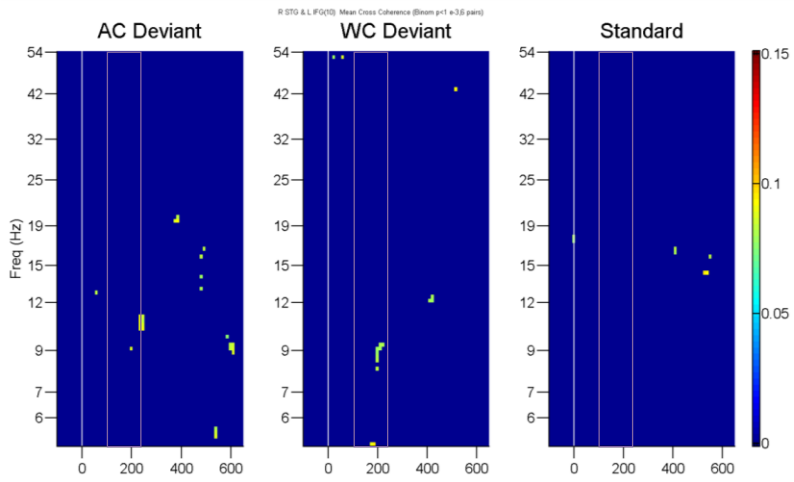

Figure G. 3. Mean cross-coherence between R STG and L IFG (BA10) for active paradigm (binomial $p < 0.001$, 6 pairs). ROI is MMN latency region 120 - 250 ms, within mauve box. No consistent frequency cross-coherence ≥ 1 frequency cycle within the latency of the MMN.

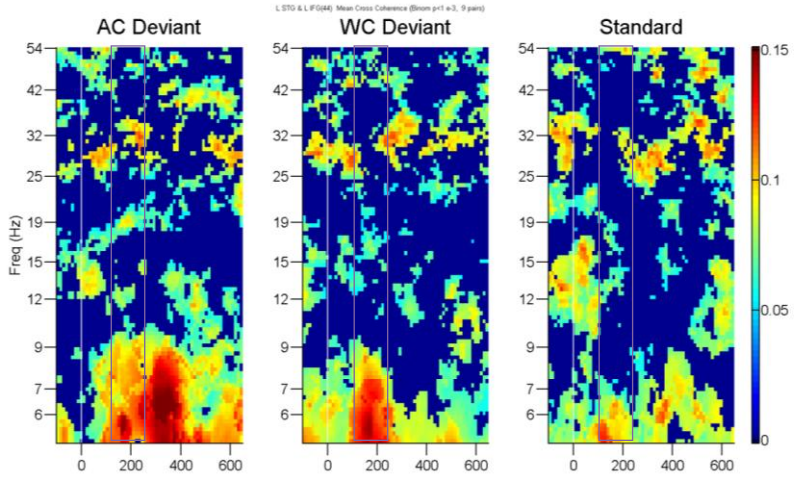

Figure G. 4. Mean cross-coherence between L STG and L IFG (BA44) for active paradigm (binomial $p < 0.001$, 9 pairs). ROI is MMN latency region 120 - 250 ms, within mauve box. Consistent cross-coherence for all frequency bands in the AC Deviant condition are significantly > the Standard condition ($p < 0.005$). Consistent theta-, beta- and gamma-band cross-coherence for WC Deviant condition are significantly > the Standard condition ($p < 0.005$).

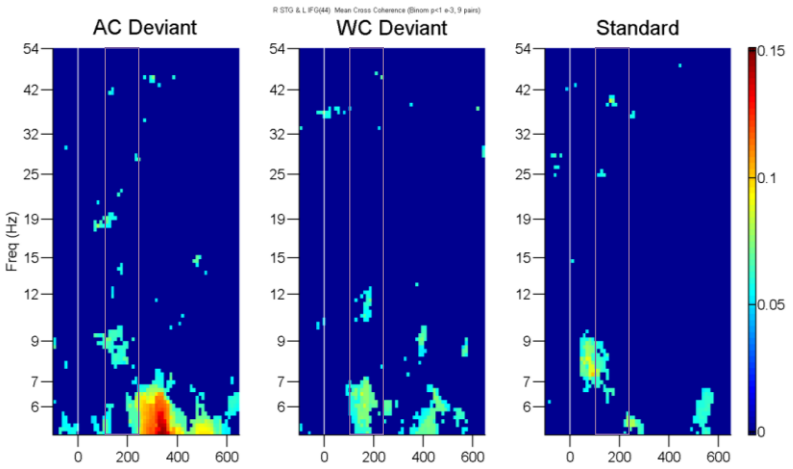

Figure G. 5. Mean cross-coherence between R STG and L IFG (BA44) for active paradigm (binomial $p < 0.001$, 9 pairs). ROI is MMN latency region 120 - 250 ms, within mauve box. No consistent frequency cross-coherence ≥ 1 frequency cycle within the latency of the MMN.

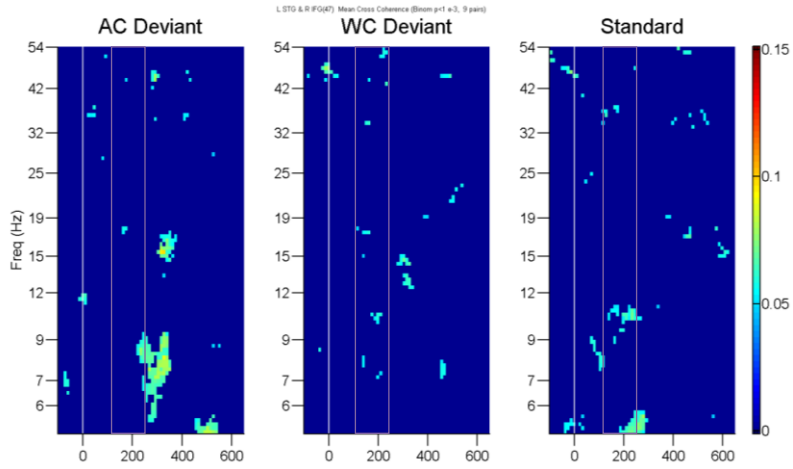

Figure G. 6. Mean cross-coherence between L STG and R IFG (BA47) for active paradigm (binomial $p < 0.001$, 9 pairs). ROI is MMN latency region 120 - 250 ms, within mauve box. No consistent frequency cross-coherence ≥ 1 frequency cycle within the latency of the MMN.

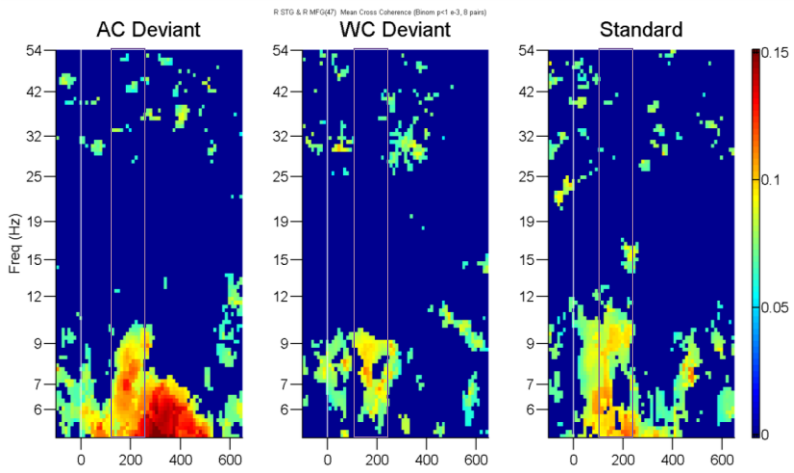

Figure G. 7. Mean cross-coherence between R STG and R IFG (BA47) for active paradigm (binomial $p < 0.001$, 8 pairs). ROI is MMN latency region 120 - 250 ms, within mauve box. Consistent theta-band cross-coherence in the AC Deviant condition is significantly > the Standard condition ($p < 0.005$). Consistent alpha- and beta-band cross-coherence for the Standard condition are significantly > the AC Deviant and WC Deviant conditions ($p < 0.005$). Consistent theta-band cross-coherence for the Standard condition is significantly > WC Deviant condition ($p < 0.005$).

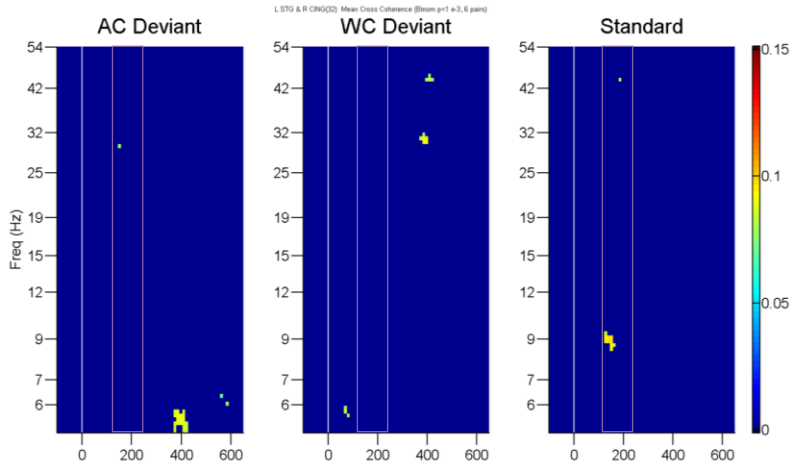

Figure G. 8. Mean cross-coherence between L STG and R CING for active paradigm (binomial $p < 0.001$, 5 pairs). ROI is MMN latency region 120 - 250 ms, within mauve box. No consistent frequency cross-coherence ≥ 1 frequency cycle within the latency of the MMN.

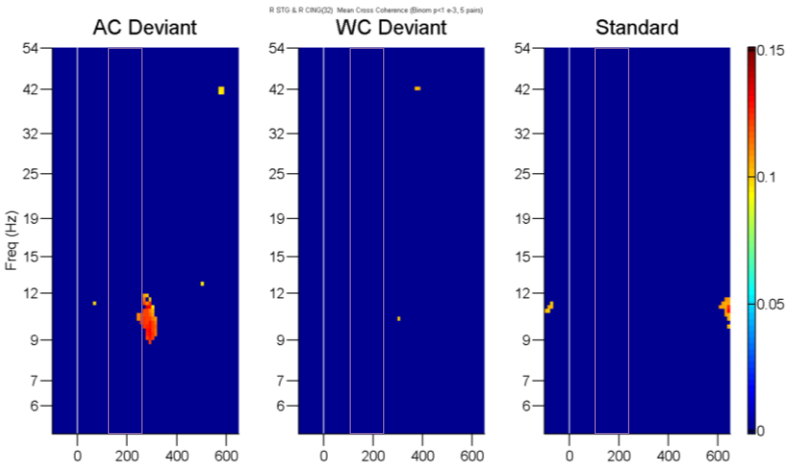

Figure G. 9. Mean cross-coherence between R STG and R CING for active paradigm (binomial $p < 0.001$, 5 pairs). ROI is MMN latency region 120 - 250 ms, within mauve box. No consistent frequency cross-coherence ≥ 1 frequency cycle within the latency of the MMN.

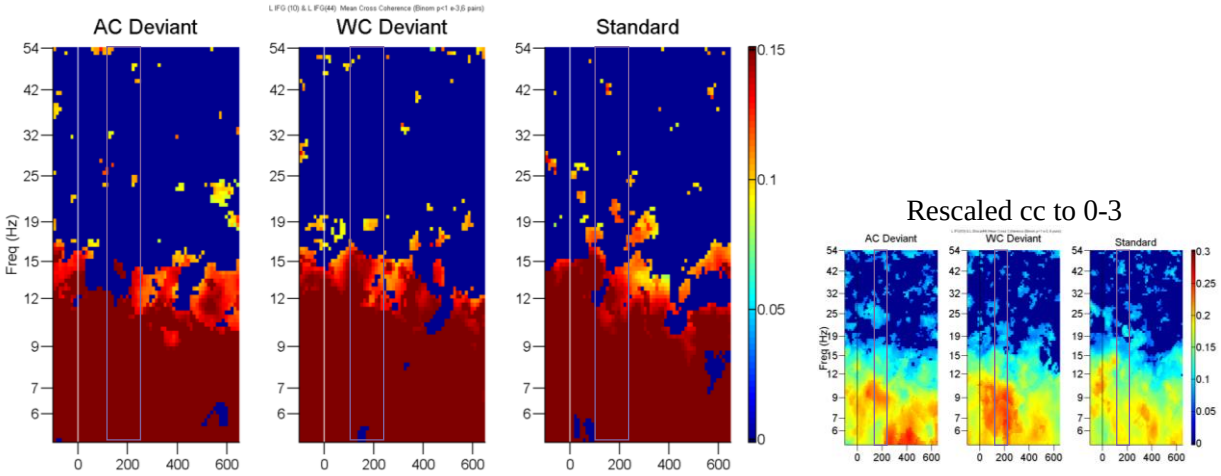

Figure G. 10. Mean cross-coherence between L IFG (BA10) and L IFG (BA44) for active paradigm (binomial $p < 0.001$, 6 pairs). ROI is MMN latency region 120 - 250 ms, within mauve box. Inset provides wider cross-coherence scale from 0-3 for better visualization. Consistent alpha-band cross-coherence for AC Deviant condition is significantly > the Standard condition ($p < 0.005$). Consistent alpha-band and theta-band cross-coherence for WC Deviant condition are significantly > the Standard condition ($p < 0.005$).

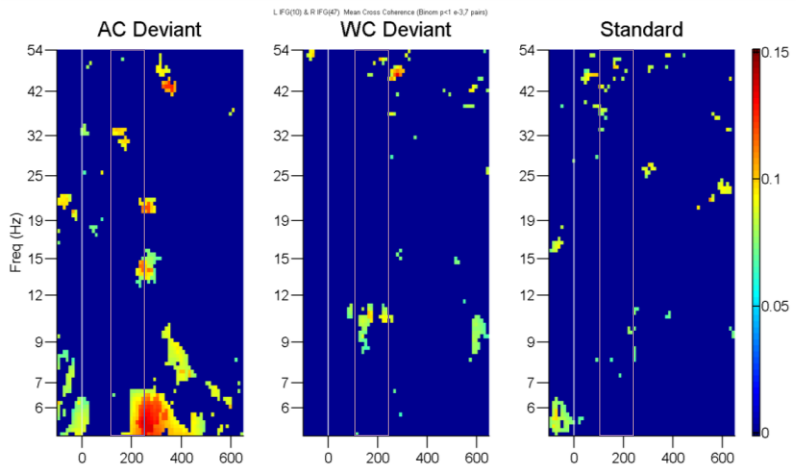

Figure G. 11. Mean cross-coherence between L IFG (BA10) and R IFG (BA47) for active paradigm (binomial $p < 0.001$, 7 pairs). ROI is MMN latency region 120 - 250 ms, within mauve box. Consistent gamma-band cross-coherence in the AC Deviant condition is significantly > the Standard condition ($p < 0.005$).

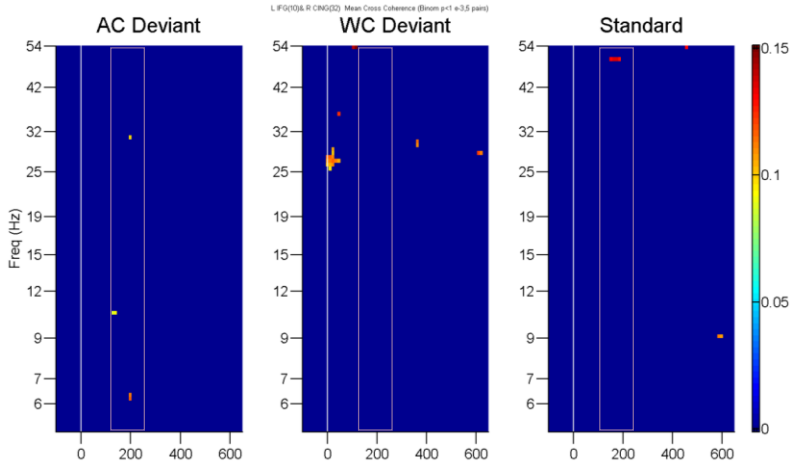

Figure G. 12. Mean cross-coherence between L IFG (BA10) and R CING for active paradigm (binomial $p < 0.001$, 5 pairs). ROI is MMN latency region 120 - 250 ms, within mauve box. Consistent gamma-band cross-coherence in the Standard condition is significantly > AC Deviant condition ($p < 0.005$).

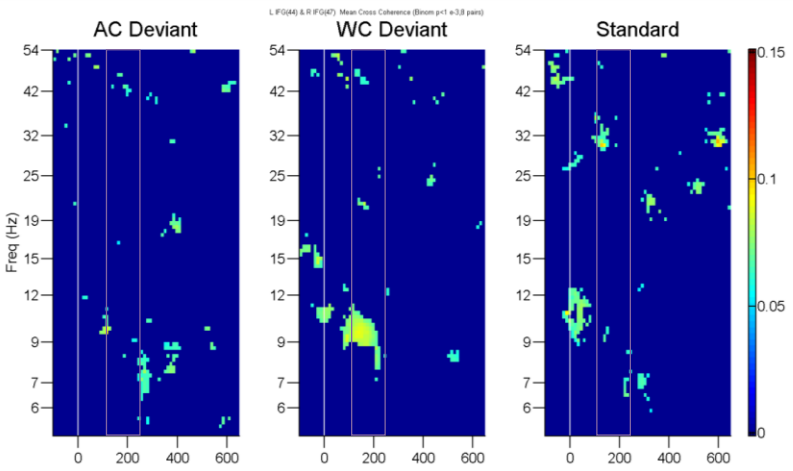

Figure G. 13. Mean cross-coherence between L IFG (BA44) and R IFG (BA47) for active paradigm (binomial $p < 0.001$, 8 pairs). ROI is MMN latency region 120 - 250 ms, within mauve box. Consistent gamma-band cross-coherence in the Standard condition is significantly > AC Deviant and WC Deviant conditions ($p < 0.005$).

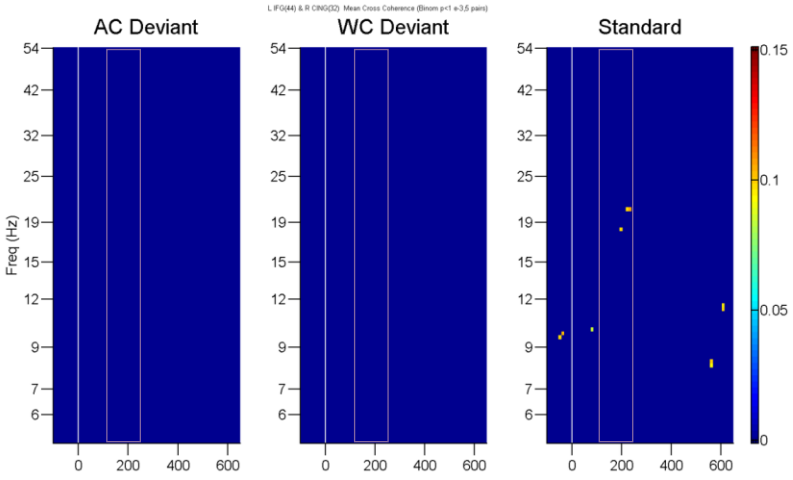

Figure G. 14. Mean cross-coherence between L IFG (BA44) and R CING for active paradigm (binomial $p < 0.001$, 5 pairs). ROI is MMN latency region 120 - 250 ms, within mauve box. No consistent frequency cross-coherence ≥ 1 frequency cycle within the latency of the MMN.

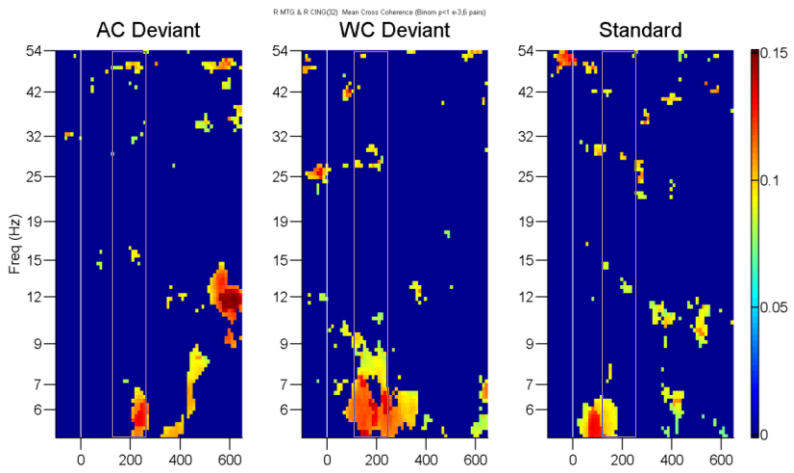

Figure G. 15. Mean cross-coherence between R IFG (BA47) and R CING for active paradigm (binomial $p < 0.001$, 6 pairs). ROI is MMN latency region 120 - 250 ms, within mauve box. Consistent gamma-band cross-coherence in the AC Deviant condition is significantly > the Standard condition ($p < 0.005$). Consistent theta- and beta-band cross-coherence for WC Deviant condition are significantly > the Standard condition ($p < 0.005$).